

**MECHANICAL PERFORMANCE OF UNDERGROUND  
EXCAVATION IN ROCK SALT FORMATION FOR  
NUCLEAR WASTE REPOSITORY IN NORTHEASTERN  
THAILAND**

**Mr. Kitcha Klayvimut**

**A Thesis Submitted in Partial Fulfillment of the Requirements for the Degree of**

**Master of Engineering in Geotechnology**

**Suranaree University of Technology**

**Academic Year 2003**

**ISBN 974-533-313-1**

ศักยภาพเชิงกลศาสตร์ของอุโมงค์ใต้ดินในชั้นเกลือหินสำหรับกักเก็บ  
กากนิวเคลียร์ในภาคตะวันออกเฉียงเหนือของประเทศไทย

นายกิจจา คล้ายวิมุติ

วิทยานิพนธ์นี้เป็นส่วนหนึ่งของการศึกษาตามหลักสูตรปริญญาวิศวกรรมศาสตรมหาบัณฑิต

สาขาวิชาเทคโนโลยีธรณี

มหาวิทยาลัยเทคโนโลยีสุรนารี

ปีการศึกษา 2546

ISBN 974-533-313-1

**MECHANICAL PERFORMANCE OF UNDERGROUND  
EXCAVATION IN ROCK SALT FORMATION FOR NUCLEAR  
WASTE REPOSITORY IN NORTHEASTERN THAILAND**

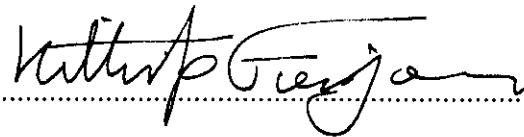
Suranaree University of Technology has approved this thesis submitted in partial fulfillment of the requirements for a Master's Degree.

Thesis Examining Committee



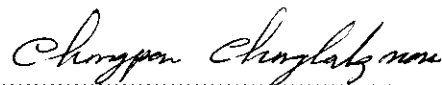
(Asst. Prof. Thara Lekuthai)

Chairman



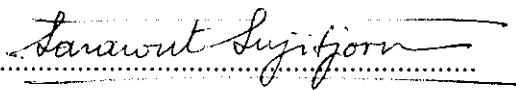
(Assoc. Prof. Dr. Kittitep Fuenkajorn)

Member (Thesis Advisor)



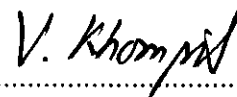
(Dr. Chongpan Chonglakmani)

Member



(Assoc. Prof. Dr. Sarawut Sujitjorn)

Vice Rector for Academic Affairs



(Assoc. Prof. Dr. Vorapot Khompis)

Dean of Institute of Engineering

กิจจา กล้ายวิมุติ: ศักยภาพเชิงกลศาสตร์ของอุโมงค์ใต้ดินในชั้นเกลือหินสำหรับกักเก็บกากนิวเคลียร์ในภาคตะวันออกเฉียงเหนือของประเทศไทย(MECHANICAL PERFORMANCE OF UNDERGROUND EXCAVATION IN ROCK SALT FORMATION FOR NUCLEAR WASTE REPOSITORY IN NORTHEASTERN THAILAND)

อาจารย์ที่ปรึกษา: รองศาสตราจารย์ ดร. กิตติเทพ เฟื่องขจร, 191 หน้า

ISBN 974-533-313-1

การประเมินศักยภาพเชิงกลศาสตร์ของชั้นเกลือหินในภาคตะวันออกเฉียงเหนือของประเทศไทยสำหรับกักเก็บกากนิวเคลียร์ประกอบด้วยสองกิจกรรมหลักคือ การทดสอบตัวอย่างเกลือหินในห้องปฏิบัติการ และการออกแบบโดยใช้วิธีคำนวณด้วยแบบจำลองทางคอมพิวเตอร์ ผลการวิเคราะห์ข้อมูลหลุมเจาะและข้อมูลสำรวจธรณีฟิสิกส์ที่มีอยู่ระบุว่าลำดับชั้นหินใน 3 พื้นที่ในหมวดหินมหาสารคามมีความเหมาะสมในการใช้ทั้งกากนิวเคลียร์ โดยการทดสอบในห้องปฏิบัติการประกอบด้วยทดสอบการเคลื่อนไหลในแกนเดียวและในสามแกนภายใต้อุณหภูมิคงที่ของตัวอย่างเกลือหิน ผลจากการทดสอบได้นำมาสอบเทียบคุณสมบัติเชิงกลศาสตร์ของเกลือหิน ซึ่งรวมไปถึงความเหนียว ความหนืด ความแข็ง ความยืดหยุ่น และการเปลี่ยนรูปตามเวลา ผลของการสอบเทียบได้นำมาใช้ในการออกแบบโดยอาศัยแบบจำลองทางคอมพิวเตอร์ การจำลองใช้สมการสำหรับความหนืดเชิงยืดหยุ่นและความหนืดเชิงพลาสติกเพื่อคาดคะเนความเค้นและการเปลี่ยนรูปเชิงเวลาของเกลือหินที่อยู่รอบอุโมงค์ และคาดคะเนการเคลื่อนตัวของหินข้างเคียง การวิเคราะห์สมมุติให้เกลือหินอยู่ภายใต้อุณหภูมิค่า โดยลำดับชั้นหินจาก 3 พื้นที่ที่คัดเลือกไว้ได้นำมาใช้ในแบบจำลอง ข้อกำหนดที่สำคัญในการออกแบบประกอบด้วย 1) เสถียรภาพเชิงกลศาสตร์ในช่วงระยะเวลา 50 ปี ระหว่างการดำเนินการ 2) ไม่มีการรั่วไหลของกากนิวเคลียร์ในระยะเวลา 500 ปี ระหว่างการกักเก็บ และ 3) การเคลื่อนตัวของหินข้างเคียงมีค่าน้อยที่สุด ผลจากการจำลองทางคอมพิวเตอร์ระบุว่าการกักเก็บกากนิวเคลียร์ในเหมืองเกลือควรใช้แนวคิดแบบ

เสาค้ำยันยาว (Long-wall pillar concept) อุโมงค์กักเก็บควรอยู่ที่ความลึกประมาณ 500 เมตร โดยมีความกว้างของแต่ละห้องกักเก็บเท่ากับ 4 เมตร สูง 4 เมตร และยาว 50 เมตร ห้องควรงั่นด้วยเสาค้ำยันยาวที่มีความกว้าง 16 เมตร เสาค้ำยันหลักที่แบ่งระหว่างทางเข้า-ออกถึงแนวอุโมงค์กักเก็บควรมีความกว้าง 400 เมตร การออกแบบลักษณะนี้ทำให้การหดตัวของอุโมงค์ก่อนที่จะทำการถมกลับมีค่าประมาณ 6 เซนติเมตร (น้อยที่สุด) และการทรุดตัวของผิวดินประมาณ 2 เซนติเมตร ในระยะเวลา 500 ปีของการกักเก็บ

สาขาวิชาเทคโนโลยีธรณี

ปีการศึกษา 2546

ลายมือชื่อนักศึกษา..... *K. Klaysemit* .....

ลายมือชื่ออาจารย์ที่ปรึกษา..... *K. Sujin* .....

**KITCHA KLAYVIMUT: MECHANICAL PERFORMANCE  
OF UNDERGROUND EXCAVATION IN ROCK SALT  
FORMATION FOR NUCLEAR WASTE REPOSITORY IN  
NORTHEASTERN THAILAND THESIS ADVISOR: ASSOC.  
PROF. KITTITEP FUENKAJORN, Ph.D., P.E. 191 pp.  
ISBN 974-533-313-1**


ROCK SALT/DISPOSAL/NUCLEAR WASTE/CREEP/VISCO-PLASTICITY/  
SOLUBILITY/LOW-LEVEL WASTE/FINITE ELEMENT/HYDROLOGY

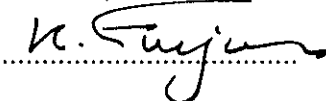
Series of mechanical laboratory testing and numerical modeling have been carried out to assess the geomechanical performance of rock salt formation in the northeast of Thailand for the nuclear waste repository. Results from the existing boreholes and geophysical data have suggested that the stratigraphic sequences in the Maha Sarakham Salt Formation of three areas pose geological suitability for the underground repository. The uniaxial and triaxial creep tests have been performed on the salt core specimens under isothermal conditions. The results are used in the calibration of the stiffness, strength, instantaneous responses and time-dependent behavior of the salt. Finite element analyses use the laboratory-calibrated properties to assist in the design of the repository dimensions and layout under a variety of loading and boundary conditions. The numerical model employing the visco-elastic and visco-plastic constitutive equations predicts the time-dependent stresses and

deformation around the salt openings, as well as the movement of the overlying formations. The analysis assumes the low temperature condition (low-level nuclear wastes). The actual stratigraphy of the three selected sites is used in the modeling. The key design requirements are 1) the mechanical stability during the emplacement period of 50 years, 2) the containment integrity for the repository during the isolation period of 500 years, and 3) minimization of the movement of the surrounding rock formations. The numerical results indicate that the repository horizon should invoke the long-wall pillar concept and should be located at about 500 meters depth. The repository rooms are 4 m wide, 4 m high and 50 m long, separated by 16 m wide pillar. The minimum width for the barrier and protective pillars is 400 meters. Under these design parameters, the predicted room convergence is about 6 cm before backfill installation, and the surface subsidence is about 2 cm through the next 500 years.

School of Geotechnology

Academic Year 2003

Student's Signature ..... 

Advisor's Signature ..... 

## **ACKNOWLEDGEMENTS**

The author wishes to acknowledge the support from the Thailand Research Fund (TRF) and the Office of Atomic Energy for Peace (OAEP) who have provided funding for this research. Asia Pacific Potash Corporation, Ltd. (APPC) has provided the salt cores for testing.

Assoc. Prof. Dr. Kittitep Fuenkajorn is the thesis advisor, Asst. Prof. Thara Lekuthai and Dr. Chongpan Chonglakmani are the thesis committee.

Kitcha Klayvimut



## TABLE OF CONTENTS

	<b>PAGE</b>
ABSTRACT (THAI) .....	I
ABSTRACT (ENGLISH).....	III
ACKNOWLEDGEMENTS .....	V
TABLE OF CONTENTS.....	VI
LIST OF TABLES .....	XI
LIST OF FIGURES .....	XIII
LIST OF SYMBOLS AND ABBREVIATIONS .....	XXX
<b>CHAPTER</b>	
<b>I INTRODUCTION .....</b>	<b>1</b>
1.1 Objectives .....	1
1.2 Problem and Rationale.....	1
1.3 Scope and Limitations of the Study .....	2
1.4 Research Procedure.....	4
1.4.1 Literature Review .....	4
1.4.2 Sample Collection and Preparation .....	6
1.4.3 Experimental Work .....	6
1.4.4 Construction of Finite Element Models .....	6
1.4.5 Computations.....	7

## TABLE OF CONTENTS (Continued)

	<b>PAGE</b>
1.4.6 Data Analysis .....	7
1.4.7 Design of Underground Layout.....	8
1.5 Expected Results.....	8
1.6 Thesis Contents.....	8
<b>II LITERATURE REVIEW .....</b>	<b>10</b>
2.1 Objectives .....	10
2.2 Hazardous Waste Disposal in Rock Salt Formations .....	10
2.3 Mechanical Properties of Rock Salt.....	13
2.4 Experimental Research on Salt.....	20
2.5 Mechanical Constitutive Laws of Rock Salt.....	28
2.6 Computer Models.....	30
2.7 Constitutive Law used in this Study .....	34
2.8 Dry Salt Mining .....	38
2.9 Salt Bearing Formation in Khorat Plateau .....	42
2.10 Research on Nuclear Waste Repository in Thailand .....	48
<b>III EXPERIMENTAL WORK .....</b>	<b>50</b>
3.1 Objectives .....	50
3.2 Sample Collection and Preparation.....	50
3.3 Uniaxial Creep Tests.....	53
3.3.1 Test Methods .....	56

## TABLE OF CONTENTS (Continued)

	<b>PAGE</b>
3.3.2 Test Results .....	56
3.3.3 Discussions .....	59
3.4 Triaxial Creep Tests .....	59
3.4.1 Test Methods .....	59
3.4.2 Test Results .....	60
3.4.3 Discussions .....	63
<b>IV CALIBRATION OF ROCK SALT PROPERTIES .....</b>	<b>64</b>
4.1 Objectives .....	64
4.2 Constitutive Law used in this Study .....	64
4.3 Calibration and Calculation of Salt Property Parameters .....	65
4.3.1 Determination of Plastoviscosity from Uniaxial Creep Test .....	65
4.3.2 Determination of Plastoviscosity from Triaxial Creep Test .....	68
4.4 Discussions .....	74
<b>V COMPUTER MODELING FOR DRY SALT MINE .....</b>	<b>76</b>
5.1 Objectives .....	76
5.2 Rock Salt Formations used in this Study .....	76
5.3 Property Parameters used in Computer Modeling .....	83
5.4 Underground Repository .....	83

## TABLE OF CONTENTS (Continued)

	<b>PAGE</b>
5.5 Finite Element Mesh for Repository Room .....	86
5.5.1 Study on the Effect of Opening Widths .....	86
5.5.2 Study on the Effect of Pillar Widths .....	89
5.5.3 Study on the Effect of Room Depths.....	99
5.6 Modeling Results .....	105
5.6.1 Results of Study on the Effect of Room Widths .....	105
5.6.2 Results of Study on the Effect of Pillar Widths .....	107
5.6.3 Results of Study on the Effect of Room Depths .....	108
5.7 Design of Underground Layout .....	110
5.8 Discussions .....	114
<b>VI DISCUSSIONS, CONCLUSIONS AND</b>	
<b>RECOMMENDATIONS .....</b>	<b>116</b>
6.1 Discussions .....	116
6.1.1 Sufficiency and Suitability of Test Results .....	116
6.1.2 Experimental Methods .....	117
6.1.3 Suitability of Constitutive Law .....	117
6.1.4 Advantages and Disadvantages of Proposed Concept ...	118
6.2 Conclusions.....	118
6.3 Recommendations for Future Research Study.....	121
<b>REFERENCES.....</b>	<b>122</b>

## TABLE OF CONTENTS (Continued)

	<b>PAGE</b>
<b>APPENDICES</b>	
APPENDIX A STRATIGRAPHIC COLUMN OF BOREHOLES USED IN THE MODELING.....	144
APPENDIX B RESULTS FROM THE COMPUTER MODELING TO STUDY THE EFFECT OF ROOM WIDTH.....	148
APPENDIX C RESULTS FROM THE COMPUTER MODELING TO STUDY THE EFFECT OF PILLAR WIDTH...	156
APPENDIX D RESULTS FROM THE COMPUTER MODELING TO STUDY THE EFFECT OF ROOM DEPTH.....	175
APPENDIX E RESULTS FROM THE COMPUTER MODELING OF THE MAIN ENTRY .....	185
<b>BIOGRAPHY .....</b>	<b>191</b>

## LIST OF TABLES

TABLE	PAGE
1.1 Relative assessment of properties of potential rocks used for the deposition of radioactive waste. Numbers indicated represent rating; 3 means a positive, 2 an intermediate, and 1 a negative property .....	3
2.1 Locations and dimensions of openings repository in rock salt.....	14
2.2 The results of uniaxial and triaxial compressive strength tests and Brazilian tensile strength tests on rock salt from ten different locations in the United States .....	22
2.3 Some computer programs used for describing the rock salt behavior .....	32
3.1 Summary of the uniaxial creep test results .....	58
3.2 Summary of the triaxial creep test results on rock salt .....	62
4.1 Properties used in computer modeling.....	66
4.2 Summary of the property parameters of the salt specimens obtained from the computer modeling for the uniaxial creep tests .....	70
4.3 Summary of the property parameters of the salt specimens obtained from the computer modeling for the triaxial creep tests.....	73
4.4 Comparison of the range of parameters and the selected values .....	75
5.1 Selected areas in Sakon Nakhon and Khorat basins used in this research.....	82
5.2 Material properties used in computer modeling .....	84

## LIST OF TABLES (Continued)

TABLE	PAGE
5.3 Shape and size of salt openings used in the modeling.....	103
5.4 Number of nodes and elements in finite element models.....	104
6.1 Comparison the advantages and disadvantages of disposal concepts between dry salt mining and solution mining.....	119

## LIST OF FIGURES

FIGURE	PAGE
1.1 Study program for the mechanical performance of underground excavations in rock salt formation for nuclear waste repository in northeastern Thailand.....	5
2.1 The typical deformation as a function of time of creep materials.....	17
2.2 Rheological components of the GEO program.....	37
2.3 Layout of square pillars mining.....	39
2.4 Layout of long-wall mining.....	41
2.5 A simplified geological map of the Khorat plateau.....	43
2.6 Stratigraphy of the Khorat Basin in the Northeast of Thailand, with a more detail section of the Maha Sarakham Formation (right).....	47
3.1 Locations where the salt cores are obtained from Sakon Nakhon Basin in the northeast of Thailand.....	51
3.2 Some salt core samples donated by Asia Pacific Potash Corporation, Udon Thani Province. They are collected from borehole no. BD99-1 located in Khumpawapi District. These core samples are from the depths ranging from 419 to 422 meters.....	52
3.3 Core sample is cut to obtain the desired length.....	54
3.4 Grinding of core samples for smooth and parallel end surfaces.....	55



## LIST OF FIGURES (Continued)

FIGURE	PAGE
3.5 Uniaxial creep test set-up. The cylindrical salt specimen is loaded vertically using the compression machine, while displacement digital gages measured the axial deformation on opposite sides of the specimen .....	57
3.6 Results of the uniaxial creep testing for different constant axial stresses ( $\sigma_{\text{axial}}$ ). .....	58
3.7 Triaxial creep test with constant axial load under confining pressure. The cylindrical specimen placed inside Hoek cell is loaded vertically using the compression machine. Digital gages measure the axial deformation .....	61
3.8 Results of the triaxial creep testing. The confining pressures ( $\sigma_3$ ) = 3.4 and 6.9 MPa. The axial stresses ( $\sigma_1$ ) vary from 16.6 MPa to 27.6 MPa .....	62
4.1 Single element mesh used in the calibration of the uniaxial creep test results ...	67
4.2 Comparisons between the simulation and the experimental results for the uniaxial creep test at constant axial stresses of 4.1, 7.1, 9.1, 11.1, and 14.1 MPa .....	69
4.3 Single element mesh used in calibration of the triaxial creep test results .....	71
4.4 Comparisons between the simulation and the experimental results for the triaxial creep test results at constant axial stress of 20.7 and 27.6 MPa (for constant confining pressure of 6.9 MPa) and 16.6 and 24.1 MPa (for constant confining pressure of 3.4 MPa) .....	72

## LIST OF FIGURES (Continued)

FIGURE	PAGE
5.1 Location of borehole in Khorat Basin in the northeast of Thailand .....	77
5.2 Location of borehole in Sakon Nakhon Basin in the northeast of Thailand.....	78
5.3 Locations of the three study areas in Khorat and Sakon Nakhon basins in the northeast of Thailand .....	80
5.4 Simplified stratigraphy of salt and associated rocks in Sakon Nakorn and Khorat basins, after reclassification into three geomechanics groups .....	81
5.5 Design parameters for repository rooms.....	85
5.6 Repository rooms in rock salt formation designed to study the effect of room width. Stratigraphy of salt and associated rocks in Ban Kao, Muang District, Udon Thani Province is used in the study. The room widths vary from 4, 6 to 8 meters.....	87
5.7 Close-up finite element mesh for model KM-R4 at Ban Khao, Muang District, Udon Thani Province. Room width is 4 meters.....	88
5.8 Close-up finite element mesh for model KM-R6 at Ban Khao, Muang District, Udon Thani Province. Room width is 6 meters.....	90
5.9 Close-up finite element mesh for model KM-R8 at Ban Khao, Muang District, Udon Thani Province. Room width is 8 meters.....	91

## LIST OF FIGURES (Continued)

FIGURE	PAGE
5.10 Repository rooms in rock salt formation defined to study the effect of pillar width. Stratigraphy of salt and associated rocks in Ban Kao, Muang District, Udon Thani Province is used in the study. The pillar widths vary from 4, 8, 12, 16, 20 to 36 meters.....	92
5.11 Close-up finite element mesh for model KM-P1 at Ban Khao, Muang District, Udon Thani Province. Room and pillar widths are 4 meters.....	93
5.12 Close-up finite element mesh for model KM-P2 at Ban Khao, Muang District, Udon Thani Province. Room and pillar widths are 4 and 8 meters, respectively .....	94
5.13 Close-up finite element mesh for model KM-P3 at Ban Khao, Muang District, Udon Thani Province. Room and pillar widths are 4 and 12 meters, respectively .....	95
5.14 Close-up finite element mesh for model KM-P4 at Ban Khao, Muang District, Udon Thani Province. Room and pillar widths are 4 and 16 meters, respectively .....	96
5.15 Close-up finite element mesh for model KM-P5 at Ban Khao, Muang District, Udon Thani Province. Room and pillar widths are 4 and 20 meters, respectively .....	97

## LIST OF FIGURES (Continued)

FIGURE	PAGE
5.16 Close-up finite element mesh for model KM-P9 at Ban Khao, Muang District, Udon Thani Province. Room and pillar widths are 4 and 36 meters, respectively .....	98
5.17 Comparisons of the disposal rooms located in rock salt formation to study the effect of room depth. Stratigraphy of salt and associated rocks in 1). Ban Kao, Muang District, Udon Thani Province (model KM-P4), 2) Ban Kudjig, Wanon Niwat District, Sakon Nakon Province (model KW-P4) and, 3) Ban Nong Plue, Borabue District, Mahasarakham Province (model NB-P4) are used in the study. The room height and width are 4 meters and 16 meters of pillar width.....	100
5.18 Close-up finite element mesh for model KW-P4 at Ban Kudjig, Wanon Niwat District, Sakon Nakon Province. Room and pillar widths are 4 and 16 meters, respectively .....	101
5.19 Close-up finite element mesh for model KW-P4 at Ban Nong Plue, Borabue District, Mahasarakham Province. Room and pillar widths are 4 and 16 meters, respectively .....	102
5.20 Underground layout for the repository at Ban Kao, Muang District, Udon Thani Province .....	111

## LIST OF FIGURES (Continued)

FIGURE	PAGE
5.21 Finite element mesh for model main entry at Ban Kao, Muang District, Udon Thani Province. The main entry is 5 m wide and 4.5 m high, separated by 20 m wide pillar .....	112
A.1 Stratigraphic column of rock salt and associated rocks at Ban Khao, Muang District, Udon Thani Province (borehole no. K-006) .....	145
A.2 Stratigraphic column of rock salt and associated rocks at Ban Kudjig, Wanon Niwat District, Maha Sarakham Province (borehole no. K-055) .....	146
A.3 Stratigraphic column of rock salt and associated rocks at Ban Nong Plue, Borabue District, Maha Sarakham Province (borehole no. K-089).....	147
B.1 Predicted surface subsidence induced by repository rooms for various room widths. The room depth is 502 meters .....	149
B.2 Predicted vertical closure of repository rooms for various room widths. The room depth is 502 meters .....	149
B.3 Predicted roof deformation of repository rooms for various room widths. The room depth is 502 meters.....	150
B.4 Predicted floor deformation of repository rooms for various room widths. The room depth is 502 meters.....	150
B.5 Contour of octahedral shear stress around repository room (model KM-R4) at 50 years after emplacement (the maximum octahedral shear stress = 450 psi). The room width is 4 meters .....	151

## LIST OF FIGURES (Continued)

FIGURE	PAGE
B.6 Contour of octahedral shear stress around repository room (model KM-R6) at 50 years after emplacement (the maximum octahedral shear stress = 450 psi). The room width is 6 meters .....	151
B.7 Contour of octahedral shear stress around repository room (model KM-R8) at 50 years after emplacement (the maximum octahedral shear stress = 500 psi). The room width is 8 meters .....	152
B.8 Contour of octahedral shear strain around repository room (model KM-R4) at 50 years after emplacement (the maximum octahedral shear strain = $27 \times 10^{-3}\%$ ). The room width is 4 meters .....	152
B.9 Contour of octahedral shear strain around repository room (model KM-R6) at 50 years after emplacement (the maximum octahedral shear strain = $33 \times 10^{-3}\%$ ). The room width is 6 meters .....	153
B.10 Contour of octahedral shear strain around repository room (model KM-R8) at 50 years after emplacement (the maximum octahedral shear strain = $39 \times 10^{-3}\%$ ). The room width is 8 meters .....	153
B.11 Principal stress vectors around repository room (model KM-R4) at 50 years after emplacement (the maximum stress = 2,575 psi). Scale is 10,000 psi/inch. The room width is 4 meters .....	154

## LIST OF FIGURES (Continued)

FIGURE	PAGE
B.12 Principal stress vectors around repository room (model KM-R6) at 50 years after emplacement (the maximum stress = 2,575 psi). Scale is 10,000 psi/inch. The room width is 6 meters .....	154
B.13 Principal stress vectors around repository room (model KM-R8) at 50 years after emplacement (the maximum stress = 2,575 psi). Scale is 10,000 psi/inch. The room width is 8 meters .....	155
B.14 Principal strain vectors around repository room (model KM-R4) at 50 years after emplacement (the maximum strain = 1.81%). Scale is 10% /inch. The room width is 4 meters.....	155
B.15 Principal strain vectors around repository room (model KM-R6) at 50 years after emplacement (the maximum strain = 2.16%). Scale is 10% /inch. The room width is 6 meters.....	156
B.16 Principal strain vectors around repository room (model KM-R8) at 50 years after emplacement (the maximum strain = 2.61%). Scale is 10% /inch. The room width is 8 meters.....	156
C.1 Predicted surface subsidence induced by repository rooms for various pillar widths. The room depth is 502 meters .....	158
C.2 Close-up predicted surface subsidence induced by repository rooms for various pillar widths. The room depth is 502 meters.....	158

## LIST OF FIGURES (Continued)

FIGURE	PAGE
C.3 Predicted vertical closure of repository rooms for various pillar widths. The room depth is 502 meters.....	159
C.4 Closure-up predicted vertical closure of repository rooms for various pillar widths. The room depth is 502 meters.....	159
C.5 Predicted roof deformation of repository rooms for various pillar widths. The room depth is 502 meters.....	160
C.6 Closure-up predicted roof deformation of repository rooms for various pillar widths. The room depth is 502 meters.....	160
C.7 Predicted floor deformation of repository rooms for various pillar widths. The room depth is 502 meters.....	161
C.8 Closure-up predicted floor deformation of repository rooms for various pillar widths. The room depth is 502 meters.....	161
C.9 Predicted pillar yielding of repository rooms for various pillar widths. The room depth is 502 meters.....	162
C.10 Closure-up predicted pillar yielding of repository rooms for various pillar widths. The room depth is 502 meters.....	162
C.11 Contour of octahedral shear stress around repository room (model KM-P1) at 50 years after emplacement (the maximum octahedral shear stress = 500 psi). The room is 4 m wide and 4 m high, separated by 4 m wide pillar.....	163



## LIST OF FIGURES (Continued)

FIGURE	PAGE
C.12 Contour of octahedral shear stress around repository room (model KM-P2) at 50 years after emplacement (the maximum octahedral shear stress = 500 psi). The room is 4 m wide and 4 m high, separated by 8 m wide pillar .....	163
C.13 Contour of octahedral shear stress around repository room (model KM-P3) at 50 years after emplacement (the maximum octahedral shear stress = 500 psi). The room is 4 m wide and 4 m high, separated by 12 m wide pillar .....	164
C.14 Contour of octahedral shear stress around repository room (model KM-P4) at 50 years after emplacement (the maximum octahedral shear stress = 500 psi). The room is 4 m wide and 4 m high, separated by 16 m wide pillar .....	164
C.15 Contour of octahedral shear stress around repository room (model KM-P5) at 50 years after emplacement (the maximum octahedral shear stress = 500 psi). The room is 4 m wide and 4 m high, separated by 20 m wide pillar .....	165
C.16 Contour of octahedral shear stress around repository room (model KM-P9) at 50 years after emplacement (the maximum octahedral shear stress = 500 psi). The room is 4 m wide and 4 m high, separated by 36 m wide pillar .....	165
C.17 Contour of octahedral shear strain around repository room (model KM-P1) at 50 years after emplacement (the maximum octahedral shear strain = $55 \times 10^{-2}$ %). The room is 4 m wide and 4 m high, separated by 4 m wide pillar .....	166

## LIST OF FIGURES (Continued)

FIGURE	PAGE
C.18 Contour of octahedral shear strain around repository room (model KM-P2) at 50 years after emplacement (the maximum octahedral shear strain = $13 \times 10^{-2}$ %). The room is 4 m wide and 4 m high, separated by 8 m wide pillar.....	166
C.19 Contour of octahedral shear strain around repository room (model KM-P3) at 50 years after emplacement (the maximum octahedral shear strain = $42 \times 10^{-3}$ %). The room is 4 m wide and 4 m high, separated by 12 m wide pillar.....	167
C.20 Contour of octahedral shear strain around repository room (model KM-P4) at 50 years after emplacement (the maximum octahedral shear strain = $24 \times 10^{-3}$ %). The room is 4 m wide and 4 m high, separated by 16 m wide pillar.....	167
C.21 Contour of octahedral shear strain around repository room (model KM-P5) at 50 years after emplacement (the maximum octahedral shear strain = $20 \times 10^{-3}$ %). The room is 4 m wide and 4 m high, separated by 20 m wide pillar.....	168
C.22 Contour of octahedral shear strain around repository room (model KM-P9) at 50 years after emplacement (the maximum octahedral shear strain = $18 \times 10^{-3}$ %). The room is 4 m wide and 4 m high, separated by 36 m wide pillar.....	168
C.23 Principal stress vectors around repository room (model KM-P1) at 50 years after emplacement (the maximum stress = 2,603 psi). Scale is 20,000 psi/inch. The room is 4 m wide and 4 m high, separated by 4 m wide pillar.....	169

## LIST OF FIGURES (Continued)

FIGURE	PAGE
C.24 Principal stress vectors around repository room (model KM-P2) at 50 years after emplacement (the maximum stress = 2,579 psi). Scale is 20,000 psi/inch. The room is 4 m wide and 4 m high, separated by 8 m wide pillar .....	169
C.25 Principal stress vectors around repository room (model KM-P3) at 50 years after emplacement (the maximum stress = 2,594 psi). Scale is 20,000 psi/inch. The room is 4 m wide and 4 m high, separated by 12 m wide pillar .....	170
C.26 Principal stress vectors around repository room (model KM-P4) at 50 years after emplacement (the maximum stress = 2,594 psi). Scale is 20,000 psi/inch. The room is 4 m wide and 4 m high, separated by 16 m wide pillar .....	170
C.27 Principal stress vectors around repository room (model KM-P5) at 50 years after emplacement (the maximum stress = 2,583 psi). Scale is 20,000 psi/inch. The room is 4 m wide and 4 m high, separated by 20 m wide pillar .....	171
C.28 Principal stress vectors around repository room (model KM-P9) at 50 years after emplacement (the maximum stress = 2,583 psi). Scale is 20,000 psi/inch. The room is 4 m wide and 4 m high, separated by 36 m wide pillar .....	171
C.29 Principal strain vectors around repository room (model KM-P1) at 50 years after emplacement (the maximum strain = 34.32%). Scale is 50% /inch. The room is 4 m wide and 4 m high, separated by 4 m wide pillar .....	172

## LIST OF FIGURES (Continued)

FIGURE	PAGE
C.30 Principal strain vectors around repository room (model KM-P2) at 50 years after emplacement (the maximum strain = 8.42%). Scale is 20% /inch. The room is 4 m wide and 4 m high, separated by 8 m wide pillar .....	172
C.31 Principal strain vectors around repository room (model KM-P3) at 50 years after emplacement (the maximum strain = 2.77%). Scale is 20% /inch. The room is 4 m wide and 4 m high, separated by 12 m wide pillar .....	173
C.32 Principal strain vectors around repository room (model KM-P4) at 50 years after emplacement (the maximum strain = 1.57%). Scale is 20% /inch. The room is 4 m wide and 4 m high, separated by 16 m wide pillar .....	173
C.33 Principal strain vectors around repository room (model KM-P5) at 50 years after emplacement (the maximum strain = 1.42%). Scale is 20% /inch. The room is 4 m wide and 4 m high, separated by 20 m wide pillar .....	174
C.34 Principal strain vectors around repository room (model KM-P9) at 50 years after emplacement (the maximum strain = 1.23%). Scale is 20% /inch. The room is 4 m wide and 4 m high, separated by 36 m wide pillar .....	174
D.1 Predicted surface subsidence induced by repository rooms for various depths. The room depths vary from 502, 603 to 817 meters .....	176
D.2 Predicted vertical closure of repository rooms for various depths. The room depths vary from 502, 603 to 817 meters .....	176

## LIST OF FIGURES (Continued)

FIGURE	PAGE
D.3 Predicted roof deformation of repository rooms for various depths. The room depths vary from 502, 603 to 817 meters .....	177
D.4 Predicted floor deformation of repository rooms for various depths. The room depths vary from 502, 603 to 817 meters .....	177
D.5 Predicted pillar yielding of repository rooms for various depths. The room depths vary from 502, 603 to 817 meters .....	178
D.6 Contour of octahedral shear stress around repository room (model KM-P4) at 50 years after emplacement (the maximum octahedral shear stress = 500 psi). The room depth is 502 meters.....	178
D.7 Contour of octahedral shear stress around repository room (model KW-P4) at 50 years after emplacement (the maximum octahedral shear stress = 500 psi). The room depth is 603 meters.....	179
D.8 Contour of octahedral shear stress around repository room (model NB-P4) at 50 years after emplacement (the maximum octahedral shear stress = 500 psi). The room depth is 817 meters.....	179
D.9 Contour of octahedral shear strain around repository room (model KM-P4) at 50 years after emplacement (the maximum octahedral shear strain = $24 \times 10^{-3}$ %). The room depth is 502 meters.....	180

## LIST OF FIGURES (Continued)

FIGURE	PAGE
D.10 Contour of octahedral shear strain around repository room (model KW-P4) at 50 years after emplacement (the maximum octahedral shear strain = $64 \times 10^{-3}$ %). The room depth is 603 meters.....	180
D.11 Contour of octahedral shear strain around repository room (model NB-P4) at 50 years after emplacement (the maximum octahedral shear strain = $24 \times 10^{-2}$ %). The room depth is 817 meters.....	181
D.12 Principal stress vectors around repository room (model KM-P4) at 50 years after emplacement (the maximum stress = 2,594 psi). Scale is 20,000 psi/inch. The room depth is 502 meters.....	181
D.13 Principal stress vectors around repository room (model KW-P4) at 50 years after emplacement (the maximum stress = 3,360 psi). Scale is 20,000 psi/inch. The room depth is 603 meters.....	182
D.14 Principal stress vectors around repository room (model NB-P4) at 50 years after emplacement (the maximum stress = 4,289 psi). Scale is 20,000 psi/inch. The room depth is 817 meters.....	182
D.15 Principal strain vectors around repository room (model KM-P4) at 50 years after emplacement (the maximum strain = 1.57%). Scale is 20% /inch. The room depth is 502 meters.....	183

## LIST OF FIGURES (Continued)

FIGURE	PAGE
D.16 Principal strain vectors around repository room (model KW-P4) at 50 years after emplacement (the maximum strain = 4.44%). Scale is 20% /inch. The room depth is 603 meters .....	183
D.17 Principal strain vectors around repository room (model NB-P4) at 50 years after emplacement (the maximum strain = 16.18%). Scale is 20% /inch. The room depth is 817 meters .....	184
E.1 Predicted surface subsidence of the main entry at the center line. The room is 5 m wide, 4.5 m high and 502 m deep, separated by 20 m wide pillar.....	186
E.2 Predicted vertical closure of the main entry for room 1 (inner) and room 2 (outer). The room is 5 m wide, 4.5 m high and 502 m deep, separated by 20 m wide pillar .....	186
E.3 Predicted roof deformation of the main entry for room 1 (inner) and room 2 (outer). The room is 5 m wide, 4.5 m high and 502 m deep, separated by 20 m wide pillar .....	187
E.4 Predicted floor deformation of the main entry for room 1 (inner) and room 2 (outer). The room is 5 m wide, 4.5 m high and 502 m deep, separated by 20 m wide pillar .....	187
E.5 Predicted pillar yielding of the main entry for room 1 (inner) and room 2 (outer). The room is 5 m wide, 4.5 m high and 502 m deep, separated by 20 m wide pillar .....	188

## LIST OF FIGURES (Continued)

FIGURE	PAGE
E.6 Contour of octahedral shear stress around main entries at 50 years (the maximum octahedral shear stress = 500 psi). The room is 5 m wide, 4.5 m high and 502 m deep, separated by 20 m wide pillar .....	188
E.7 Contour of octahedral shear strain around main entries at 50 years (the maximum octahedral shear strain = $14 \times 10^{-3}\%$ ). The room is 5 m wide, 4.5 m high and 502 m deep, separated by 20 m wide pillar .....	189
E.8 Principal stress vectors around main entries at 50 years (the maximum stress = 2,572 psi). Scale is 15,000 psi/inch. The room is 5 m wide, 4.5 m high and 502 m deep, separated by 20 m wide pillar.....	189
E.9 Principal strain vectors around main entries at 50 years (the maximum strain = 1.0 %). Scale is 10 % /inch. The room is 5 m wide, 4.5 m high and 502 m deep, separated by 20 m wide pillar.....	190



## LIST OF SYMBOLS AND ABBREVIATIONS

$A$	=	initial cross-section area
$C$	=	deterioration coefficient
$c$	=	cohesion
$D_s$	=	diameter of specimen
$D_m$	=	new diameter of specimen
$D_{ro}$	=	original diameter of specimen
$D_2$	=	hydrostatic elastoviscosity
$E_1$	=	elastic modulus
$f_D$	=	deteriorating function
$m$	=	Lode parameter
$G_1$	=	shear modulus
$G_2$	=	retarded shear modulus
$G_{21}$	=	retarded shear moduli for short-term viscoelastic strain
$G_{22}$	=	retarded shear modulus for medium-term viscoelastic strain
$G_{23}$	=	retarded shear modulus for long-term viscoelastic strain
$K_1$	=	ultimate bulk modulus
$K_2$	=	retarded bulk modulus
$K_O$	=	octahedral shear strength
$K^A$	=	unconfined octahedral shear strength
$K^B$	=	ultimate octahedral shear strength

## LIST OF SYMBOLS AND ABBREVIATIONS (Continued)

$K^R$	=	residual strength
$\Delta K_O$	=	variance portion of the strength
$\Delta l$	=	axial deformation
$l_o$	=	original specimen length
$L$	=	thickness of specimen
$P$	=	plastic transition pressure
$P_{bf}$	=	failure load of Brazilian tensile test
$P_{uf}$	=	failure load of uniaxial compressive test
$VE$	=	viscoelastic behavior
$V_{oil}$	=	hydraulic oil bleeding from Hoek cell
$V_{steel}$	=	volume of the moving steel plate
$V_m$	=	new rock volume
$V_{ro}$	=	original rock volume
$L_m$	=	new length of specimen
$L_{ro}$	=	original length of specimen
$\alpha$	=	yield surface coefficient
$\epsilon_1$	=	maximum principal strain
$\epsilon_2$	=	intermediate principal strain
$\epsilon_3$	=	minimum principal strain
$\epsilon_{VD}$	=	non-recoverable volumetric dilation
$\epsilon_{axial}$	=	axial strain

## LIST OF SYMBOLS AND ABBREVIATIONS (Continued)

$\epsilon_{\text{vol}}$	=	volumetric strain
$\epsilon_{\text{lat}}$	=	lateral strain
$\epsilon_{\text{m}}$	=	mean strain
$\epsilon_{ij}$	=	total strain tensor
$\epsilon_{ij}^e$	=	elastic strain tensor
$\epsilon_{ij}^p$	=	plastic strain tensor
$\epsilon_f$	=	failure strain
$\eta_2$	=	elastoviscosity
$\eta_4$	=	plastoviscosity
$\eta_{21}$	=	elastoviscosity coefficient for short-term
$\eta_{22}$	=	elastoviscosity coefficient for medium-term
$\eta_{23}$	=	elastoviscosity coefficient for long-term
$\gamma_{\text{total}}^{\text{VE}}$	=	total viscoelastic creep strain rate
$\gamma_{21}^{\text{VE}}$	=	short-term viscoelastic strain rate
$\gamma_{22}^{\text{VE}}$	=	medium-term viscoelastic strain rate
$\gamma_{23}^{\text{VE}}$	=	long-term viscoelastic strain rate
$\gamma_c$	=	critical strain of elastic limit
$\gamma_o$	=	induced octahedral shear strain
$\Delta\gamma_o$	=	excess octahedral shear strain

## LIST OF SYMBOLS AND ABBREVIATIONS (Continued)

$\gamma_{\text{oct}}$	=	octahedral shear strain
$\gamma_{\text{oct}}^i$	=	viscoelastic octahedral shear strain
$\dot{\gamma}_{\text{oct}}^s$	=	octahedral shear strain rate in steady state
$\lambda$	=	Lame constant
$\phi$	=	angle of internal friction
$\sigma$	=	normal stress
$\sigma_1$	=	maximum principal stress
$\sigma_2$	=	intermediate principal stress
$\sigma_3$	=	minimum principal stress
$\sigma_1 - \sigma_3$	=	differential stress
$\sigma_B$	=	Brazilian tensile strength
$\sigma_c$	=	uniaxial compressive strength
$\sigma_m$	=	mean stress
$\tau$	=	shear stress
$\tau_{\text{oct}}$	=	octahedral shear stress
$\tau_{\text{oct}}^1$	=	octahedral shear stress in the first stage
$\tau_{\text{oct}}^2$	=	octahedral shear stress in the second stage
$\nu$	=	Poisson's ratio

# **CHAPTER I**

## **INTRODUCTION**

### **1.1 Objectives**

The objective of this research is to study the mechanical behavior of rock salt in the Maha Sarakham Formation for nuclear waste disposal. The research effort includes laboratory testing on rock salt samples and computer modeling on the designed excavations. The parameters used in the computer models are determined from the laboratory testing results. The suitability of the repository will be evaluated in terms of the mechanical stability and hydrological integrity of the host salt for the following 500 years after waste emplacement.

### **1.2 Problem and Rationale**

The increasing amounts of radioactive waste from hospitals, chemical industries and agriculture in Thailand calls for a permanent and long-term solution, or requires an isolation period as long as 500 years or at least until the radionuclide level is acceptably low (depending upon the half-life of the elements). More important in the future, Thailand as a developing country may have to rely on nuclear power plants to serve the energy consumption of her citizens, as the fossil fuel (oil and gas) is rapidly depleting. One of the problems resulted from the nuclear energy is the radioactive wastes obtained from the cooling ponds, fuel rods, plant facilities, etc. (Viboonsawat, 1998). The Office of Atomic Energy for Peace (OAEP) has taken the

responsibility on collecting liquid nuclear waste about 20,000 liters with an increasing amount of 30 m<sup>3</sup> per year. A common solution to this problem, that has been practiced internationally, is to dispose such wastes into deep geological media, for example rock salt bearing formations. It is necessary for Thailand that a preliminary study is carried out to assess the possibility of using the rock salt formation as a host rock for the waste repository.

During the past 30 years extensive research has been conducted on the performance of rock salt under repository environment. Such efforts have been made in the United States, Canada and Germany with the main objective to develop their national repository site. Rock salt is one of the prime candidates for the repository, due to its low permeability, healing capacity and availability (Wallner, 1984; Matalucci and Hunter, 1984; Berest et al., 1988; Habib and Berest, 1993; Broek and Heilbron, 1997). The assessment of the main properties of several potential host rocks (e.g. granite, basalt, shale and rock salt) are composed and rated in Table 1.1. The comparison clearly shows the advantage of rock salt as the prime geological media for nuclear waste deposition (Herrmann, 1998).

### **1.3 Scope and Limitations of the Study**

This research involves laboratory testing and computer modeling to predict the behavior of rock salt around the openings for radioactive or nuclear waste disposal. Since there is neither a plan for nuclear waste disposal nor a specific site, the study will not include in-situ testing or measurements and will not focus on any site selection. Rock salt samples from the Maha Sarakham Formation (Sakon Nakhon Basin) will be used in the laboratory experiments. The current radioactive waste in

**Table 1.1** Relative assessment of properties of potential rocks used for the deposition of radioactive waste (Herrmann, 1998). Numbers indicated represent rating; 3 means a positive, 2 an intermediate, and 1 a negative property.

<b>Property</b>	<b>Granite</b>	<b>Basalt</b>	<b>Shale</b>	<b>Rock salt</b>
Natural water content of the rock	3	3	2	3
Strength	3	3	2	1
Linear expansion coefficient	3	3	3	2
Heat capacity	2	2	2	3
Heat conductivity	2	1	2	3
Solubility	3	3	3	1
Permeability	3	3	3	3
Porosity	3	3	1	3
Tendency of fracturing	1	1	1	3
Tendency of getting open joints	1	1	1	3
Tendency of plastic deformation	1	1	1	3

Thailand is classified as low-level waste (becoming harmless after 500 years). In the computer models the horizontal variations of the chemical compositions and mechanical properties have not been taken into consideration since such variations remain unknown. The in-situ stresses are equivalent to the hydrostatic pressure of the rock. All simulations will be carried out up to 500 years and under constant and ambient temperature. Since the long-term behavior is of interest, it is assumed that all openings in the model are simultaneously excavated. The design recommendations obtained for the rock salt formation in northeastern Thailand therefore may not be applicable to rock salt formations from other locations.

## **1.4 Research Procedure**

The research efforts are divided into seven tasks, including literature review, sample collection and preparation, laboratory testing, construction of finite element models, computations, data analysis, and design of the underground layout. Some tasks are performed in parallel. Figure 1.1 shows the path of the main activities performed in this research.

### **1.4.1 Literature Review**

All relevant information and data will be requested from the Department of Mineral Resources (DMR) and the Office of Atomic Energy for Peace (OAEP). These data will include detailed geological information in relation to the rock salt sequences in northeastern Thailand, mechanical, physical, chemical and rheological (if available) properties of the rock salt, in-situ stress states, etc. (Japakset, 1985; Gevantman et al., 1981). Relevant literatures on the mechanical and hydrological behaviour of rock salt and on the geologic repository will be searched and reviewed to



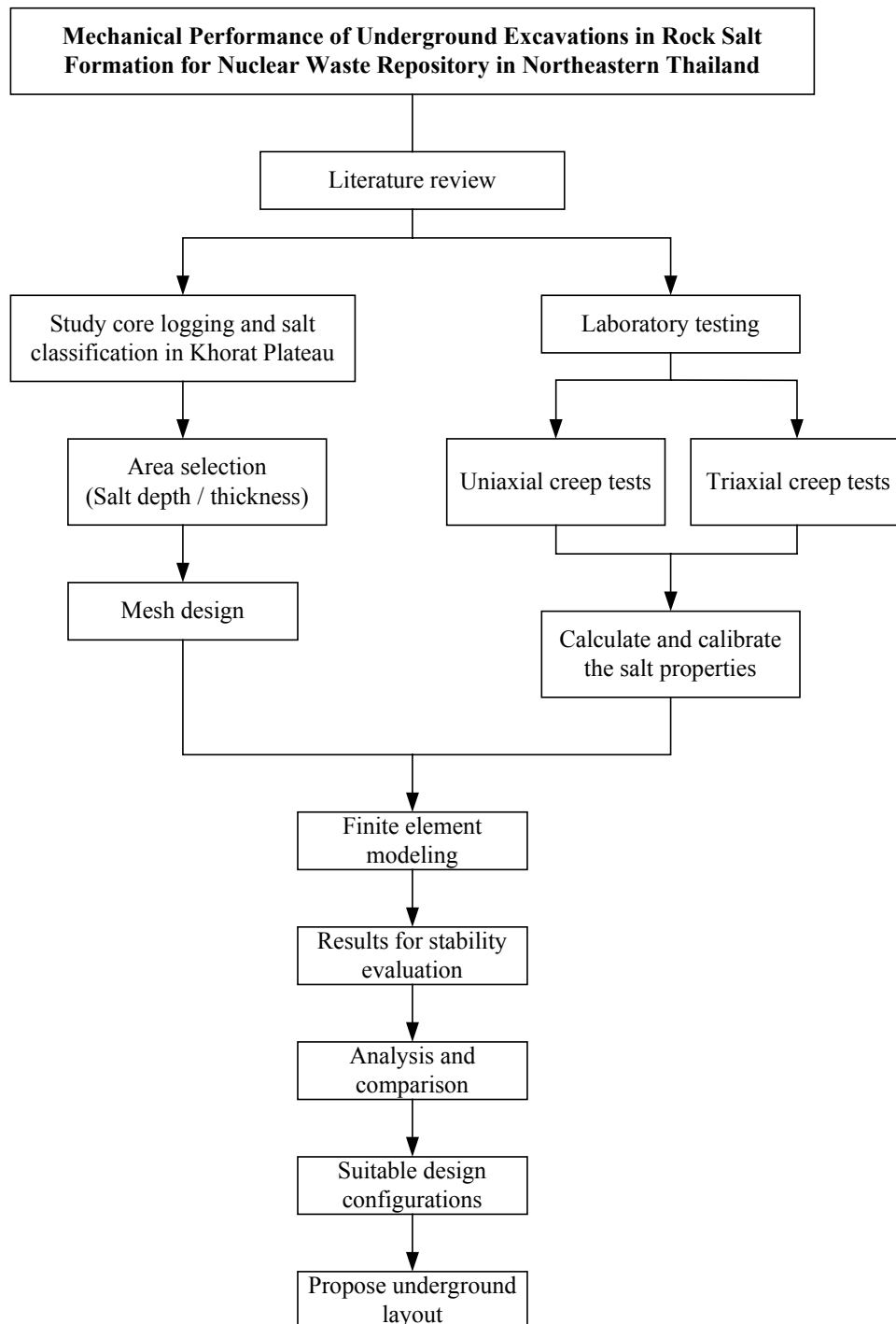


**Figure 1.1** Study program for the mechanical performance of underground excavations in rock salt formation for nuclear waste repository in northeastern Thailand.

understand the state-of-the-art in these fields. Results from the literature study will be summarized in the thesis.

#### **1.4.2 Sample Collection and Preparation**

Rock salt samples used in this research have been donated by Asia Pacific Potash Corporation Limited, Udon Thani Province. The salt cores have a diameter of 6 centimeters. They are drilled from the Middle and Lower Salt members of the Maha Sarakham Formation in Sakon Nakhon Basin. Preparation of these samples will follow, as much as practical, the standard practices of the American Society for Testing and Materials (ASTM D4543-85).

#### **1.4.3 Experimental Work**

The laboratory mechanical testing will be performed on salt specimens prepared from task 1.4.2. The essential laboratory testing includes uniaxial and triaxial creep testing on salt specimens. There are five specimens for each test. The testing period is about one month for each specimen. The constant axial stresses, used in the uniaxial creep testing, are varied from 4 to 14 MPa. The constant axial stresses used in the triaxial creep testing are between 14 and 34 MPa and constant confining pressures are between 3 and 7 MPa. The test results are used to calibrate the rock salt property parameters for the computer simulations.

#### **1.4.4 Construction of Finite Element Models**

Vertical finite element models will be constructed in 2-D to graphically represent the formations of rock salt and associated rocks around the openings in the repository. The dry salt mining concept will be used to develop the disposed openings. The opening shapes will be determined with different room and pillar widths. The salt roof and floor will be varied for different depths selected to

determine the most suitable design. The spacing between the adjacent openings will be varied depend on the pillar width. A minimum of three depths will be simulated to determine the most suitable repository horizon.

#### **1.4.5 Computations**

The non-linear finite element code “GEO” will be used in the computation of the creep stress and strain induced in the rock salt around the openings through 500 years of the isolation. The algorithm of the computer code is designed to compute the stress and displacement in time domain. It consists of eight main modules; elastic, visco-elastic, visco-plastic, strain-softening, strain-hardening, deterioration, dilation and permeability increase. This program can therefore disclose a more realistic rheological behavior of the rock salt, than other conventional computer codes (Serata and Fuenkajorn, 1991, 1992a, 1992b; Stormont and Fuenkajorn, 1994; Fuenkajorn and Serata, 1994). Information and model in tasks 1.4.3 and 1.4.4 will be used to calibrate the property parameters of the constitutive equations in the GEO program. These parameters include the elastic modulus, Poisson’s ratio, shear modulus, bulk modulus, visco-elastic and visco-plastic parameters, deterioration, and dilation.

#### **1.4.6 Data Analysis**

The results will be graphically presented in terms of the principal stresses and strains, displacement of the salt roof, floor and pillar, and the subsidence of overlying formations and ground surface. Comparison of the results will be made to determine the optimum opening geometry and depths. The final result will reveal the most suitable excavation layout and depth for long-term isolation of the nuclear wastes.

#### **1.4.7 Design of Underground Layout**

The underground layout will be designed, including mine depths, configurations, positions, and dimensions of the repository room, accesses (shafts or ramps), adits, and main entry. Accommodation for the amount of wastes collected through the next 50 years (repository life) will be considered in the design.

### **1.5 Expected Results**

The research results will disclose if the salt in the Maha Sarakham Formation has the mechanical potential for the nuclear waste repository. The suitability will be determined in terms of the long-term mechanical stability and hydrological integrity of the salt around the openings. The mechanical and rheological properties of the salt will be revealed. The expected results will be in accordance with the research objectives in task 1.1. The concept of using dry salt mining for geologic disposal in northeastern Thailand will be verified. The magnitude of the surface subsidence as well as the distribution of the stress, strain and permeability of the host rock salt will be predicted up to 500 years after the waste emplacement.

### **1.6 Thesis Contents**

The objectives of this research, the problems and rationale, the research procedure, and the expected results are described in Chapter I. Chapter II presents summary of the literature review on the hazardous waste disposal in rock salt formations, the salt properties, the experimental research on salt, the mechanical constitutive laws, the computer modeling, the dry salt mining technology, and the salt formations in the Khorat Plateau. Chapter III explains the salt sample collection and

preparation, and laboratory testing. Chapter IV describes the constitutive laws and the salt parameter calibrations. Chapter V presents the computer modeling and proposes the conceptual design for the nuclear waste disposal. Chapter VI summarizes the research results, and provides recommendations for future research studies.

## **CHAPTER II**

### **LITERATURE REVIEW**

#### **2.1 Objectives**

Literatures related to the dry salt mining technology for nuclear waste repository created in rock salt formations and salt domes have been reviewed in this research. This research emphasizes the mechanical potential of rock salt formations to be applied in this technology. The related knowledge is categorized into eight groups: 1) hazardous waste disposal in rock salt formation, 2) salt properties, 3) experimental research on salt, 4) mechanical constitutive laws, 5) computer modeling, 6) dry salt mining technology, 7) salt bearing formations in Khorat Plateau, and 8) previous research on waste disposal in Thailand.

#### **2.2 Hazardous Waste Disposal in Rock Salt Formations**

During the past 30 years, extensive research has been conducted on the disposal of hazardous waste in geological media. Several performance aspects within the parameters of geological media under repository environments have been investigated. The researches have been conducted in the United States of America, Germany, Finland, and Canada for the primary objective of developing the national hazardous waste repository sites. Rock salt formations are one of the prime candidates for the host rock, because they have favorable characteristics, such as low

permeability, ability to healing, resisting to high temperature, and low humidity (Bechthold et al., 1999).

Matalucci and Hunter (1984) reported that the US Department of Energy (DOE) is developing the Waste Isolation Pilot Plant (WIPP) Project in southeastern New Mexico as a research and development (R&D) facility to demonstrate the safe disposal of radioactive wastes in bedded (layered) salt. This project is resulted from earlier work on the disposal of nuclear waste in geological media, originated in 1957 when a National Academy of Sciences committee recommended guidelines for permanent deep disposal in bedded salt deposit or other sedimentary basins. In 1960, the Oak Ridge National Laboratories (ORNL) conducted in-situ experimental programs in Lyons, Kansas called Project Salt Vault. Subsequent evaluations of salt basins in the United States by ORNL and the United States Geological Survey (USGS) in 1970 lead to the field investigation of the southeastern New Mexico salt deposits and the conceptual definition of the WIPP Project.

A conceptual plan for in-situ measurements in access shafts and underground openings was developed in the WIPP project. This was soon followed by a preliminary plan and by proposed test room configurations for the underground experimental program. These plans, combined with update technical and institutional information obtained from WIPP and other waste management R&D programs, resulted in a baseline documentation defining an in-situ testing program to address technical issues of waste disposal in bedded salt (Matalucci and Munson, 1988).

Harrington et al. (1984) analyzed the WIPP room geometry at about 650-meter depth under isothermal conditions. The analysis evaluated the stability of the room design over a ten-year period. The presence of stiff anhydrite layers and clay seams,

as determined from field investigations, was implemented. The clay seams were treated as joints in the model with the influence of the joint properties evaluated parametrically. The results indicated that the behavior of the room was governed by the locations and properties of the clay seams and stiff anhydrite layers. Hence, for the design of actual mine rooms which were required to remain open for several years, the determination of the exact local geology and the properties of the clay seams or joints and other interbeds was of prime importance.

Germany disposed short-lived low and intermediate level radioactive wastes from the operation of nuclear power plants and the application of radionuclides in research, medicine, and industry, in the former German Democratic Republic in abandoned salt mine located near the village of Morsleben (now in the State of Sachsen-Anhalt). The salt was excavated to form room and pillar down to a depth of about 500 meters so that mine openings resulted with a maximum length of about 150 meters, a maximum width of 30 meters and a maximum height of about 30 meters. In total, a volume of about  $7.6 \times 10^6 \text{ m}^3$  was excavated and partly backfilled ( $2.1 \times 10^6 \text{ m}^3$ ). Until 1991, radioactive wastes with a total emplacement volume of approximately  $14,500 \text{ m}^3$  and about 6,200 radiation sources were disposed. In total, this represents an activity of  $1.8 \times 10^{14} \text{ Bq}$ . The activity of alpha emitters amounted to  $1.6 \times 10^{11} \text{ Bq}$ , and the activity of beta/gamma emitters, to  $1.8 \times 10^{14} \text{ Bq}$ . The waste was mainly delivered by combined rail-and-road transports using standardized freight containers. About 2,900 of such containers were delivered until 1991.

The Gorleben salt dome has been under scrutiny since 1979 to host a repository at depth between 840 and 1200 m, mainly for high level and/or alpha bearing wastes and spent fuel. Site investigations and planning are at pressure based



on a nuclear capacity of 2500 GWa, leading to a total activity of about  $10^{21}$  Bq and an alpha activity of about  $10^{19}$  Bq. The following work from above ground was carried out between 1979 and 1985 to investigate the geology and hydrogeology of the Gorleben site (Langer and Rothemeyer, 1996).

Heusermann et al. (1998) reported that the German concept for the final disposal of radioactive waste comprised both reprocessing and direct disposal of spent fuel elements used at Asse salt mine in Germany. The disposal involved placing the fuel rods in self-shielding Pollux casks which were emplaced in drifts of a repository in rock salt. These drifts were backfilled with crushed salt. The planned disposal drifts were several hundred meters in length and are designed to contain up to 30 casks. There are two parallel drifts at the 800 meters level in the Asse salt mine, several observation drifts at the 750 meters and 800 meters levels and several access drifts. The two test drifts are each 70 m long, 3.5 m high and 4.5 m wide. The drift axes are 14.5 m apart. Each drift contains three heater casks of 5.5 m length, diameter 1.5 m and mass 65 t.

Table 2.1 summarizes locations and dimensions of nuclear wastes repository in rock salt formation.

### **2.3 Mechanical Properties of Rock Salt**

Researchers from the field of material sciences believe that rock salt behavior shows many similarities with that of various metals and ceramics (Chokski and Langdon, 1991; Munson and Wawersik, 1993). However, because alkali halides are ionic materials, there are some important differences in their behavior. Aubertin et al. (1992, 1993, 1998, 1999) conclude that the rock salt behavior should be brittle-to-

**Table 2.1** Locations and dimensions of openings repository in rock salt.

<b>Locations</b>	<b>Depth</b>	<b>Dimension</b>	<b>References</b>
New Mexico, USA	659 m	10 x 100 x 4 m	Matalucci and Munson (1988)
Asse salt mine, Germany	800 m	4.5 x 70 x 3.5 m	Heusermann et al. (1998)
Gorleben, Germany	840 m	N/A	Langer and Rothemeyer (1996)
Morsleben, Germany	500 m	30 x 150 x 30 m	

ductile materials or elastic-plastic behavior. This also agrees with the finding by Fuenkajorn and Daemen (1988), Fokker and Kenter (1994), and Fokker (1995, 1998).

Jeremic (1994) discusses the mechanical characteristics of the salt. They are divided into three characteristics: the elastic, the elastic-plastic, and the plastic behavior. The elastic behavior of rock salt is assumed to be linearly elastic with brittle failure. The rock salt is observed as linear elastic only for a low magnitude of loading. The range of linear elastic mainly depends on the content of elastic strain and can be used to formulate the modulus of elasticity. Normally, the modulus of elasticity of rock salt is relatively low. The elastic and plastic behavior of rock salt can be investigated from the rock salt specimen. The confined rock salt specimen at the beginning of incremental loading shows linear elastic deformation but with further load increases the plastic behavior is induced, which continues until yield failure. Elastic deformation and plastic deformation are considered as separated modes of deformability in the great majority of cases. The salt material simultaneously exhibits both elastic strain and plastic strain. The difference between elastic behavior and plastic behavior is that elastic deformation is temporary (recoverable) and plastic deformation is permanent (irrecoverable). The degree of permanent deformation depends on the ratio of plastic strain to total strain. The elastic and plastic deformation can also be observed by short-term loading, but at higher load magnitude. The plastic behavior of rock salt does not occur if the applied stress is less than the yield stress. The rock salt is deformed continually if the high stress rate is still applied and is more than the yield stress. Increasing the load to exceed the strain limit of the rock salt beyond its strength causes it to fail. The deformation of

rock salt by the increase of temperature can also result in the transition of brittle-to-ductile behavior.

The time-dependent deformation (or creep) is the process at which the rock can continue deformation without changing stress. The creep strain seldom can be recovery fully when loads are removed, thus it is largely plastic deformation. Creep deformation occurs in three different phases, as shown in Figure 2.1, which relatively represents a model of salt properties undergoing creep deformation due to the sustained constant load. Upon application of a constant force on the rock salt, an instantaneous elastic strain ( $\epsilon_e$ ) is induced. The elastic strain is followed by a primary or transient strain, shown as Region I. Region II, characterized by an almost constant slope in the diagram, corresponds to secondary or steady state creep. Tertiary or accelerating creep leading to rather sudden failure is shown in Region III. Laboratory investigations show that removal of applied load in Region I at point L will cause the strain to fall rapidly to the M level and then asymptotically back to zero at N. The distance LM is equal to the instantaneous strain  $\epsilon_e$ . No permanent strain is induced here. If the removal of stress takes place in the steady-state phase the permanent strain ( $\epsilon_p$ ) will occur. From the stability point of view, salt structure deformations after constant load removal have only academic significance, since the stresses imposed underground due to mining operations are irreversible. The behavior of the salts with time-dependent deformation under constant load is characterized as a visco-elastic and visco-plastic phenomenon. Under these conditions the strain criteria are superior to the strength criteria for design purposes, because failure of most salt pillars occurs during accelerated or tertiary phase of creep, due to the almost constant applied load. The dimensions of a pillar in visco-elastic and visco-plastic rock should be

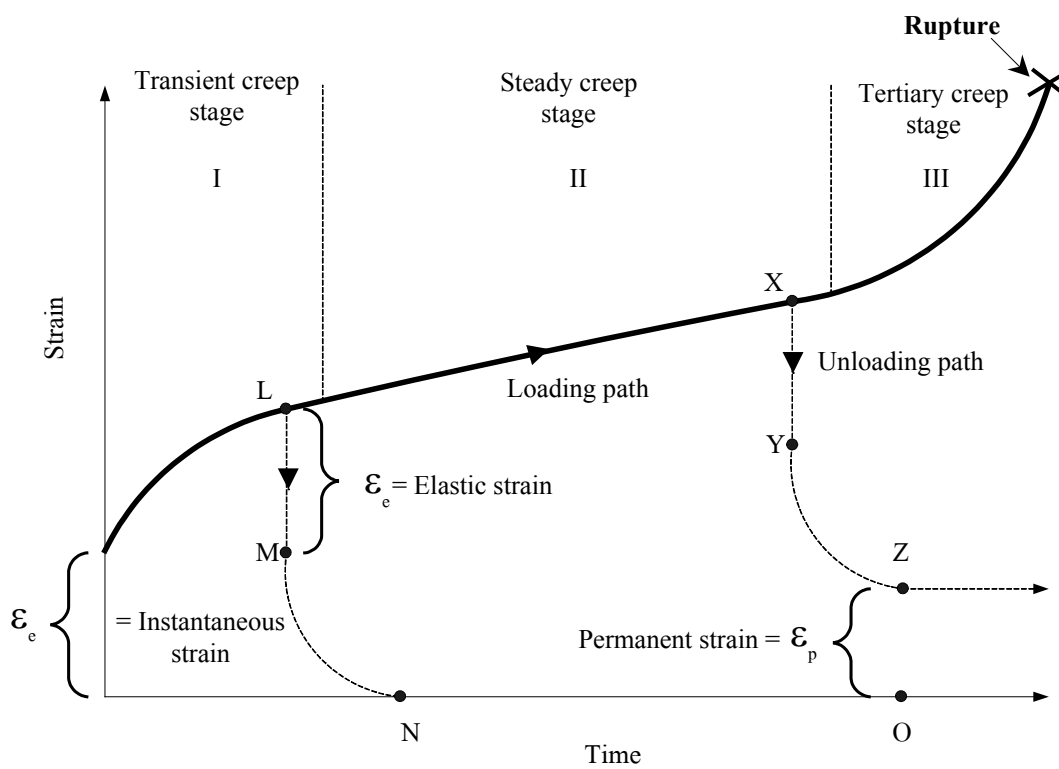


**Figure 2.1** The typical deformation as a function of time of creep materials  
(modified from Jeremic, 1994).

established on the basis of a prediction of its long-term strain, to guard against adequate safety factor accelerating creep (Fuenkajorn and Daemen, 1988; Dusseault and Fordham, 1993; Jeremic, 1994; Knowles et al., 1998).

The mechanical behavior of rock salt is complex and is affected by many factors, such as grain size, bonding between grains, time, temperature, humidity, and inclusions, and more. The effects on rock salt characteristics by these factors are normally shown by the differences in deformation and creep properties.

The effects of grain size on the creep behavior and strength of rock salt in laboratory and field conditions are described by Fokker (1998). The average grain size of salt visually observed from the core and post-failure specimens is 5 mm × 10 mm × 10 mm. It is concluded that the large size of the salt crystals increases the effect of the crystallographic features (i.e. cleavage planes) on the mechanics of deformation and failure of the samples. This also agrees with the finding by Aubertin (1996). The dislocations and plastic flows in single crystals of halite are studied by several researchers (Franssen and Spiers, 1990; Raj and Pharr, 1992; Senseny et al., 1992; Wanten et al., 1996). They conclude that the shear strength and deformation of halite crystals are orientation-dependent. The small size of the sample may not provide good representative test results. This also reflects on the specifications by ASTM (ASTM D2664, D2938 and D3967). The ASTM standard methods specify that to minimize the effect of grain size the sample diameter should be at least ten times the average grain size.

Bonding between grains can affect the creep rate and the strength of salt. Allemandou and Dusseault (1996) observe the post-failure from the Brazilian strength tests and uniaxial compressive strength tests. They report that strength

depends on the boundary between grains. This also agrees with the laboratory results obtained by Fuenkajorn and Daemen (1988) who report that weakness or brittleness of the crystal boundary of salt is observed during sample preparation. It is unlikely that a long intact core can drill through the salt formation.

The time-dependent behavior of salt under differential stress raises the question of the significance of time-related test parameters such as loading rate, testing period, and loading sequence. The effects of stress rate and strain rate on the deformation and strength of salt samples have long been recognized (Farmer and Gilbert, 1984; Dusseault and Fordham, 1993). The loading rate must be maintained constant and measured as precisely as possible during the test. The loading sequence and the duration for which each load is sustained by the salt specimens are important since salt tends to behave as a plastic creep material with low yield stress. This situation is found in the triaxial compressive strength test where the confining pressure is applied to the salt cylinder prior to the axial load. Due to the nonlinear behavior of salt, the analysis of stress induced in a salt specimen is complex and the Boltzmann law of superposition cannot be used.

Temperature or heating affects the creep deformation, because they increases the plastic property of salt and long-term deformation (Broek et al., 1994; Pudewills et al., 1995). Jeremic (1994) postulates that rock salts lose their brittleness after extension tempering at approximately 600 °C and exhibit a critical shear stress up to 1 MPa. Hamami et al. (1996) study the effect of temperature and conclude that the temperature increase, as for the deviatoric stress, results in an increase of the material deformation. Cristescu and Hunsche (1996) study the temperature effect on the strain rate suitable for laboratory testing. They suggest that the appropriate strain rate for

testing at 100 °C and 200 °C is  $10^{-8} \text{ s}^{-1}$  and  $10^{-7} \text{ s}^{-1}$  because the temperature can affect the creep deformation and strength of salt under high temperatures.

Humidity affects salt properties by reducing the strength of rock salt (Hunsche and Schulze, 1996; Cleach et al., 1996). Hydrated reaction between water and salt occurs when salt contacts with air humidity. The temperature effects can catalyze the hydration. They find that when subjected to air humidity, the strength of salt can be decreased by up to 1 MPa (normally, strength of 30 MPa).

Inclusions and impurities in salt have an effect on to the creep deformation and strength of salt. The degree of impurity is varying for different scales of the rock salt. On a small scale, such as for laboratory specimens, the impurities of salt involve ferruginous inclusions and thin clay seams along grain boundaries or bedding planes. The impurities distribute uniformly in the salt may affect the strength of rock salt. This can decrease the creep deformation and strength of rock salt. These phenomena have been reported by Franssen and Spiers (1990), Raj and Pharr (1992) and Senseny et al. (1992), as well.

## **2.4 Experimental Research on Salt**

Rock salt has mechanical behavior that differs from most rocks. Basic mechanical laboratory tests that have been carried out on rock salt include uniaxial compressive strength testing, triaxial strength testing, uniaxial creep testing, multi-steps testing, triaxial creep testing, tensile strength testing, cyclic loading testing and permeability measurement testing. The main objective of these tests is to study the strength and the time-dependent deformations of the rock.



The uniaxial compression tests determine the compressive strength of rock salt under unconfined condition. The salt specimens are subjected to the uniaxial load until failure. The compressive strength can be varied with the applied stress and strain rates. Hansen et al. (1984) performs the uniaxial compressive strength tests on rock salt from ten different locations in the United States. The results indicated that compressive strengths vary from 13.3 to 33.6 MPa (see Table 2.2). Fuenkajorn and Daemen (1988) study the compressive strength of rock salt from Permian basin, New Mexico. The results are 18.44 MPa of compressive strength, 36 degrees of internal friction angle, 3.42 GPa of tangent modulus, and 5.13 GPa of secant modulus. Ratigan and Vogt (1993) summarize the compressive strengths of salt with values ranging from 15 MPa to 30 MPa. Wanten et al. (1996) studies the uniaxial compressive strength under different strain rates. The strain rate ranging from  $10^{-4} \text{ s}^{-1}$  to  $10^{-7} \text{ s}^{-1}$  is applied on the crystal (salt grain) at temperature of 20 °C to 200 °C. The results indicate that the salt samples show work hardening behavior. Microstructure studies revealed high dislocation densities but little or no sub-grain development or cross-slip. Comparison of the results with micro-physical models suggests that obstacle limited dislocation glide is the controlling deformation mechanism. Boontongloan (2000) studies the uniaxial compressive strength with controlled loading rate on salt cores drilled in Sakon Nakhon Basin in Udon Thani Province, Thailand. The uniaxial load is applied within 5 to 10 minutes. The results indicate that the Upper Salt has the uniaxial compressive strength of 18.5 MPa and the Middle Salt has uniaxial compressive strength of 26 MPa. The tangent and secant elastic moduli equal 5.6 GPa and 9.9 GPa. The Lower Salt has uniaxial compressive strength of 25 MPa. The tangent and secant elastic moduli equal 6.4 GPa and 11.4

**Table 2.2** The results of uniaxial and triaxial compressive strength tests and Brazilian tensile strength tests on rock salt from ten different locations in the United States (from Hansen et al., 1984).

Locations	Uniaxial compressive strength test	Brazilian tensile strength test	Triaxial compressive strength test	
	$\sigma_c$ (MPa)	$\sigma_B$ (MPa)	C (MPa)	$\phi$ (degrees)
S. E. New Mexico (1900' level)	16.9	1.26	2.31	59.5
S. E. New Mexico (2700' level)	25.7	1.63	3.24	61.7
Lyons	25.2	1.56	3.14	62.1
Permian	22.1	1.72	3.08	58.8
Paradox	33.6	2.61	4.68	58.9
Jefferson Island	24.0	1.54	3.04	61.6
Week's Island	13.9	1.24	2.08	56.7
Cote Blanche	25.2	1.93	3.49	59.1
Avery Island	23.1	1.17	2.60	64.6
Richton	13.3	1.32	2.10	55.0
Vacherie	15.3	1.12	2.07	59.7

**Notes:**  $\sigma_c$  = Uniaxial compressive strength    C = Cohesion compressive strength

$\sigma_B$  = Brazilian tensile strength     $\phi$  = Internal friction angle

GPa. The Poisson's ratio varies between 0.35 and 0.42. Wetchasat (2002) performs the uniaxial compressive strength with controlled loading rates. The loading rate ranging from 0.01 to 1.0 MPa/s are applied on salt specimens from Sakon Nakhon basin in Udon Thani Province, Thailand. The results indicated that the average compressive strength from thirteen specimens is 27.4 MPa.

The triaxial testing is conducted to determine the compressive strengths of rock salt under confined conditions. The axial load and the confining pressure are increased simultaneously, until the predetermined test level for the confining pressure is reached. Subsequently, the confining pressure shall be maintained to within 2 % of the prescribed value. The axial load on the specimen shall then be increased continuously at a constant stress rate such that failure will occur within 5 to 10 minutes of loading. The maximum axial load and the corresponding confining pressure on the specimen are recorded. Hansen et al. (1984) performs the triaxial compressive strength tests on rock salt from ten different locations in the United States. The results indicated that cohesion compressive strengths (C) are varying from 2.07 to 4.68 MPa and 55 to 64.6 degrees of internal friction angle ( $\phi$ ), as shown in Table 2.2. Fuenkajorn and Daemen (1988) perform strain rate-controlled triaxial tests on Salado salt samples at confining pressures ranging from 1.54 MPa to 8.18 MPa and constant strain rates ranging from  $2.25 \times 10^{-5}$  to  $2.08 \times 10^{-4} \text{ s}^{-1}$ . The salt tends to behave as brittle material (strain-softening) when it is subjected to high strain rates and as ductile material (strain-hardening) for lower strain rates. The sample volume tends to decrease at the beginning of loading and it starts increasing shortly before the peak stress has been reached. Therol and Ghoreychi (1996) study the triaxial compressive strength tests on rock salt with measurements of the volumetric

strains. They report that the initiation of damage is supposed to be linked to the change of curvature of volumetric strain from compressibility to dilatancy due to microcracking. Wetchasat (2002) conducts the triaxial compressive strength tests on rock salt from salt cores in Sakon Nakhon Basin in Udon Thani Province, Thailand. The results are 8 MPa of cohesion compressive strength and 49 degrees of internal friction angle. The linear equation of Coulomb's criterion is given by  $\tau = 8 + \sigma \tan 49^\circ$  MPa.

The cyclic loading test consists of the loading and unloading system, which causes the fatigue in salt specimen and reduces the ultimate compressive strength (Allemandou and Dusseault, 1996). Results of these tests can be shown by the stress, strain, and numerical cycle's graph. The graph shows fatigue concentration of each cycles and ultimate strength at failure. The cyclic loading test can be modified for long-term testing called creep-cyclic loading tests. These results are presented as the relationship between strain and time. Results of all creep-cyclic loading test show a classical creep response with high strain rates at the beginning, gradually decreasing with time towards an identical asymptotic value from cycle to cycle (Thoms and Gehle, 1984). Wetchasat (2002) performs the uniaxial cyclic loading tests on rock salt from salt cores in Sakon Nakhon Basin in Udon Thani Province, Thailand to determine the uniaxial compressive strength and the elastic modulus. The average uniaxial compressive strength from eighth specimens is 23.6 MPa and 19.9 GPa for the average elastic modulus.

Uniaxial creep testing is conducted to determine the time-dependent deformation of rock salt. The uniaxial loading is maintained constant during the test while recording the axial strain and time. The results are commonly shown as a strain

and time curve. Normally, the curve of creep testing is divided into three stages: 1) transient or preliminary creep stage, 2) steady or secondary creep stage, and 3) tertiary creep stage (Figure 2.1). Hunsche and Schulze (1996) perform the uniaxial creep testing, and find that different layer formations have different creep properties. The temperature of test varies from 22 °C to 630 °C. The salt is close to the plastic behavior under a high temperature. Pudewills and Hornberger (1996) study the uniaxial creep testing at different temperatures. The result shows that the creep deformation (strain) at 200 °C is higher than the creep deformation at 100 °C. A study by Fuenkajorn and Daemen (1988) demonstrated that the strain rate at steady state is  $17 \times 10^{-6} \text{ hours}^{-1}$  and equal zero when the time of testing is about 300 to 800 hours. Yin (1998) performs uniaxial creep tests on rock salt from different areas (Canada and Thailand). The results indicate that lateral and axial deformations are about 60% and 70% of sample length. The deformation increases rapidly when axial stress is more than the yield stresses (8 MPa). Micro-cracks are developed when axial stress is equal 12 MPa. Wetchasat (2002) performs uniaxial creep tests to determine time-dependent parameters of rock salt from Sakon Nakhon basin in Udon Thani Province, Thailand. The results are 1.1 GPa of retarded shear modulus ( $G_2$ ), 9.1 GPa-day of elasto-viscosity ( $V_2$ ), and 4.9 GPa of retarded bulk modulus ( $K_2$ ).

Triaxial creep testing is conducted to determine the time-dependent deformation of rock salt under confined conditions. The triaxial creep test is close to in-situ stress conditions when applying confining pressures. Ong et al. (1998) study creep deformation of salt and potash from Patience Lake Member in the United States. They perform the long-term triaxial creep tests. Adjustment of the desired axial and confining stress levels is quick. The axial and confining stresses are

maintained. The test is either a single stage test or multiple stage test which lasts for 90 days. The data storage interval at the start of a test is usually 5 minutes; it is changed to one hour when the creep rate decreased. Upon unloading, the sample is inspected and measured dimensionally. They find that the salt is close to plastic behavior under high confining pressure. Hamami et al. (1996) study the triaxial creep testing on salt with low deviatoric stress under an axial stress varying between 5.5 and 15 MPa with a step of 2.5 MPa each 3 months. The triaxial creep test with constant deviatoric stress (under an axial stress of 13 MPa) and decreasing (and increasing) the temperature from 20 °C to 90 °C (and 90 °C to 20 °C) with a step of 10 °C each 1.5 months. They summarize that if the temperature increases, the deviatoric stress results in an increase of the material deformation. A decrease in temperature remarkably reduces the sample deformation, which is subjected to a deformation at higher temperatures in the beginning of test. This phenomenon is called strain hardening. The strain rate depends on the stress, the temperature and the previous strain. This also agrees with the finding by Korthaus (1996).

Hansen et al. (1984) compare the Brazilian tensile strength of rock salt from ten different locations in the United States. The results indicated that tensile strengths are varying from 1.12 to 2.61 MPa (see Table 2.2). Senseny et al. (1992) perform Brazilian tensile strength on rock salt obtained from Permian basin. During the test, the axial load is applied along diametrical specimen with loading rates of 0.057 to 0.342 MPa/s until the specimen fails. The Brazilian tensile strength is ranging from 1.3 MPa to 1.6 MPa. The high loading rate reduces the tensile strength. Studies by Hunsche (1993) show the suitable loading rates for the tensile strength test which are from 0.017 MPa/s to 0.248 MPa/s. These rates do not affect the tensile strength of

rock salt. Hardy (1998) uses fine-grained rock salt for tensile strength tests under conditions of direct-pull, diametric loading (Brazilian tensile strength test), and hoop-stress loading. Acoustic emission is monitored during these tests. The tests use the loading rates ranging from 0.003 MPa/s to 0.059 MPa/s. The results of direct-pull, diametric loading and hoop-stress loading are 1.63 MPa, 3.97 MPa and 0.68 MPa, respectively. Wetchasat (2002) performs Brazilian tensile strength test on the Maha Sarakham Formation in the Sakon Nakhon Basin. The tensile strength averaged from thirteen specimens is 1.5 MPa.

In the past decade, many researchers studied the permeability of salt by laboratory and field tests. Gas or brine is pressurized through salt specimen and crushed salt specimen for permeability measurement. The permeability of in-situ and undisturbed salt ranges from  $10^{-21} \text{ m}^2$  to  $10^{-20} \text{ m}^2$  (Stormont et al., 1992; Fuenkajorn, 2000). The permeability of crushed salt depends on the bulk density. Brodsky et al. (1998) report that the fractional density from 0.85 to 0.90 of the crushed salt, gives permeability ranging from  $10^{-15} \text{ m}^2$  to  $10^{-12} \text{ m}^2$ . The permeability of crushed salt is normally higher than the permeability of salt specimens. The permeability of salt is still very low but salt may increase its permeability with mechanical damages such as induced cracks around openings on caverns in the salt formations. Phueakphum (2003) performs fracture healing tests under uniaxial and radial loading on rock salt from Sakon Nakhon Basin. The result indicated that confining pressure has an advantage over uniaxial loading, in term of the maximum applied pressures on the tested salt fracture. The applied load is limited by the compressive strength of the salt. The maximum axial stress used is therefore limited to 7.8 MPa or about 30% of the strength. For the confined conditions, the specimen can subject to the confining

pressure as high as 20 MPa. The results suggest that both applied pressure and time are important factors for fracture healing. The healing effectiveness of salt fractures depends heavily on the origin of the fractures. If a fracture is formed by the separation or splitting of salt crystals, it can be easily healed even under relatively low stress for a short period. The splitting failure of salt crystals occurs by a separation of cleavage planes. This means that healing is effective if the salt crystals on both sides of the cleavage plane return to their original position. For the fractures formed by separation of inter-crystalline boundaries or by crystals with different orientations on the opposite sides, healing will not be easily achieved. The hydraulic conductivity for all salt fractures decreases with increasing applied confining pressure and time. This implies that the fracture healing is accompanied by the fracture closure. Both processes are time-dependent. The closure involves the visco-plastic deformation for the salt on both sides of the fracture. The healing involves a chemical process. It is permanent and remains even after the load is removed. Owing to the surface smoothness, the polished fractures show a lower permeability than do the tension-induced fractures. This however does not necessarily mean that the polished fractures heal more effectively than do the tension-induced fractures. A reduction of fracture permeability does not necessarily mean that the healing has occurred. This is evidenced by that even the polished fracture has been compressed until its hydraulic conductivity becomes lower than  $10^{-8}$  m/s, no healing has taken place in the fracture (Phueakphum, 2003).

## **2.5 Mechanical Constitutive Laws of Rock Salt**

During the past two decades, several mechanical constitutive laws of rock salt have been developed, which vary from simple visco-elastic models to complicated



dislocation theory models. Most of the laws emphasize long-term mechanical behavior under a variety of pressures, and temperatures. The constitutive models for salt can be divided into three groups: 1) rheological, 2) empirical, and 3) physical models.

The rheological models describe the mechanical behavior of salt but ignore the actual mechanisms of deformation. The deformational characteristics are assumed to be governed by two basic physical elements: spring elasticity and dashpot viscosity. The mechanical behavior of salt is modeled by a combination of these elements. Since the structure of the rheological models is not related to any particular test, the model can be applied to general problems of time-dependent behavior without requiring additional assumptions. The theories of rheological models have been studied by Fuenkajorn and Daemen (1988), Serata and Fuenkajorn (1992a), Fuenkajorn and Serata (1992, 1994), Stormont and Fuenkajorn (1994), Cristescu (1996), Massier (1996) and Jin and Cristescu (1998)

The empirical models generally are arbitrary functions formulated to fit a set of experimental results. Similar to the rheological approach, developing the empirical laws ignores the actual mechanism of deformation of salt. By fitting curves to a set of data, certain relationships among the data can be established. The empirical laws can be presented in several forms (power, exponential, polynomial, etc.), depending upon the characteristics of the data. Several forms of empirical model can be studied from Farmer (1982), Fokker and Kenter (1994), Pudewills and Hornberger (1996), Zhang et al. (1996), Callahan et al. (1998), and Spiers and Carter (1998).

The physical theory models start from the analysis of the microscopic structural variation of the material observed under loading, and incorporate a

theoretical explanation of the basis of the time-dependent behavior. The method originated in metallurgy and is later introduced into rock mechanics. Rocks, however, are a much more complex material than metals. The atomic bond in natural rock is always a chemical bond rather than a metallic bond; furthermore, most rocks are multigranular-structured in contrast to the relatively homogeneous structure of metals. The physical theory models are therefore considered inappropriate for describing the time-dependent behavior of rock salt (Korthaus, 1996; Durup and Xu, 1996; Eduardo et al., 1996; Weidinger et al., 1998; Senseny and Fossum, 1998; Aubertin et al., 1998, 1999; Hampel et al., 1998; Korthaus, 1998).

## **2.6 Computer Models**

The main objective of this section is to address several computer models (programs) and analytical methods for describing the rock salt behavior. The computer models have been generally developed to simulate the time-dependent brittle-ductile behavior of rock salt and to analyze of complex material behavior under a variety of loading and thermal conditions (Juliend et al., 1998). It is difficult to obtain an accurate calculation of salt behavior with respect to time by human. Advantages of the computer programs are easy to use and rapidly computing. So, the computer programs are used for simulating and predicting the rock salt behavior under in-situ conditions. The computer models for continuous media such as rock salt can be divided into two groups: 1) boundary methods and 2) domain methods. The boundary methods include boundary element method (BEM) and displacement discontinuity method (DDM). The domain methods include finite element method

(FEM) and finite difference method (FDM). Several computer programs for these two groups are listed in Table 2.3.

The boundary element method derives its name from the fact that only the boundaries of the problem geometry are divided into elements. In other words, only the excavation surfaces, the free surface for shallow problems, joint surfaces where joints are considered explicitly and material interfaces for multi-material problems are divided into elements. Several types of boundary element methods are collectively referred to as the boundary element method. These models may be grouped as follows. Direct method, so named because the displacements are solved directly for the specified boundary conditions. Displacement discontinuity (indirect) method, so named because it represents the result of an elongated slit in an elastic continuum being pulled apart. Fictitious stress (indirect) method, so named because the first step in the solution is to find a set of fictitious stresses which satisfy prescribed boundary conditions. These stresses are then used in the calculation of actual stresses and displacements in rock mass.

The finite element method is well suited to solving problems involving heterogeneous or non-linear material properties, since each element explicitly models the response of its contained material. However, the finite element method is not well suited to modeling infinite boundaries, such as in underground excavation problems. One technique for handling infinite boundaries is to discretize beyond the zone of influence of the excavation and to apply appropriate boundary conditions to the outer edges. Another approach has been to develop elements for which one edge extends to infinity (i.e. so-called infinity finite element). Efficient pre- and post-processors allow the user to perform parametric analyses and assess the influence of

**Table 2.3** Some computer programs used for describing the rock salt behavior.

<b>Code Names</b>	<b>Methods</b>	<b>References</b>
BEFE	BEM (3D)	Beddoes (1994)
VELMINA	DDM (3D)	Frayne (1998)
VNFOLD	DDM (3D)	Beddoes (1994)
FLAC	FDM (2D)	Itasca (1992)
FLAC	FDM (3D)	Itasca (1994), and Frayne (1996, 1998)
ADINA	FEM (2D)	Pudewills and Hornberger (1996)
ANSALT	FEM (2D)	Heusermann et al. (1998)
ANSPRE	FEM (2D)	Honecker and Wulf (1988)
ANTEMP,ANSPP	FEM (2D)	Honecker and Wulf (1988)
ASTHER	FEM (2D)	Rolnik (1988)
CODE-BRIGHT	FEM (2D)	Olivella et al. (1996, 1998a, 1998b)
COYOTE	FEM (2D)	Gartling (1981a)
DAPROK	FEM (2D)	Harrington et al. (1991)
FAST-BEST	FEM (2D)	Pudewills (1998)
GEO/REM	FEM (2D)	Serata (1991), and Serta and Fuenkajorn (1993)
GEOMECH	FEM (2D)	Nguyen-Minh and Menezes (1996)
GEOROC	FEM (2D)	Rizkalla (1991)
JAC	FEM (2D)	Biffle (1984)
LUBBY-1	FEM (2D)	Rokahr and Staudtmeister (1996)
LUBBY-2	FEM (2D)	Lux and Schmidt (1996)
MARC	FEM (2D)	Van Eekelen (1988)
MERLIN	FEM (2D)	Gartling (1981b)
SANCHO	FEM (2D)	Stone et al. (1985), and Hansen (1996)
SPECTROM-32	FEM (2D)	Callahan et al. (1989)
VIPLEF	FEM (2D)	Vouille et al. (1996)
VISCOT	FEM (2D)	INTERA (1982), and Frayne (1996)
SUVIC-D	FEM (2D/3D)	Julien et al. (1998)
VISAGE	FEM (3D)	Ong (1994)

**Note:** FEM is finite element method, FDM is finite difference method, DDM is displacement discontinuity method, BEM is boundary element method, 2D is two-dimension, and 3D is three-dimension.

approximated far-field boundary conditions. The time required for this process is negligible compared to the total analysis time. Joints can be represented explicitly using a specific joint element. Once the model has been divided into elements, material properties have been assigned and loads have been prescribed, some technique must be used to redistribute any unbalanced loads and thus determine the solution to the new equilibrium state. Available solution techniques can be broadly divided into two classes, implicit and explicit. Implicit techniques assemble systems of linear equations, which are then solved using standard matrix reduction techniques. Any material non-linearity is accounted for by modifying stiffness coefficients (secant approach) and/or by adjusting prescribed variables (initial stress or initial strain approach). These changes are made in an iterative manner such that all constitutive and equilibrium equations are satisfied for the given load state. Several computer programs for the finite element methods can be studied from INTERA (1982), Honecker and Wulf (1988), Honecker and Wulf (1988), Rolnik (1988), Callahan et al. (1989), Blanquer-Fernandez (1991), Harrington et al. (1991), Serata and Fuenkajorn (1993), Ong (1994), Nguyen-Minh and Menezes (1996), Lux and Schmidt (1996), Rokahr and Staudtmeister (1996), Vouille et al. (1996), de Vries and Callahan (1998), Heusermann et al. (1998), Salzer and Scheriner (1998), Julien et al. (1998), and Pudewills (1998).

The finite difference method is well suited to solving problems involving inhomogeneous, complicated geometry, and non-linear material properties. The FDM is a method for approximating derivatives in the equations of motion. Continuous derivatives in differential equations are replaced by finite difference approximations at a discrete set of points in space and time. The resulting set of equations, with

appropriate restrictions, can then be solved by algebraic methods. A finite difference model is one, which employs finite difference methods. The resolution of a finite difference model is determined by the spacing of the discrete set of points (grid points) used to approximate the derivatives. The FDM is applied for modeling geomechanical problems that consist of several stages, such as sequential excavation, backfilling and loading. Some computer programs for describing the rock salt behavior can be studied from Itasca (1992, 1994).

## 2.7 Constitutive Law used in this Study

The constitutive law used in this study is developed by Fuenkajorn and Serata (1992, 1993, 1994) and Serata and Fuenkajorn (1992). The rheological constitutive model used here is capable of simulating the elastic, viscoelastic, viscoplastic, strain-softening and dilation behavior of time-dependent materials, such as rock salt. These equations have been incorporated into a finite element code, named GEO. A brief discussion identifying its unique derivation of the constitutive equations is given below.

The von Mises criterion is used to describe the failure surface and to develop a strain-softening model for geologic materials. It is proposed that the octahedral shear strength  $K_O$  increases with an increase of the mean stress  $\sigma_m$  toward an ultimate value. The rate change of  $K_O$  with respect  $\sigma_m$  can be expressed as,

$$\partial K_O / \partial \sigma_m = \alpha (K^B - K_O), \quad (2.1)$$

where  $\alpha$  is a yield surface coefficient, and  $K^B$  is an ultimate octahedral shear strength. Equation (2.1) leads to the following expression of a compressive failure criterion, which is applicable for brittle to ductile materials,

$$K_O = K^A + (K^B - K^A) [1 - \exp(-\alpha\sigma_m)], \quad (2.2)$$

where  $K^A$  is an unconfined octahedral shear strength. During strain softening, the strength of rock decreases or deteriorates. The ultimate deterioration of the material is defined as the state at which the inter-crystalline cohesive bonds are completely lost, as in a mass of loose sand. The strength  $K_O$  in this state then becomes the residual strength  $K^R$ , which reflects the internal friction strength in the pulverized mass, given by the function of confinement  $\sigma_m$ ,

$$K^R = K^B \sigma_m/P, \quad (2.3)$$

where  $K^B/P$  is friction tangent ( $\tan \theta$ ),  $P$  is the plastic transition pressure, and  $\theta$  is the angle of internal friction. Rock deterioration progresses from the intact to the residual strength ( $K_O$  to  $K^R$ ) with an increase in the excess octahedral shear strain  $\Delta\gamma_O$ . The  $K_O$  of the deteriorated rock can be determined by adding the residual strength  $K^R$  to the variable portion  $\Delta K_O$ , which varies from 0 to 100 %, depending on the amount of the deterioration. Thus the strength can be defined as,

$$K_O = f_D \Delta K_O + K^R, \quad (2.4)$$

where  $f_D$  is the deteriorating function and  $\Delta K_O$  is the variance portion of the strength which equals  $[K^A + (K^B - K^A) (1 - \exp(-\alpha\sigma_m))] - K^R$ .  $f_D$  can be related to the excess octahedral shear strain as,

$$f_D = \exp[-C(\gamma_O - \gamma_C)/\gamma_C]; \gamma_O > \gamma_C, \quad (2.5)$$

where  $C$  is a deterioration coefficient,  $\gamma_C$  is a critical strain of elastic limit, and  $\gamma_O$  is the induced octahedral shear strain. By introducing equation (2.5) into equation (2.4), the strength deterioration function describing the strain-softening behavior of rock after  $\gamma_O$  exceeds  $\gamma_C$ , can be established,

$$K_O = \exp[-C(\gamma_O - \gamma_C)/\gamma_C] \{ [K^A + (K^B - K^A) (1 - \exp(-\alpha\sigma_m))] - K^B \sigma_m/P \}$$

$$+ K^B \sigma_m / P. \quad (2.6)$$

For viscoelastic behavior (VE), its state is defined as the state in which the octahedral shear stress  $\tau_o$  is less than the octahedral shear strength  $K_o$ . No viscoplastic creep tanks place in this state. The VE strain can be directly identified using the results from creep testing (Serata et al., 1991). The time-dependent strain resulting from viscoelastic creep can best be described by a set of three or more Kelvin components as,

$$\begin{aligned} \gamma_{total}^{VE} &= \gamma_{23}^{VE} + \gamma_{22}^{VE} + \gamma_{21}^{VE} \\ &= (\tau_o / V_{21}) \exp(-G_{21}t / V_{21}) + (\tau_o / V_{22}) \exp(-G_{22}t / V_{22}) \\ &\quad + (\tau_o / V_{23}) \exp(-G_{23}t / V_{23}). \end{aligned} \quad (2.7)$$

Where:  $\gamma_{23}^{VE}, \gamma_{22}^{VE}, \gamma_{21}^{VE}$  = short-, medium-, and long-term viscoelastic strain rates;  $G_{21}, G_{22}, G_{23}$  = retarded shear moduli for short-, medium-, and long-term VE strain;  $V_{21}, V_{22}, V_{23}$  = elastoviscosity coefficients for short-, medium-, and long-term VE strains.

Figure 2.2 shows the behavioral system of GEO model. The formulation separates the octahedral shear stress-strain ( $\sigma_m$ - $\epsilon_m$ ) relation. These relations act in parallel and are related via failure and post-failure conditions (i.e. deterioration coefficient C). The program carries out the explicit time-domain integration, and hence allows updating the element strength and state (elastic or plastic) through different time steps. The formulation is designed such that when the induced shear strain ( $\gamma_o$ ) is less than the critical shear strain ( $\gamma_c$ ), element behaves as an elastic or visco-elastic, and does not dilate. Immediately after  $\gamma_o$  exceeds  $\gamma_c$  and  $\sigma_m$  is less than



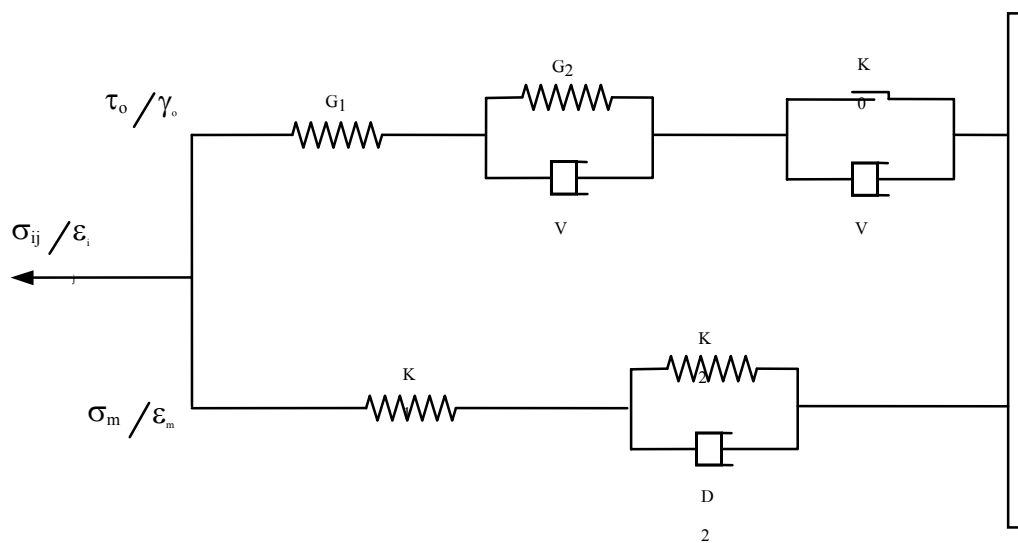


**Figure 2.2** Rheological components of the GEO program (modified from Serata and Fuenkajorn, 1993).

$P$ ,  $K_O$  decreases, and results in a strain-softening behavior. Under this condition, the calculation for a new failure surface and volumetric dilation will be carried out for that particular element. The new  $K_O$  is then returned to the main algorithm to compare with the current stress state. The calculated  $\varepsilon_{VD}$  is added to the elastic and plastic strain components in the minimum principal stress direction. Under large confinements ( $\sigma_m > P$ ), the strength will not deteriorate, and dilation will not occur. The element may deform in strain hardening mode or may flow plastically, depending on the amount of  $\gamma_O$ .

## 2.8 Dry Salt Mining

The dry salt mining method can be divided into two types based on the configurations and layout of the excavations, room-and-pillar and long-wall mining.

For room-and-pillar mining, there are a wide variety of angular pillar shapes, either by design or by irregularities of the deposit. Room and pillar mining can be planned as either a one-pass advanced mining system, where the pillars are left in place, or as a two-pass advance and retreat sequence, where the pillars are partially or totally recovered in the retreat phase. To a large part, the layout of the angular pillar is influenced by the excavation methods and equipment. Mining can be drilling and blasting (cyclic mining), by road headers, drum miners, and more (Jeremic, 1994).

Square pillars have been used extensively in the mining of all types of evaporite deposits. The common application is in flat-bedded deposits with thickness up to 2.5 m which are sandwiched between rock strata. Figure 2.3 shows the layout example for square pillar mining.

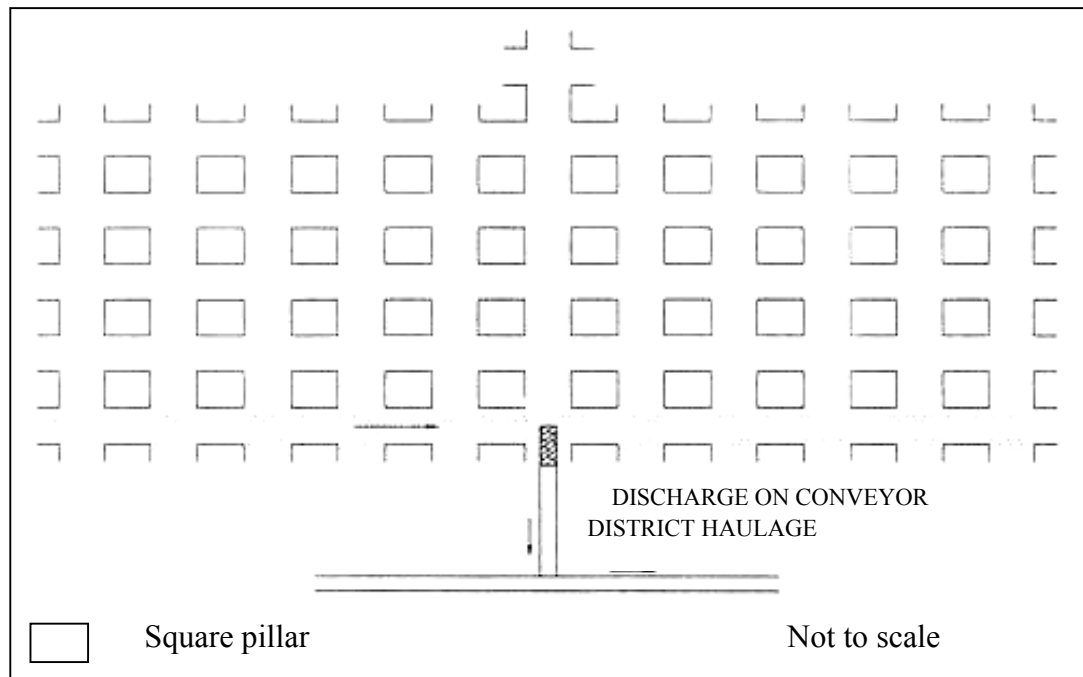


**Figure 2.3** Layout of square pillars mining. (modified from Michalk, 1980).

Rectangular pillars have also been applied to the mining of evaporite deposits in a close parallel to square pillar mining. It is currently limited generally to drill and blast operations (Jeremic, 1994).

Long-wall mining of potash beds is widely practiced in Europe, including the USSR. The first long-wall face was set up in France in 1948, and was then adapted to the more regular deposits of Spain in 1963 and the USSR in 1972. Long-wall mining was a complete departure from the normal room and pillar operations used in evaporite deposit mines with flat and moderate thick beds. Success depended on the close cooperation between the mine operators and mine equipment manufacturers. This allowed equipment, designed for long-wall coal mining, to be modified for use in the very different strata conditions and ground behavior associated with the mining of salt. Long-wall salt mining, at the beginning, followed the coal mining practice of face undercutting followed by blasting. Loading was done manually or with a scraper-hoist system. Developments in mechanized long-wall coal extraction were immediately transferred to salt mining operations. Figure 2.4 shows the example of layout by square pillar mining (Herget, 1986; Jeremic, 1994).

Jeremic (1982, 1985a, and 1985b) reported that the most common and simplest approach to pillar loads is through the tributary area theory, which depends on a number of simplifications. The pillars have an open face on all four sides and thus are uniaxially loaded by the superimposed overburden. The average stress in pillars with an adequate size in relation to mine depth to not fail, is calculated on the assumption that the pillars uniformly support the entire load of the overlying strata above both the pillars and the mine-out areas. The effects of deformation and failure of the roof strata are disregarded. The concept of abutment pillar design was

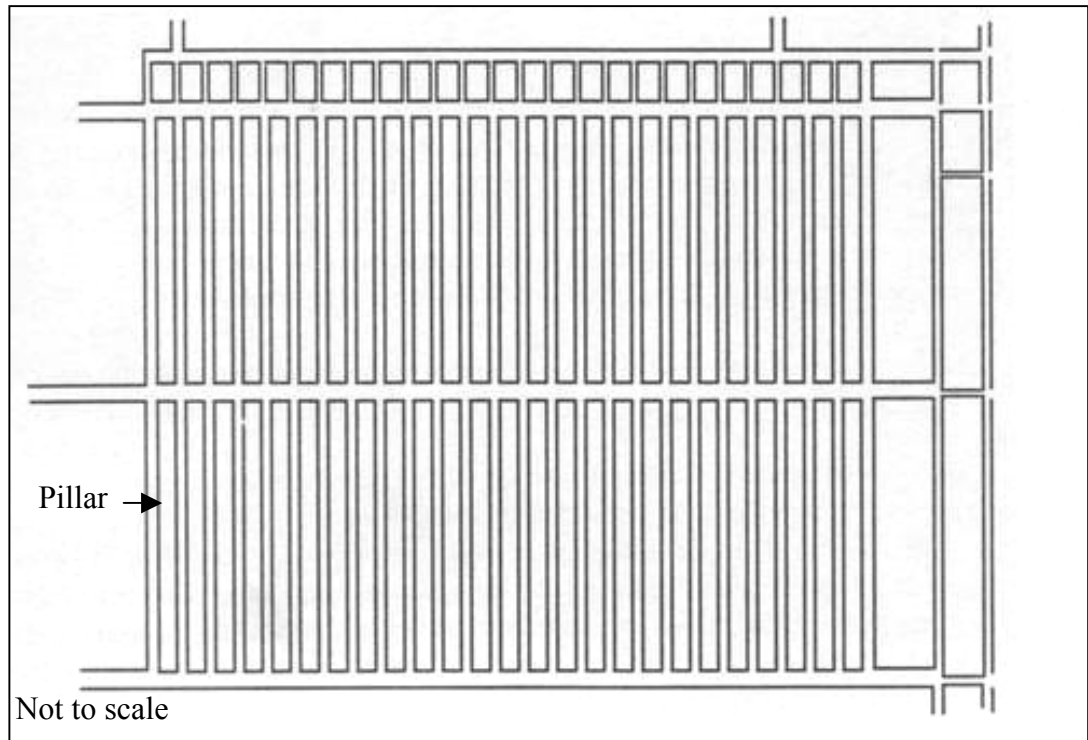


**Figure 2.4** Layout of long-wall mining. (modified from Molavi and Wooley, 1986).

introduced in underground mining long ago to improve ground conditions in ore extraction areas. The concept is based on the stress diversion from the mining extraction panel onto the abutment pillars. It is accomplished through the use of inter-room yielding pillars which can only support a limited load. The magnitude of the load resting on the abutment pillars depends on the shape and size of the arch of equilibrium above the mining panel. For the practical purpose of the load calculation on abutment pillars, an arch of equilibrium is approximated by a trapezoidal shape (Jeremic, 1994).

Van Sambeek (1998) presented that specification of properly sized pillars to support the overburden is one of the most challenging aspects of salt mine design. Consideration of salt mine design include average vertical pillar stress, average horizontal stresses, average effective stress, pillar creep rates, and pillar strength. Kwon and Miller (1998) reported that prediction of the deformational behavior of excavation in rock salt is complex due to the time-dependent behavior of rock salt as well as many other parameters, which can exert an influence on the deformation mechanism of these openings. Important parameters may include, as follows; depth, width and height of excavation, pillar size and elapse time.

## **2.9 Salt Bearing Formation in Khorat Phateau**

The rock salt formation in Thailand is located in the Khorat plateau as shown in Figure 2.5. The Khorat plateau covers 150,000 square kilometers, from 14° to 19° northern latitude and 101° to 106° eastern longitude. It has high escarpment up to 900 meters above mean sea level along the western and southern edges and mesa topography over parts of its area whereas its middle area elevation is about 140 meters

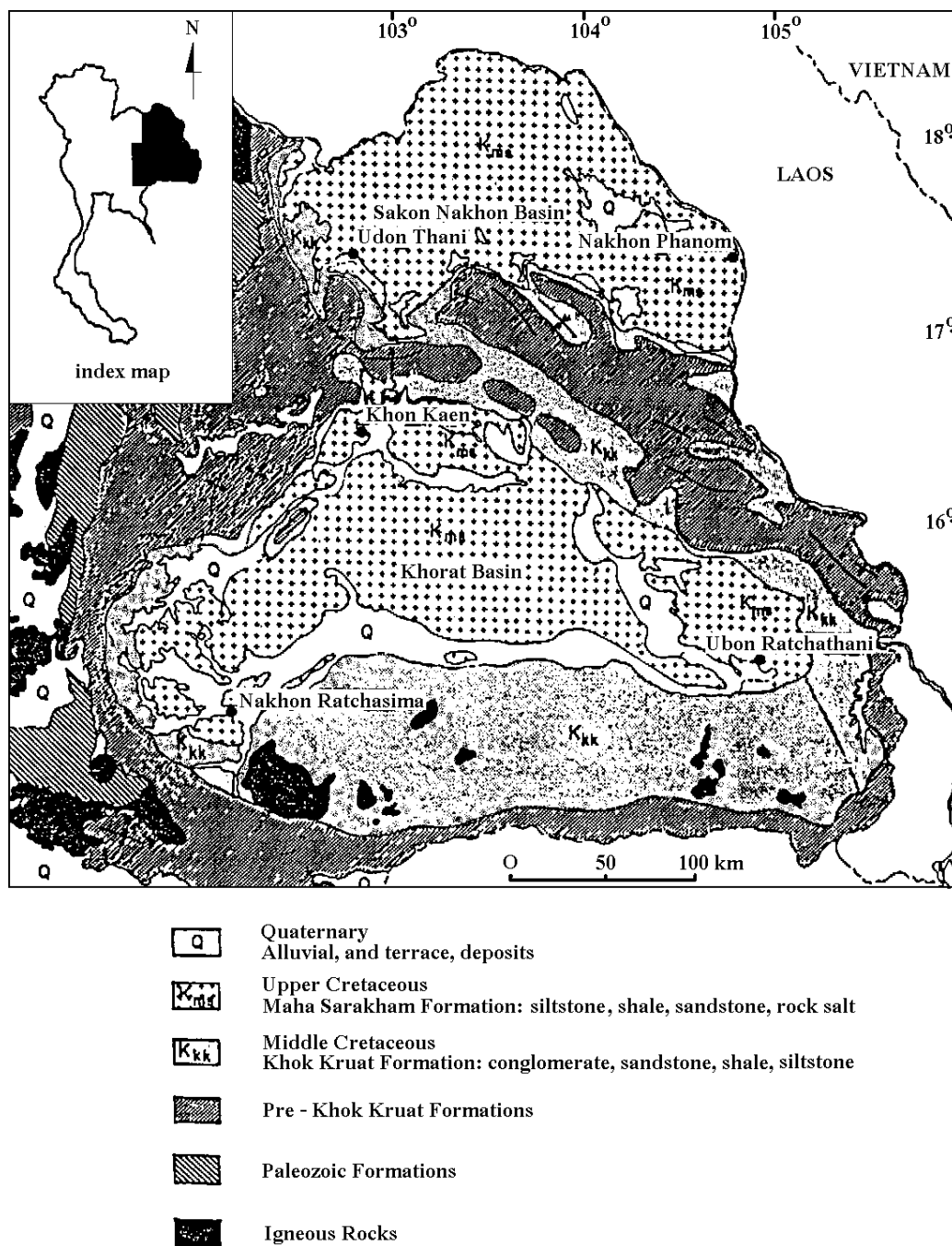


**Figure 2.5** A simplified geological map of the Khorat plateau. (modified from Utha-aaron, 1993 adapted from DMR's Geological Map of Thailand scale 1:2,500,000).

above mean sea level. The northern and eastern edges of the plateau lie close to Laos and the southern one close to Cambodia (Utha-aroon, 1993).

The Khorat plateau is divided into two features: the edge group and the basin group. The edge group consists of Huai Hin Lat Formation, Nam Phong Formation, Phu Kradung Formation, Phra Wihan Formation, Sao Khua Formation and Phu Pan Formation. The basin group consists of Khok Kruat and Maha Sarakham Formations. Yumuang et al. (1986), Supajanya et al. (1992), Utha-aroon (1993) and Warren (1999) describe these formations from the youngest to oldest, as follows.

- 1) Phu Thok Formation consists of brown to reddish brown sandstone, siltstone, and mudstone in the upper Tertiary age.
- 2) Maha Sarakham Formation consists of three evaporation cycles (e.g., rock salt) and clastic rocks (e.g., sandstone, siltstone, and shale), upper cap anhydrite and basal anhydrite in the top and bottom of the formations. They are in the Lower Cretaceous age.
- 3) Khok Kruat Formation consists of sandstone, reddish brown mudstone, and conglomerate in the Middle Cretaceous age.
- 4) Phu Phan Formation consists of conglomerate and white and light gray sandstone in the Upper Cretaceous age.
- 5) Sao Khua Formation consists of sandstone, siltstone, mudstone, and red conglomerate in the Lower Jurassic age.
- 6) Phra Wihan Formation consists of white sandstone, reddish brown shale and massive sandstone with conglomerate in the Middle Jurassic age.
- 7) Phu Kradung Formation consists of reddish brown mudstone and siltstone in the Upper Jurassic age.



8) Nam Phong Formation consists of sandstone and reddish brown conglomerate. The top and bottom of the bed are mudstone interbedded with siltstone in the Upper Jurassic age.

Rock salt in the Khorat plateau is separated into 2 basins: Sakon Nakhon basin and Khorat basin. The Sakon Nakhon basin in the north has an area of about seventeen thousand square kilometers. It covers the area of Nong Khai, Udon Thani, Sakon Nakorn, Nakorn Phanom, and Muk Dhahan Provinces and extends to some part of Laos. The Khorat basin is in the south, which has about thirty thousand square kilometers. The basin covers the area of Nakhon Ratchasima, Chaiyaphum, Khon Kaen, Maha Sarakham, Roi Ed, Kalasin, Yasothon, Ubol Ratchathani provinces and the north of Buri Ram, Surin and Si Sa Ket provinces (Suwanich, 1986).

Both basins contain three cycles of evaporated deposits within the Maha Sarakham salt-bearing strata (Suwanich and Rattanajaruraks, 1982). The lower cycles consist of the lower clastic cycle and the lower evaporated cycle. The lower clastic cycle (the marine transgression) has been formed as a substratum to the evaporated deposits and mainly consists of ferruginous clastic sediments and calcareous sandstone. The lower evaporated cycle (the marine regression) has been formed which causes penesaline conditions inducing anhydrite precipitation. By further concentration of the saline, water halite and the sylvite are deposited marking the termination of the restricted environment. The middle cycles consisted of the middle clastic cycle and the middle evaporated cycle. The middle clastic cycle (the marine transgression) has been formed after the lower evaporated cycle ceases and is replaced by sedimentation of mudstone and clay stone. The middle evaporated cycle (the marine regression) has under restrictive marine conditions. The brine concentration

increased due to saline conditions and the lower middle halite sub-facies reprecipitated. Increasing in the salinity of basin water is interrupted by marine influxes as evidenced by thin anhydrite layers. The rejuvenation of brine concentrations results in precipitation of the upper middle halite sub-facies. The upper cycles consisted of the upper clastic cycle and the upper evaporated cycle. The upper clastic cycle (the marine transgression) has been formed after the deposition of the halite sub-facies ceased because the depositional basin was opened for sedimentation of fine grain clastic sediments, namely, mudstone and clay stone. The upper evaporated cycle (the marine regression) marked the end of both the evaporated and clastic sedimentation (Suwanich, 1986).

From 1973 to 1983, the Department of Mineral Resources (DMR) explored the potash deposits in the Korat Basin and drilled 118 exploratory boreholes (Japakasetr and Workman, 1981). Some boreholes are drilled into the Khok Kruat Formation. The core logs reveals the stratigraphy of the Maha Sarakham sequence and its relationship to the underlying Khorat Group as shown in Figure 2.6. The Maha Sarakham Formation can be briefly described from top to bottom as follows (Suwanich, 1978; Yumuang, 1983; Sattayarak, 1985; Tabakh et al., 1995).

- 1) Clay and claystone are reddish brown. Some siltstone and sandstone may occur occasionally.
- 2) Upper anhydrite is thin layer with white to gray.
- 3) Upper salt is dirty, light brown to smoky or orange when it is filled with clay. The thickness is between 3 to 65 meters.
- 4) Middle clastic includes reddish brown clay and mudstone, and some interbedded gypsum.

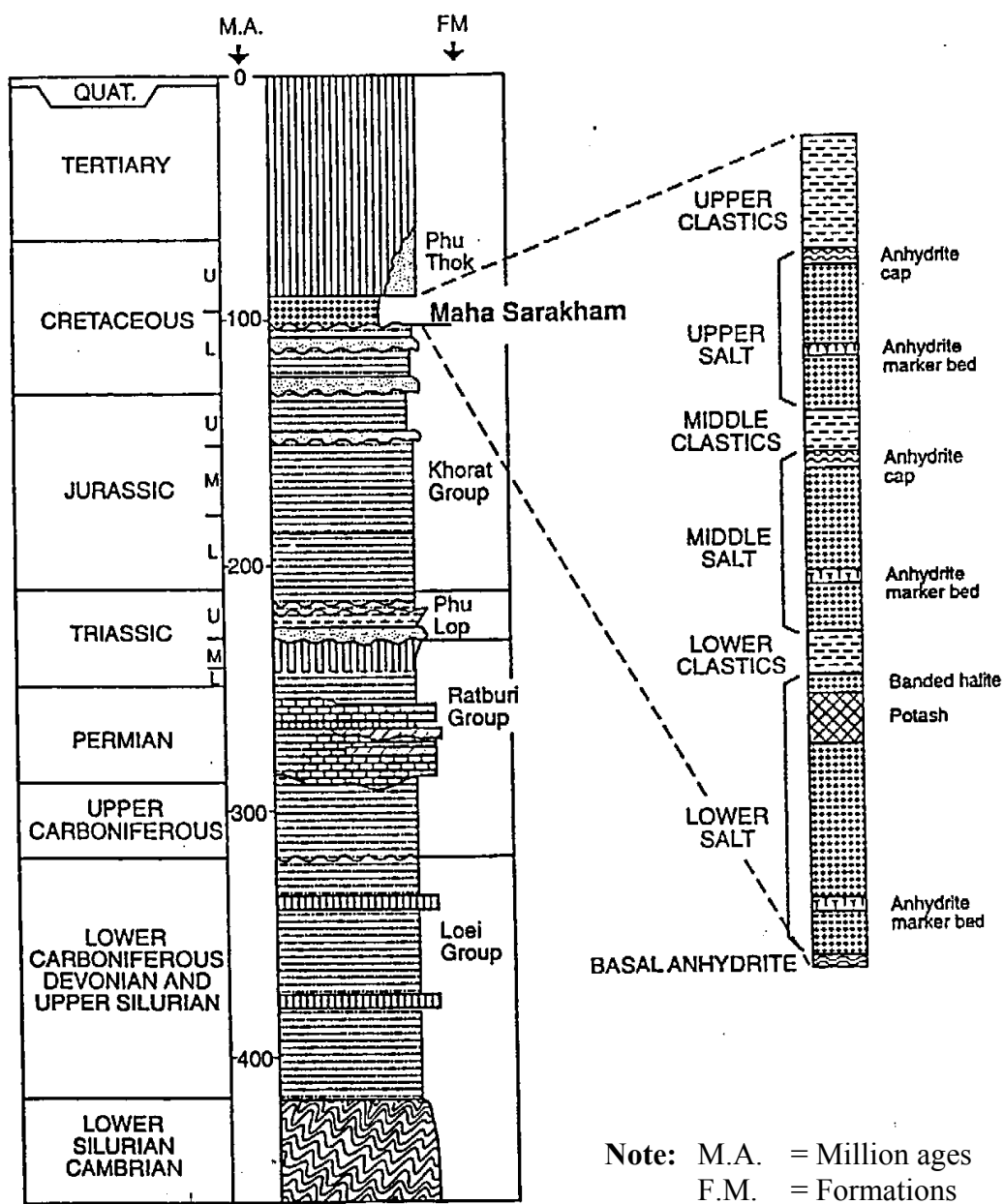


**Figure 2.6** Stratigraphy of the Khorat Basin in the Northeast of Thailand, with a more detail section of the Maha Sarakham Formation (right).  
(From Utha-aroon et al., 1995).

- 5) Middle salt is dirty, light brown to smoky, thicker than the upper salt with 70 meters in thickness. The lower part may contain carnallite or sylvinite.
- 6) Lower clastic includes reddish brown clay and mudstone.
- 7) Rock salt, very thin layer (three meters thick) with various colors such as red, orange, brown, gray, and white.
- 8) Potash found in the study areas can be divided into two types: Carnallite ( $\text{KCl}\cdot\text{MgCl}_2\cdot 6\text{H}_2\text{O}$ ) and Sylvite ( $\text{KCl}$ ). Carnallite is commonly orange, red, and pink while sylvinite is white or light orange that may be occurred by the chemical changing of carnallite nearby salt domes. Another mineral named tachyhydrite ( $\text{CaCl}_2\cdot 2\text{MgCl}_2\cdot 12\text{H}_2\text{O}$ ) that likely occurs accompanied with carnallite. It is orange or yellow, and can be easily dissolved in water.
- 9) Lower rock salt is the thickest and clean salt unit in the Maha Sarakham Formation. Lower rock salt formation in some areas is over 400-1000 meters thick. The average thickness is 134 meters.
- 10) Basal anhydrite is found at the base of the Maha Sarakham Formation throughout both the Khorat and the Sakon Nakhon Basins. It overlies Khok Kruat sandstones of the Khorat Group. Generally reddish-color sandstones of the Khok Kruat are typically greenish and may be Cu-stained in proximity to this contact.

## **2.10 Research on Nuclear Waste Repository in Thailand**

Wetchasat (2002) studies the mechanical performance of the rock salt formations for the nuclear waste disposal. The concept of salt solution mining is

used. Research procedures are divided into three tasks: 1) mechanical laboratory testing, 2) salt property calibrations, and 3) computer model simulation. The computer models are constructed from 5 geologically favorable areas. A time-dependent finite element analyses determine the mechanical stability of the caverns under isothermal conditions during the waste emplacement for the next 500 years. The results from the computer prediction suggest that the spherical shape shows the most suitable geometry for the disposal cavern. The effects of depths and thickness of salt formations has also been studied. The results suggest that the disposal caverns should be solution-mined below 585 meters depth. The diameter of the spherical shaped cavern should be 40 meters. The vertical and horizontal cavern closures are calculated to be less than 0.5 %. The surface subsidence is calculated to be less than 0.22 meter for the next 500 year after waste emplacement.

## **CHAPTER III**

### **EXPERIMENTAL WORK**

#### **3.1 Objectives**

Laboratory experiments have been performed to determine the mechanical and rheological properties of the Maha Sarakham rock salt. The experiments concentrate on the instantaneous and long-term mechanical response to obtain the relationship between stress, strain and time for use in the calibrations of the visco-plastic properties and the prediction via computer modeling. The experiments include long-term uniaxial and triaxial creep tests. All experiments are conducted under isothermal conditions (room temperature). The sample preparation, test methods, results, and discussions for both experiments are described in the following sections.

#### **3.2 Sample Collection and Preparation**

Rock salt samples used in this research are obtained from Asia Pacific Potash Corporation, Udon Thani Province. They are collected from two deep boreholes (BD99-1 and BD99-2) located in Khumpawapi District. They are obtained from the Sakon Nakhon Basin (Figure 3.1). The core specimens have been drilled from the Middle Salt and the Lower Salt members at the depths ranging between 250 meters and 400 meters. They are cylindrical shaped with 60 millimeters in diameter. Some rock salt cores are shown in Figure 3.2. Preparation of these samples follows, as much as practical, the ASTM standard practice (ASTM D4543-85). There are two

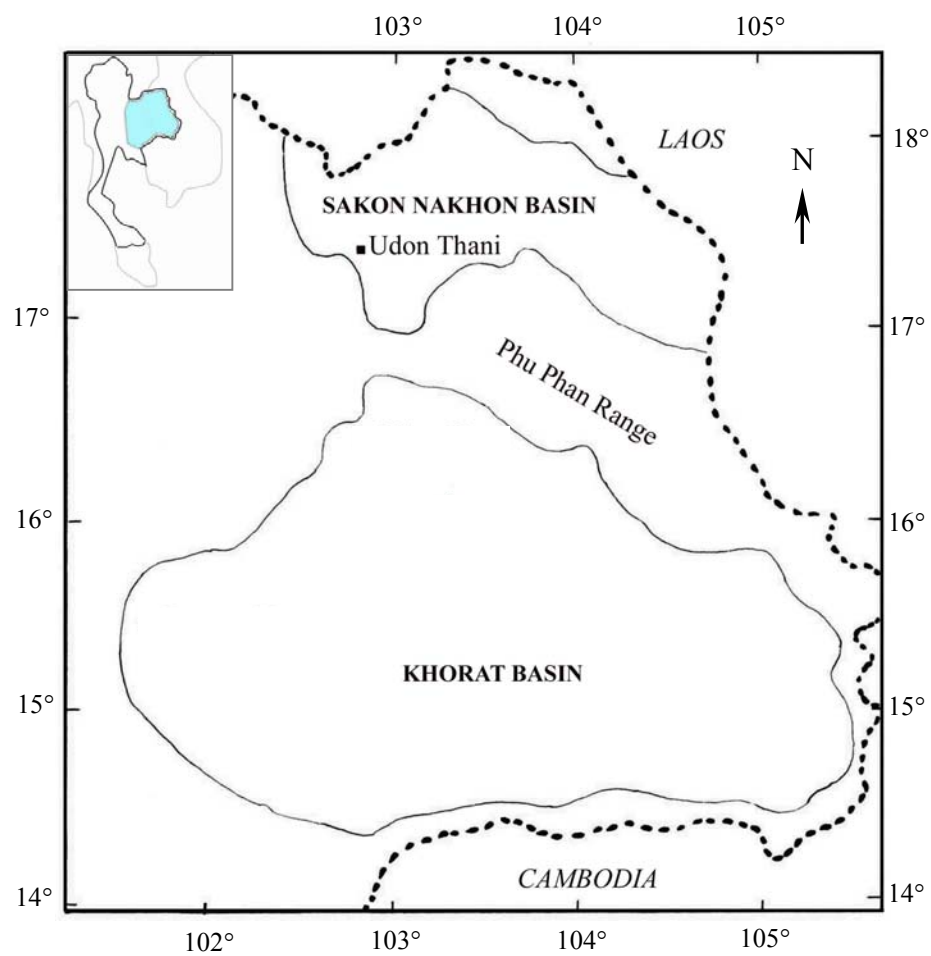


**Figure 3.1** Locations where the salt cores are obtained from Sakon Nakhon Basin in the northeast of Thailand. (modified from Japan International Cooperation Agency, 1981).



**Figure 3.2** Some salt core samples donated by Asia Pacific Potash Corporation, Udon Thani Province. They are collected from borehole no. BD99-1 located in Khumpawapi District. These core samples are from the depths ranging from 419 to 422 meters.



groups of specimens for different test methods, i.e. uniaxial and triaxial creep tests. Five specimens are prepared to have a nominal length to diameter ratio (L/D) equal to 2.5 for the uniaxial creep tests. Four specimens are prepared to have L/D ratio of 2.0 for the triaxial creep tests. The specimens are cut by cutting machine using saturated brine as cutting fluid (Figure 3.3). The saw-cut surfaces are ground flat by the grinding machine (Figure 3.4). All specimens are measured to determine the precise dimensions to the nearest 0.01 in. The depth is determined and recorded on each specimen. The rock characteristics (mineral composition, grain size, density, color, etc.) are described. After finishing the preparation, the specimens are labeled and wrapped with plastic film. The identification of specimens is given, which includes rock type, borehole number, core number, core diameter, type of experiment and sample number. Rock salt from boreholes in Udon Thani Province has more than 99 percent halite (NaCl). The mineral composition is determined by X-ray Diffractometer. The salt is coarsely crystalline. The crystal size varies from 1 millimeter to 10 millimeters. The average density is  $2,160 \text{ kg/m}^3$ . The color is clear or white, but sometimes pink and gray can be found. Most often the crystals are rough, vitreous, and transparent to translucent.

### **3.3 Uniaxial Creep Tests**

The objective of the uniaxial creep tests is to determine visco-plastic parameters of the salt specimens under unconfined condition. The time-related parameters are monitored, recorded and analyzed.



**Figure 3.3** Core sample is cut to obtain the desired length.



**Figure 3.4** Grinding of core samples for smooth and parallel end surfaces.

### 3.3.1 Test Methods

The uniaxial creep tests have been performed on five salt specimens. The salt specimens are loaded by constant uniaxial stresses at 4.1, 7.1, 9.1, 11.1, and 14.1 MPa (one stress per specimen). The experimental procedure follows the ASTM standards (ASTM D4405 and D4341). A compression machine (Consolidation machine, capacity of 5,000 kN) is used to apply constant axial load onto the specimens. The digital gages with a precision of 0.001 millimeter are installed to measure the axial displacement of the specimens (Figure 3.5). The specimens are loaded continuously for a period of 22 to 56 days, depending on the displacement results. During the test, the axial deformation, time, and failure modes are recorded. The frequency of readings is once every minute at the beginning of the test, and gradually reducing to once a day after the first few days of the test. This also depends on the deformation rate of each specimen. The results are presented by strain-time curves. The axial stress and axial strain values are calculated by :

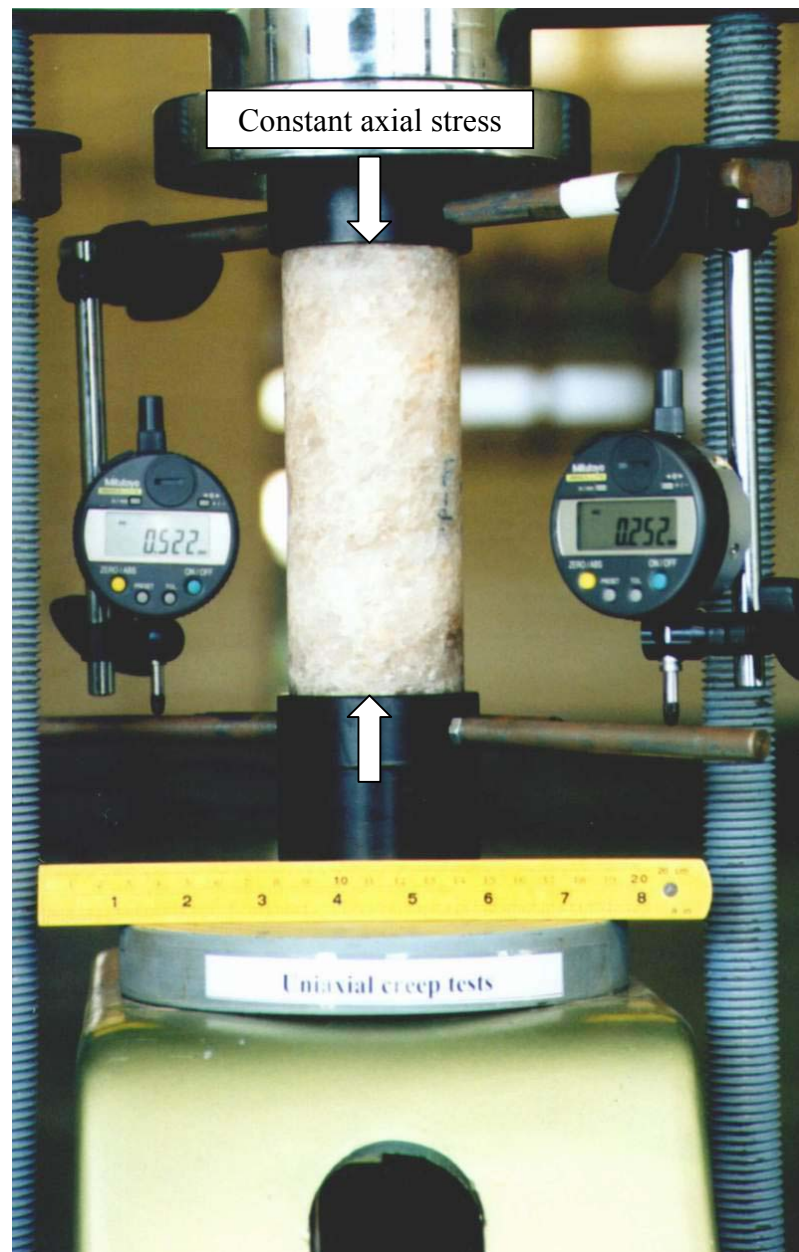
$$\sigma_{\text{axial}} = P_a/A, \quad (3.1)$$

$$\varepsilon_{\text{axial}} = \Delta L/L, \quad (3.2)$$

where  $\sigma_{\text{axial}}$  is axial stress,  $P_a$  is applied axial load,  $A$  is the cross-section area normal to the direction of load,  $\varepsilon_{\text{axial}}$  is engineering axial strain,  $\Delta L$  is the axial deformation, and  $L$  is the original length.

### 3.3.2 Test Results

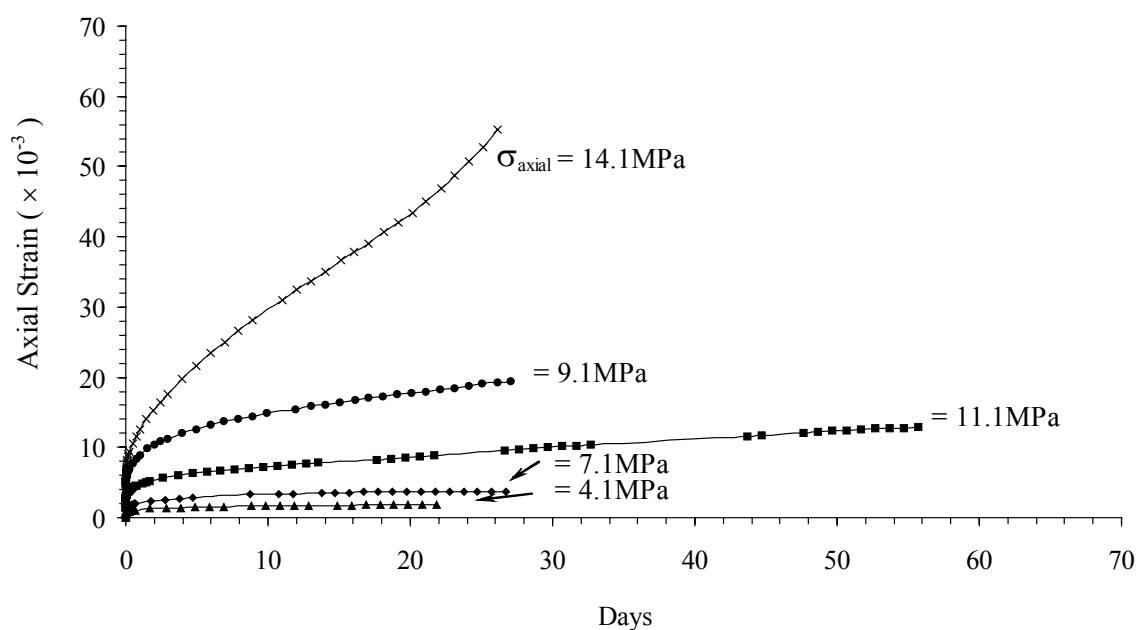
Table 3.1 summarizes the uniaxial creep test results. The axial strain-time curves are given in Figure 3.6. The curve represents instantaneous, transient, and tertiary creep states of salt specimens under a constant axial load. The specimens are rapidly loaded and subsequently the axial strains increase. The instantaneous



**Figure 3.5** Uniaxial creep test set-up. The cylindrical salt specimen is loaded vertically using the compression machine, while displacement digital gages measured the axial deformation on opposite sides of the specimen.

**Table 3.1** Summary of the uniaxial creep test results.

Specimen No.	Depth (m)	Average Diameter <b>D</b> (mm)	Average Length <b>L</b> (mm)	Constant Axial Stress $\sigma_{axial}$ (MPa)
BD99-1-CP01	402.80	61.11	155.21	7.1
BD99-1-CP02	403.00	61.17	154.27	11.1
BD99-1-CP03	403.20	61.12	155.07	4.1
BD99-1-CP06	266.20	61.08	152.06	9.1
BD99-1-CP07	266.36	61.08	156.48	14.1

**Figure 3.6** Results of the uniaxial creep testing for different constant axial stresses ( $\sigma_{axial}$ ).

strains range from  $0.8 \times 10^{-3}$  to  $8.0 \times 10^{-3}$ . Four specimens, under constant axial stress of 4.1, 7.1, 9.1, and 11.1 MPa, show the transient and steady creep phases. Only one specimen, under constant axial stress of 14.1 MPa, shows complete creep phase: the transient, steady, and tertiary creep phases.

### **3.3.3 Discussions**

The value of instantaneous creep strain increases with the constant axial stress. Figure 3.6 gives the strain-time curves of salt specimens tested under high and low constant axial stresses. The axial stress also increases the creep strains. In the transient creep phase, the strain rate increases with the applied stresses. In most cases the strain rate under high axial stresses is greater than the one under low axial stresses. The effect of inclusion in specimen may make the strain rate under low stress higher than the one under higher stress, as found in specimen no. BD-99-1-CP02. The steady state strain rate determined here is higher than the one given by Fuenkajorn and Daemen (1988),  $408 \times 10^{-6} \text{ day}^{-1}$ . This is probably due to the significant amount of inclusions, which include anhydrite and iron oxides.

## **3.4 Triaxial Creep Tests**

The objective of the triaxial creep tests is to determine visco-plastic parameters of the salt specimens under confined condition. The time-related parameters are monitored, recorded and analyzed. The salt specimens tested are selected from borehole no. BD99-1.

### **3.4.1 Test Methods**

Four salt specimens are tested under constant axial stresses from 16.6 to 27.6 MPa and constant confining pressures between 3.4 and 6.9 MPa for a period of

about one month. The experimental procedure follows the ASTM standard (ASTM D4406-93). A compression machine (Consolidation machine, capacity of 5,000 kN) is used to apply constant axial load onto the specimens. The salt specimens are placed into a triaxial (Hoek) cell to provide constant confining pressure. The digital gages are installed to measure the axial deformation (Figure 3.7). The specimens are instantaneously loaded to desired axial stress at 16.6 and 24.1 MPa for confining pressure of 3.4 MPa, and at 20.7 and 27.6 MPa for confining pressures of 6.9 MPa. During the test, the axial deformation and time are recorded. The frequency of reading is once every minute at the beginning of the test, and gradually reducing to once a day after the first few days of the test. This also depends on the deformation rate of each specimen. The results are presented by strain-time curves. The axial stress and axial strain values are calculated by Equations (3.1) and (3.2).

### 3.4.2 Test Results

Table 3.2 summarizes the triaxial creep test results. The axial strain-time curves are given in Figure 3.8. The curve represents instantaneous and transient creep states of salt specimens under a constant axial load and confining pressure. The instantaneous strains observed immediately after loading range from  $4.0 \times 10^{-3}$  to  $17.0 \times 10^{-3}$ . All specimens show the transient and steady creep phases until the end of the test. The axial strain rates in the steady state creep phase are  $0.1 \times 10^{-3}$  to  $0.6 \times 10^{-3}$  day<sup>-1</sup>. Post-tested observations the deformation increases rapidly at the beginning to the first few days of the test and tends to remain constant after that. All specimens have not been failed after finished test duration.



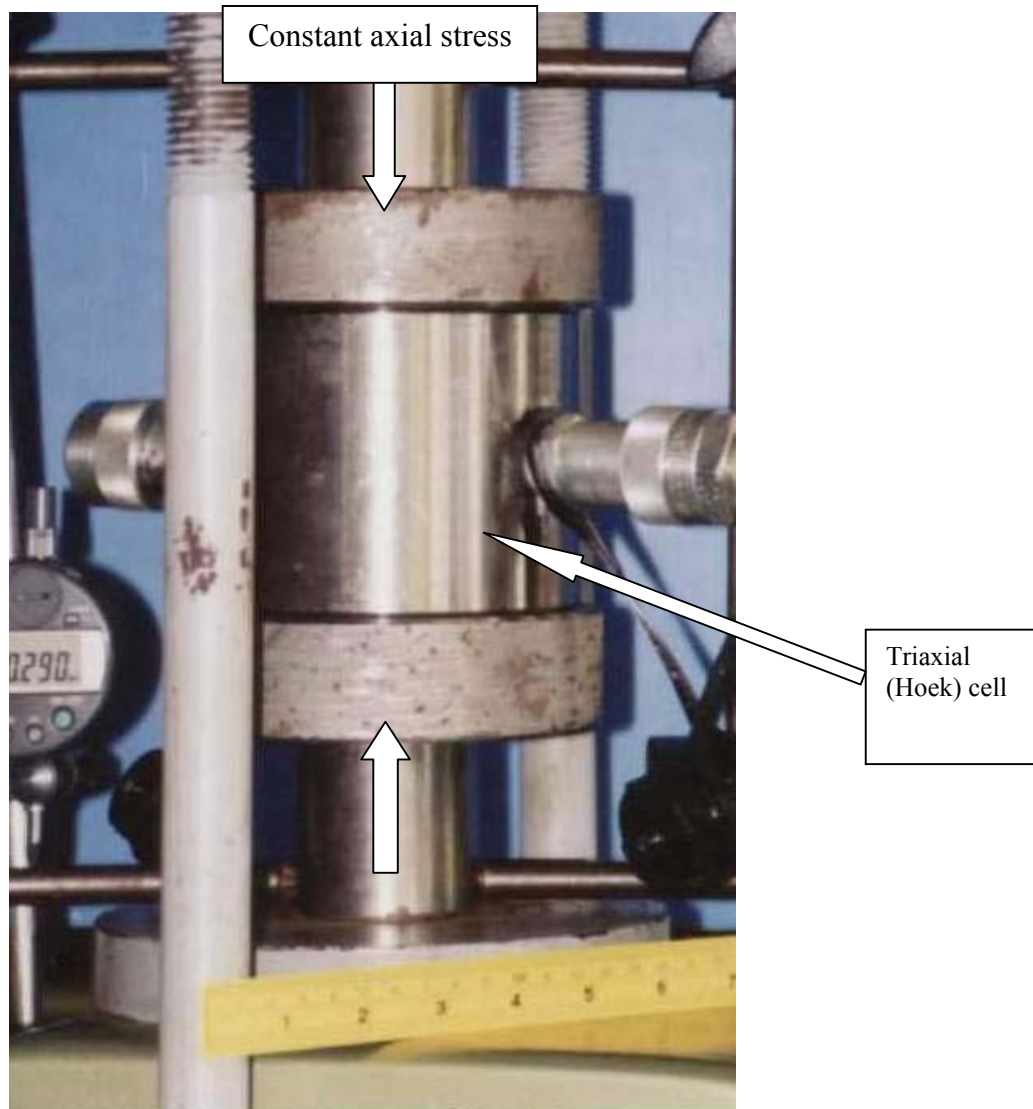


**Figure 3.7** Triaxial creep test with constant axial load under confining pressure. The cylindrical specimen placed inside Hoek cell is loaded vertically using the compression machine. Digital gages measure the axial deformation.

**Table 3.2** Summary of the triaxial creep test results on rock salt.

Specimen No.	Depth (m)	Average Diameter <b>D</b> (mm)	Average Length <b>L</b> (mm)	Constant Axial Stress $\sigma_1$ (MPa)	Constant Confining Pressure $\sigma_3$ (MPa)
BD99-1-TC01	419.03	55.42	113.00	24.1	3.4
BD99-1-TC03	419.95	55.47	111.33	16.6	3.4
BD99-1-TC10	210.99	55.52	110.00	20.7	6.9
BD99-1-TC11	325.17	55.57	110.00	27.6	6.9

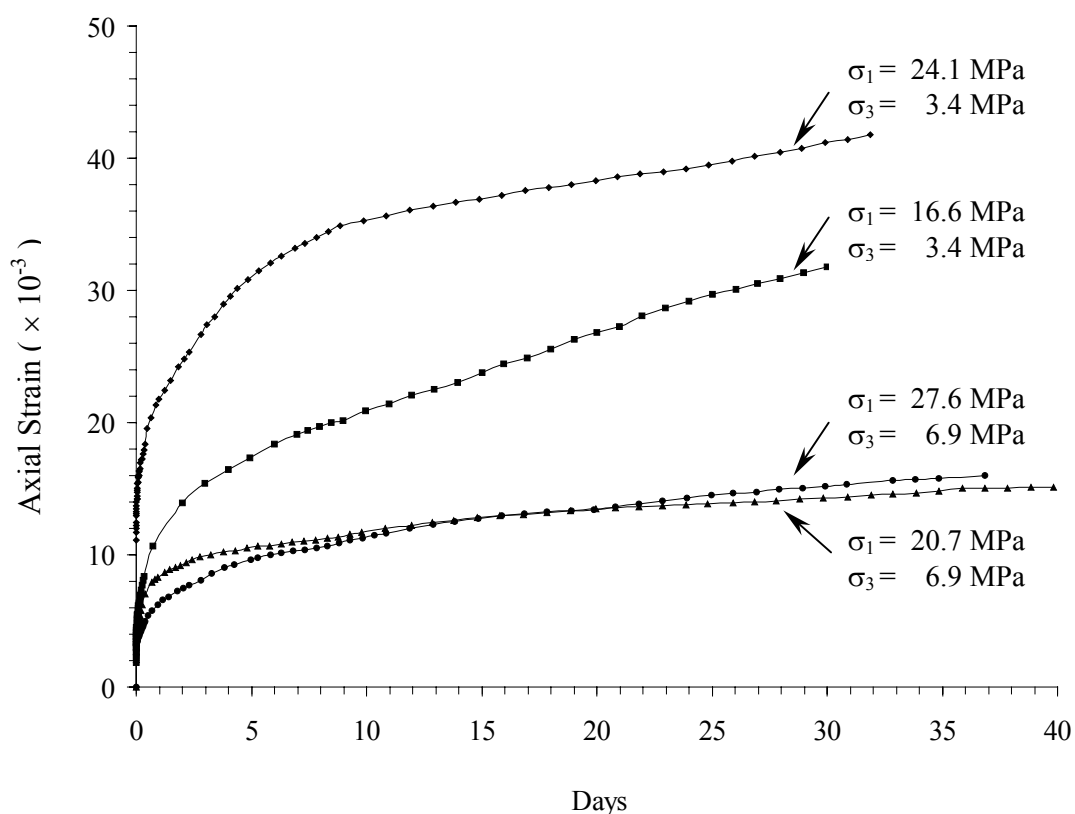


**Figure 3.8** Results of the triaxial creep testing. The confining pressures ( $\sigma_3$ ) = 3.4 and 6.9 MPa. The axial stresses ( $\sigma_1$ ) vary from 16.6 MPa to 27.6 MPa.

### 3.4.3 Discussions

The instantaneous creep strain depends on the axial stress and confining pressure. In general the increase of the constant axial stress induces a larger axial strain. The strain rate under higher axial stresses is greater than the one under lower axial stresses for the same constant confining pressure. The larger the confining pressure, the smaller the induced strain. Comparison of the results obtained from Maha Sarakham salt with those from other rock salts indicates that the strain rate depends on the stress and the previous strain. This also agrees with the finding by Korthaus (1996) and Ong et al., (1998) who describe that the salt is close to plastic behavior under high confining pressure. The axial strain rates in the steady state creep phase of Patience Lake Member are  $2.0 \times 10^{-3}$  to  $9.4 \times 10^{-3} \text{ day}^{-1}$  (Ong et al., 1998).

# **CHAPTER IV**

## **CALIBRATION OF ROCK SALT PROPERTIES**

### **4.1 Objectives**

The objective of this chapter is to describe the methods to determine the property parameters (constitutive parameters) for the rock salt by using the data from laboratory experiments. These properties include the shear modulus ( $G_1$ ), the retarded shear modulus ( $G_2$ ), the elastoviscosity ( $V_2$ ), the plastoviscosity ( $V_4$ ), the ultimate bulk modulus ( $K_1$ ), the retarded bulk modulus ( $K_2$ ), the critical shear strain ( $\gamma_c$ ), and the density gradient ( $\rho$ ). The test results in terms of stress-strain-time relationship have been used to calibrate these properties via the computer simulation. These tests include the uniaxial creep tests and the triaxial creep tests.

### **4.2 Constitutive Law used in this Study**

The constitutive law used here is called GEO (Fuenkajorn and Serata, 1992; Serata and Fuenkajorn, 1993). It is capable of simulating the elastic, visco-elastic, visco-plastic, strain softening and dilation behavior of time-dependent materials, such as rock salt. The detailed formulation and algorithm of the constitutive equations are described in Chapter II. These equations have been incorporated into a finite element code, named GEO.

### **4.3 Calibration and Calculation of Salt Property Parameters**

Wetchasat (2002) performs the uniaxial cyclic loading tests and the short and long-term uniaxial creep test on rock salt specimens from the same source of this research. The results are used to determine the basic parameters for salt properties. The average shear modulus, the ultimate bulk modulus, the retarded shear modulus, the retarded bulk modulus, the elastoviscosity, the plastoviscosity and the critical shear strain equal 8.8 GPa, 41.1 GPa, 1.1 GPa, 4.9 GPa, 9.1 GPa·day, 17.2 GPa·day and  $2 \times 10^{-3}$ , respectively (see Table 4.1). By assuming that the results obtained from Wetchasat are applicable to the rock salt tested in this research, his properties are therefore used as basic properties here. The plastoviscosity represent the time-dependent deformations of the salt. Wetchasat performed only the uniaxial creep tests on three salt specimens for determination of plastoviscosity. The in-situ conditions of the salt are under confined conditions. The triaxial creep tests will be necessitated to determine the plastoviscosity.

#### **4.3.1 Determination of Plastoviscosity from Uniaxial Creep Test**

The objective of this task is to determine the visco-plastic coefficient of the salt. A single element mesh (Figure 4.1) is constructed to represent a vertical cross-section of the salt specimen. The mesh is designed for axisymmetric analysis by using the salt specimen axis as a centerline. It represents the top-right quarter of a salt specimen. It is 30 millimeters wide and 78 millimeters long. The left boundary of the mesh represents the centerline of the specimen. It is fixed in lateral direction. The bottom boundary of the mesh does not allow vertical displacement. The right

boundary of the mesh can be freely deformed in both lateral and vertical directions.

The top boundary of the mesh is subject to the uniform loads.

**Table 4.1** Properties used in computer modeling (Wetchasat, 2002).

Behavior	Properties	Units	Ranges	Average values	Test types
Elastic	Shear Modulus	GPa	8.7 - 9	8.8	CY
	Ultimate Bulk Modulus	GPa	40.6 - 42	41.1	CY
Visco-Elastic	Retarded Shear Modulus ( $\tau_0 < K_0$ )	GPa	0.2 - 2.1	1.1	CR
	Retarded Bulk Modulus	GPa	0.9 - 9.8	4.9	CR
	Elastoviscosity ( $\tau_0 < K_0$ )	GPa·day	0.1 - 17	9.1	CR
Visco-Plastic	Plastoviscosity ( $\tau_0 < K_0$ )	GPa·day	6.9 - 27.6	17.2	CP
Strength	Critical Shear Strain at Failure	$10^{-3}$	2	2	CY

**Note:** CY = Uniaxial cyclic loading tests; CR = Short-term uniaxial creep tests

CP = Long-term uniaxial creep tests

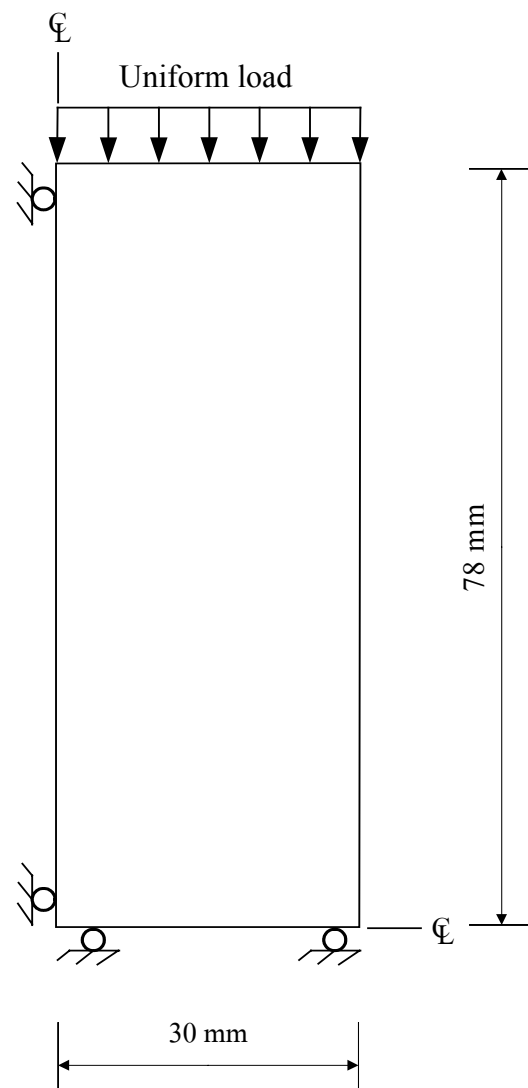


**Figure 4.1** Single element mesh used in the calibration of the uniaxial creep test results.

Initial (average) values of the shear modulus, the ultimate bulk modulus, the retarded shear modulus, the retarded bulk modulus, the elastoviscosity and the critical shear strain obtained from Wetchasat (2002) are set in the computer modeling. The instantaneous strain in the strain-time curves (Figure 4.2) is adjusted from the initial values until the instantaneous strain from the computer simulation matches the actual experimental results. The slopes and the curvatures (in visco-elastic phase) are also adjusted from the initial values until the slopes and the curvatures from the simulation match the actual experimental results. The best value of plastoviscosity is obtained by adjusting the computer simulation until it matches the actual experimental results. Table 4.2 summarizes the property parameters of the salt specimens obtained from the computer modeling for the uniaxial creep tests. The average value from three specimens is 12.4 GPa·day.

#### **4.3.2 Determination of Plastoviscosity from Triaxial Creep Test**

Figure 4.3 shows the single element mesh used in calibration of the triaxial creep test results to determine plastoviscosity. It has the same characteristics and properties as the single element mesh used in calibration of the uniaxial creep test results, except the right boundary of the element mesh is compressed by confining pressure.

Results from the long-term triaxial creep tests are used to determine plastoviscosity. Methods of calibration are similar to the calibration of the uniaxial creep test results. Figure 4.4 shows calibration results. Table 4.3 summarizes the property parameters of the salt specimens obtained from the computer modeling for the triaxial creep test. The average plastoviscosity from four specimens is 52.0 GPa·day.



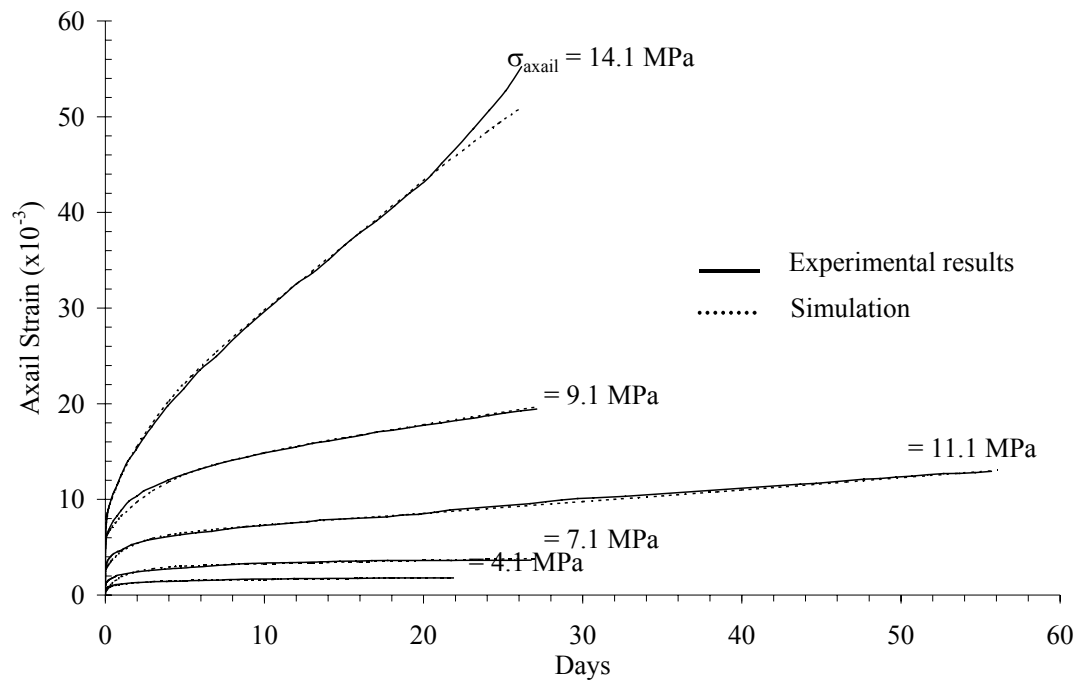


**Figure 4.2** Comparisons between the simulation and the experimental results for the uniaxial creep test at constant axial stresses of 4.1, 7.1, 9.1, 11.1, and 14.1 MPa.

**Table 4.2** Summary of the property parameters of the salt specimens obtained from the computer modeling for the uniaxial creep tests.

Property	Symbol	Unit	Initial value	Constant axial stresses					Results from calibration (average)
				7.1 MPa	11.1 MPa	4.1 MPa	9.1 MPa	14.1 MPa	
Shear modulus	$G_1$	GPa	8.8	2.1	1.2	1.7	0.4	0.4	-
Retarded shear modulus	$G_2$	GPa	1.1	0.9	0.8	1.4	0.3	0.4	-
Elastoviscosity	$V_2$	GPa·day	9.1	1.2	1.4	1.4	0.6	0.8	-
Plastoviscosity	$V_4$	GPa·day	-	27.6	17.2	6.9	7.7	2.4	12.4
Ultimate bulk modulus	$K_1$	GPa	41.1	9.7	5.8	7.6	27.6	27.6	-
Retarded bulk modulus	$K_2$	GPa	4.9	4.1	3.9	7.6	4.8	4.8	-
Critical shear strain at failure	$\gamma_c$	$10^{-3}$	2	2	2	2	2	2	-

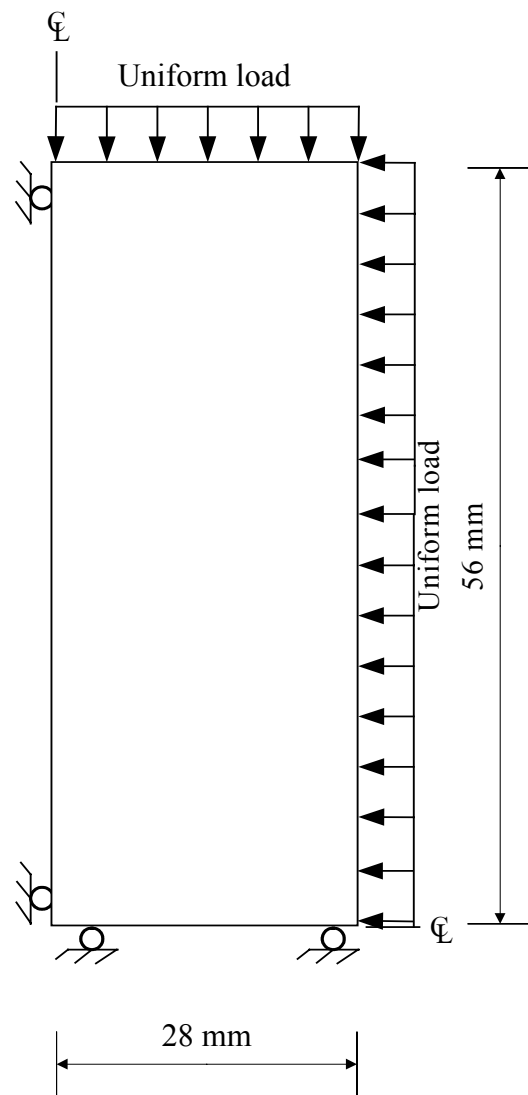


**Figure 4.3** Single element mesh used in calibration of the triaxial creep test results.

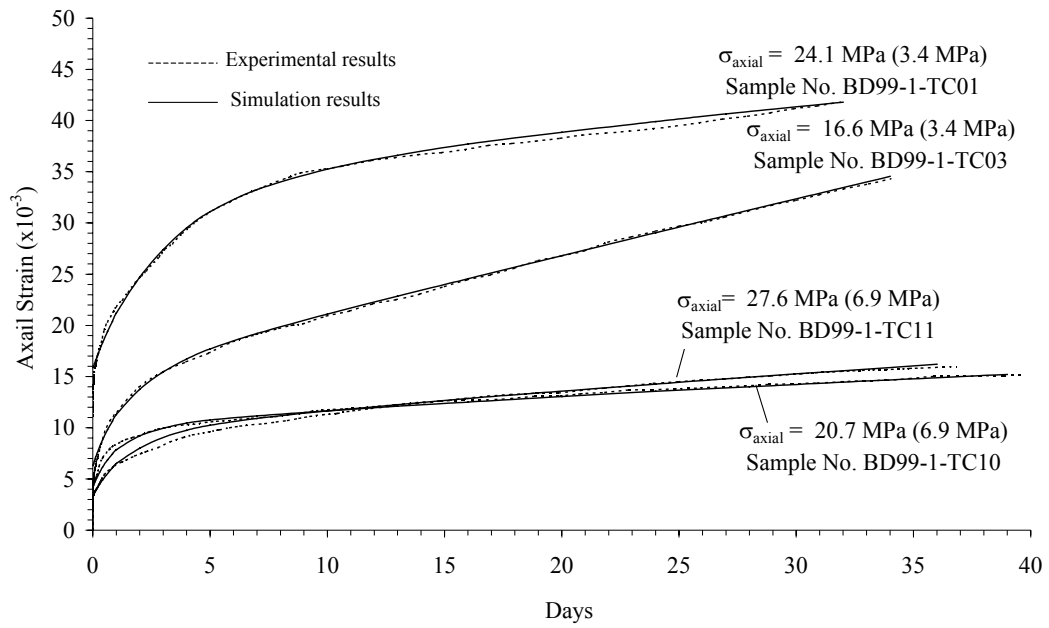


**Figure 4.4** Comparisons between the simulation and the experimental results for the triaxial creep test results at constant axial stress of 20.7 and 27.6 MPa (for constant confining pressure of 6.9 MPa) and 16.6 and 24.1 MPa (for constant confining pressure of 3.4 MPa).

**Table 4.3** Summary of the property parameters of the salt specimens obtained from the computer modeling for the triaxial creep test.

Property	Symbol	Unit	Initial value	24.1 MPa* (500 psi **)	16.6 MPa* (500 psi **)	20.7 MPa* (1000 psi **)	27.6 MPa* (1000 psi **)	Results from calibration (average)
Shear modulus	$G_1$	GPa	8.8	1.1	0.5	0.93	2.4	-
Retarded shear modulus	$G_2$	GPa	1.1	0.003	0.03	0.04	3.4	-
Elastoviscosity	$V_2$	GPa·day	9.1	3.7	1.3	3.80	3.4	-
Plastoviscosity	$V_4$	GPa·day	-	5.8	29.9	93.10	79.3	52.0
Ultimate bulk modulus	$K_1$	GPa	41.1	12.1	1	13.10	6.6	-
Retarded bulk modulus	$K_2$	GPa	4.9	0.4	0.7	0.70	0.6	-
Critical shear strain at failure	$\gamma_c$	$10^{-3}$	2	1	1	1.00	1.0	-

**Note:** \* Constant axial stresses

\*\* Constant confining pressure

#### **4.4 Discussions**

By using the finite element code GEO, the property parameters of the salt specimens are simulated and compared with the experimental results. The model simulations provide good fit to the experimental results. Table 4.4 compares the range of parameters and the selected values.

The values of the plastoviscosity obtained from the uniaxial and triaxial creep tests vary from 2.4 to 93.1 GPa-day (specimens no. CP02, CP06, CP07, TC01, TC03, TC10, and TC11). In most cases the plastoviscosity are calibrated from test results of specimens under high axial stresses is greater than the one under low axial stresses. The long-term creep simulations provide a good fit for each constant stress. The actual experimental results have sufficient data to simulate the value of plastoviscosity. Variations may be caused by intrinsic variabilities of salt such as inclusion (anhydrite and iron oxide). The plastoviscosity is relatively high as compared with those from Serata and Fuenkajorn (1993) and Wetchasat (2002).

**Table 4.4** Comparison of the range of parameters and the selected values.

Phase	Properties	Units	Ranges	Average values	Test types
Elastic	Shear Modulus	GPa	8.7 – 9.0	8.8	CY
	Ultimate Bulk Modulus	GPa	40.6 – 42.0	41.1	CY
Visco-Elastic	Retarded Shear Modulus ( $\tau_0 < K_0$ )	GPa	0.2 – 2.1	1.1	CR
	Retarded Bulk Modulus	GPa	0.9 – 9.8	4.9	CP
	Elastoviscosity ( $\tau_0 < K_0$ )	GPa·day	0.1 – 17.0	9.1	CR
Visco-Plastic	Plastoviscosity	GPa·day	2.4-93.1	33.6	CP & TC
Strength	Critical Shear Strain at Failure	$10^{-3}$	2	2	CY

**Note:** CY = cyclic loading tests,

CR = short-term uniaxial creep tests,

CP = long-term uniaxial creep tests, and

TC = long-term triaxial creep tests

# **CHAPTER V**

## **COMPUTER MODELING**

### **5.1 Objectives**

The objective of the computer modeling is to determine the time-dependent ground surface subsidence through 500 years after emplacement, the vertical opening closure, the salt pillar, roof and floor deformations, the octahedral shear stress and strain and the principal stresses and strains around the salt opening through 50 years. The results are compared to study the effect of opening widths, pillar widths and depths for three example areas. The results are compared to select the most suitable opening width, pillar width and opening depth for the repository. The non-linear finite elements program, GEO (Serata and Fuenkajorn, 1991, 1992a, 1992b; Stormont and Fuenkajorn, 1994; Fuenkajorn and Serata, 1994) and the salt property parameters (in Chapter IV) are used in the computer modeling. The GEO constitutive equations are given in Chapter II.

### **5.2 Rock Salt Formations used in this Study**

The sequences of rock salt in Thailand have been compiled by many investigators (Japan International Cooperation Agency, 1981; Suwanich et al., 1982; Suwanich and Ratanajaruraks, 1986). They are obtained from the logging of 194 exploratory boreholes drilled as part of the potash exploration project in the northeast of Thailand. The locations of the 194 boreholes are shown in Figures 5.1 and 5.2



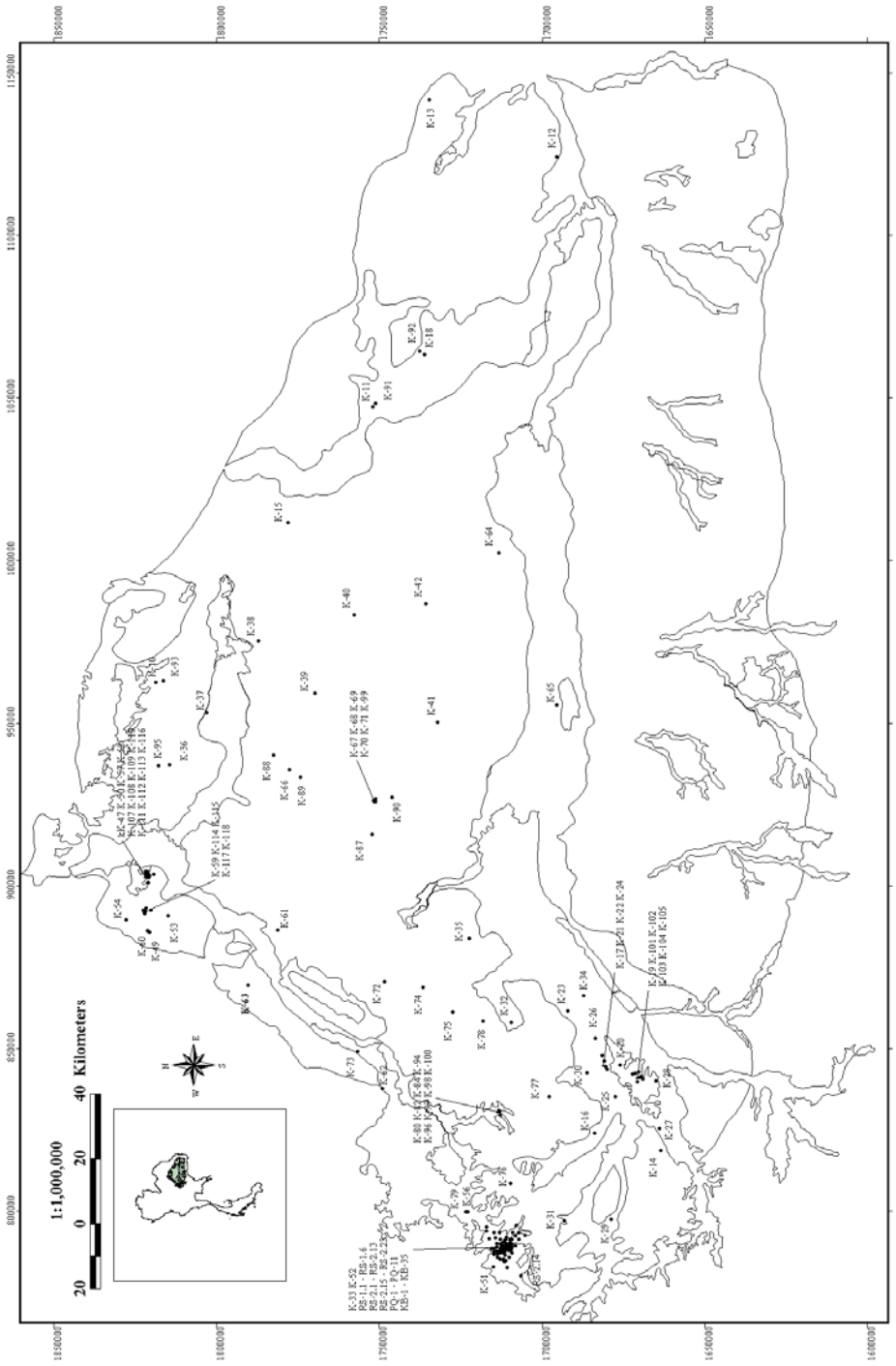
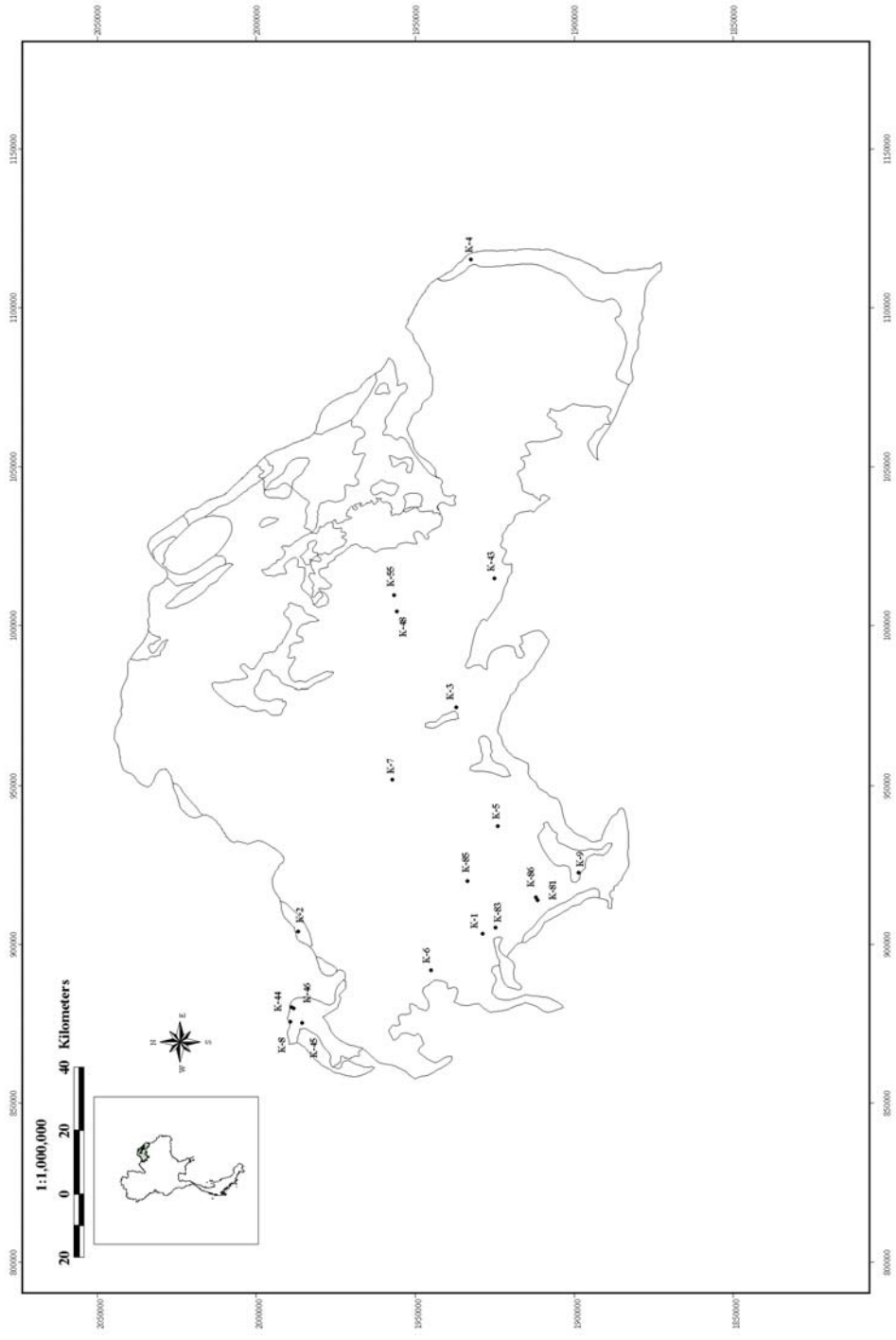


Figure 5.1 Location of borehole in Khorat Basin in the northeast of Thailand.



**Figure 5.2** Location of borehole in Sakon Nakhon Basin in the northeast of Thailand.

(Japakasetr, 1985). For this research, no attempt has been made at performing additional in-situ drilling or conducting any geological and geophysical exploration. It is assumed here that the pre-existing information is correct and reliable.

For an ease of modeling and design, the stratigraphic formations of rock salt and associated rocks have been reclassified here into three main geomechanics groups: 1) associated rocks, 2) rock salt, and 3) sandstone/siltstone groups. The associated rocks include all geological formations between and above the salt formations (e.g., anhydrite, mudstone, clay, clay stone, siltstone, conglomerate, terrain sediment, alluvial deposits, and more). The rock salt group represents the Upper Salt, Middle Salt and Lower Salt members. The sandstone/siltstone group represents all rock formations above and below the Lower Salt member.

One of the difficulties in selecting a suitable repository site is that the salt formations in Thailand are relatively thin and shallow. The selected criteria used here are the thickness and depth of the rock salt formations as compares with other repository sites as described in chapter II (see Table 2.1). Based on these case studies and from the available information from the drilled holes, three areas in the Khorat Plateau have been taken into consideration. These areas will be used as case examples because they provide suitable geology in terms of salt thickness and depth. The study areas are shown in Figure 5.3. Figure 5.4 shows the simplified stratigraphy of the three areas that have been reclassified in this study based on the above criteria. The locations are referred to by using the name of the areas where the corresponding original drilled holes are located. The original stratigraphy is shown in Figures A.1 - A.3 in Appendix A. Table 5.1 lists the names of these locations for both Sakon Nakhon and Khorat basins.

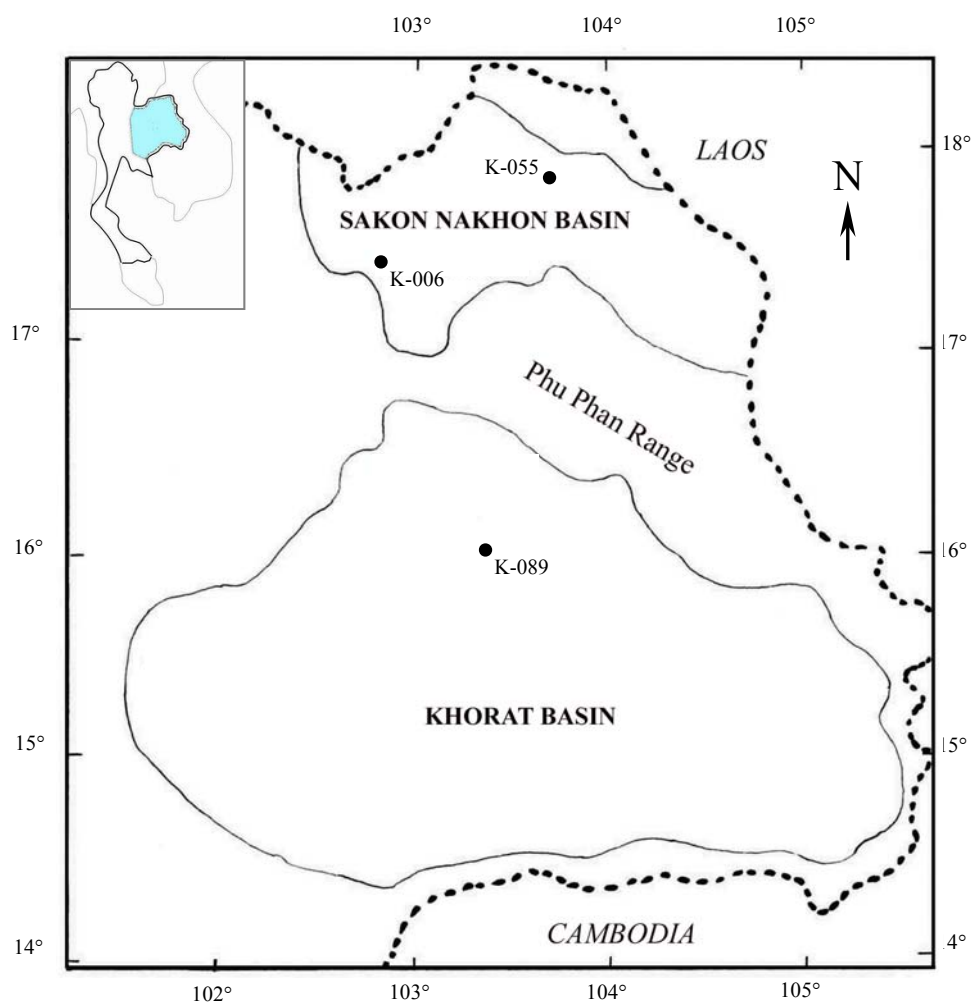


**Figure 5.3** Locations of the three study areas in Khorat and Sakon Nakhon basins in the northeast of Thailand.

K-006 = Ban Kao, Muang District, Udon Thani Province

K-055 = Ban Kudjig, Wanon Niwat District, Sakon Nakhon Province

K-089 = Ban Nong Plue, Borabue District, Maha Sarakham Province

(modified from Japan International Cooperation Agency, 1981)

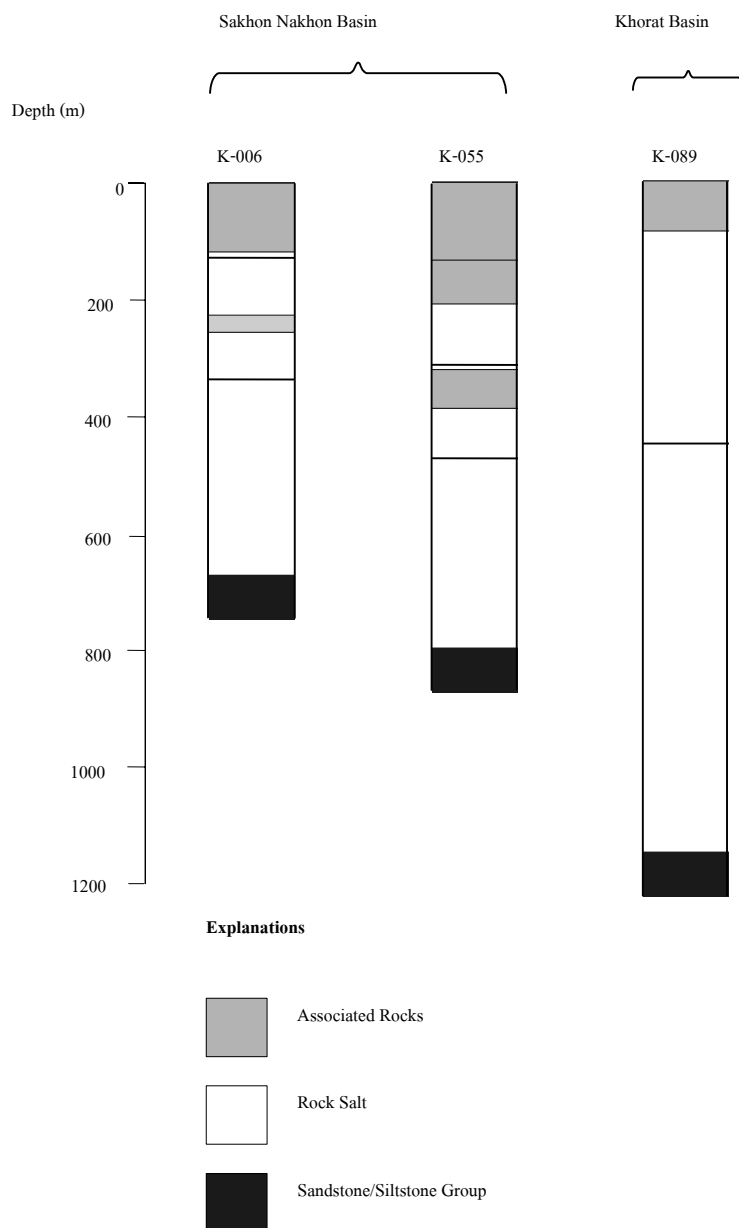


**Figure 5.4** Simplified stratigraphy of salt and associated rocks in Sakon Nakhon and Khorat basins, after reclassification into three geomechanics groups.

**Table 5.1** Selected areas in Sakon Nakhon and Khorat basins used in this research.

<b>Basin</b>	<b>Location</b>	<b>Borehole No.</b>	<b>Model</b>
Sakon Nakhon	1) Ban Kao, Muang District, Udon Thani Province	K-006	KM-P1, KM-P2, KM-P3, KM-P4, KM-P5, KM-P9, KM-R4, KM-R6, KM-R8
	2) Ban Kudjig, Wanon Niwat District, Sakon Nakhon Province	K-055	KW-P4
Khorat	1) Ban Nong Plue, Borabue District, Maha Sarakham Province	K-089	NB-P4

**Notes:** KM = Ban Kao, Muang District, Udon Thani Province

KW = Ban Kudjig, Wanon Niwat District, Sakon Nakhon Province

NB = Ban Nong Plue, Borabue District, Maha Sarakham Province

P1, P2, P3, P4, P5, P9 = Pillar width = 4, 8, 12, 16, 20, 36 meters

R4, R6, R8 = Room width = 4, 6, 8 meters

### **5.3 Property Parameters used in Computer Modeling**

Table 5.2 summarizes the property parameters for three material groups used in the computer model. Three material groups include of associated rocks, rock salt, and sandstone/siltstone formations. Numerical values of the salt property parameters are obtained from the calculation and calibration in Chapter IV and Wetchasat (2002). The average numerical values are selected for the computer modeling for a conservative approach. The properties of associated rocks and the sandstone/siltstone are taken from GEO database because the specimens are not available for testing. Conservative approach has also been taken into the assignment of each parameter.

In-situ stress is taken to be hydrostatic for conservative assumption. The density gradient of rock salt is 21.1 kPa/m and 27.1 kPa/m of clay stone and silt/sand stone.

### **5.4 Underground Repository**

This task describes the concept used to design the repository rooms. The key design requirements include, 1) the mechanical stability during the emplacement period of 50 years, 2) the containment integrity for the repository during the isolation period of 500 years, and 3) minimization of the movement of the surrounding rock formations. To meet these requirements, the longwall pillar concept is proposed. The repository rooms are arranged in a parallel pattern, connecting to a main entry. The height of the repository room is defined to be 4 meters to satisfy most available equipment. The longwall pillar mining method is described in detail by Jeremic (1994). The design parameters for the repository room are shown in Figure 5.5. An important advantage of this method is that nuclear wastes can be removed from

**Table 5.2** Material properties used in computer modeling (from Wetchasat, 2002).

<b>Behavior</b>	<b>Properties</b>	<b>Units</b>	<b>Associated Rocks</b>	<b>Rock Salt</b>	<b>Sandstone/Siltstone</b>
Elastic	Shear Modulus	GPa	0.3	8.8	13.8
	Ultimate Bulk Modulus	GPa	1.7	41.1	82.8
Visco-Elastic	Retarded Shear Modulus	GPa	0.3	1.1	13.8
	Retarded Bulk Modulus	GPa	1.4	4.9	82.8
	Elastoviscosity	GPa-day	0.3	9.1	3.4
	Plastoviscosity	GPa-day	2.8	33.6	13.8
Strength	Critical Shear Strain at Failure	$10^{-3}$	10	2	2
	Density Gradient	MPa/m	0.027	0.021	0.027



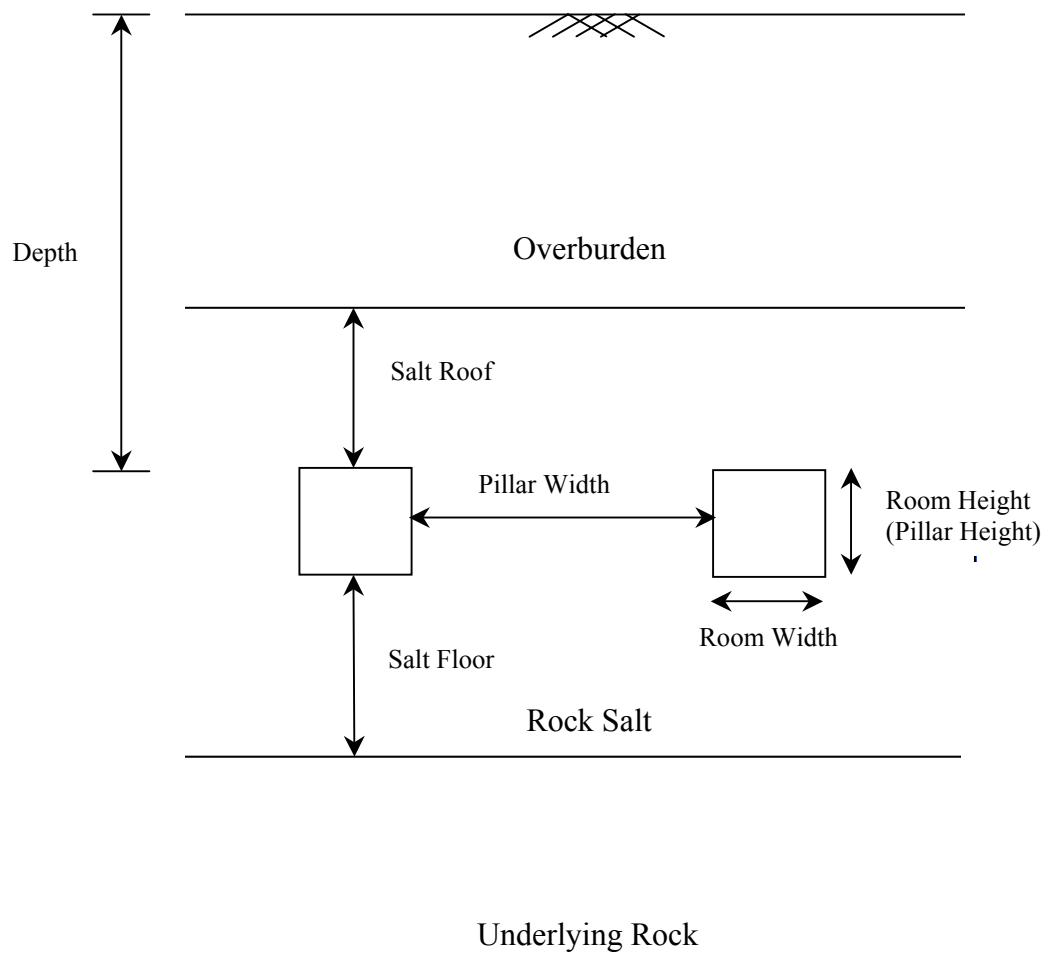


**Figure 5.5** Design parameters for repository rooms.

underground if later proved that the repository is unsafe. This study assumes that the backfills are installed at 50 years after emplacement. The computations of room behavior are concentrated at 50 years after waste emplacement. The surface subsidence is however calculated at 500 years after opening.

## **5.5 Finite Element Mesh for Repository Room**

Three series of finite element analyses have been carried out to design the most suitable width and depth of the repository room and pillar size. Details of the mesh design for each series of analysis are given in the following subsections.

### **5.5.1 Study on the Effect of Opening Widths**

The geologic sequence at Ban Kao, Muang District, Udon Thani Province is used to construct three finite element models (models KM-R4, KM-R6 and KM-R8) that have the room widths varying from 4, 6 to 8 meters. Figure 5.6 shows the geometry and geology of the repository room in rock salt formation for these models. The finite element models include square and rectangle openings with different widths. Figure 5.7 shows the close-up finite element mesh of model KM-R4. The complete mesh is constructed to represent a vertical cross-section of the repository room. The surrounding rocks are discretized from the ground surface to the depth of 800 meters. The mesh is designed for plane strain analysis using the opening and pillar axes as centerlines. It covers a horizontal distance of 40 meters. The left boundary represents the opening centerline and is laterally constrained. The right boundary represents the pillar centerline. In order to show the opening boundaries, the elements inside the room are not drawn in the Figure. The top and bottom of the repository room are located at depths of 502 meters and 506 meters. The opening is

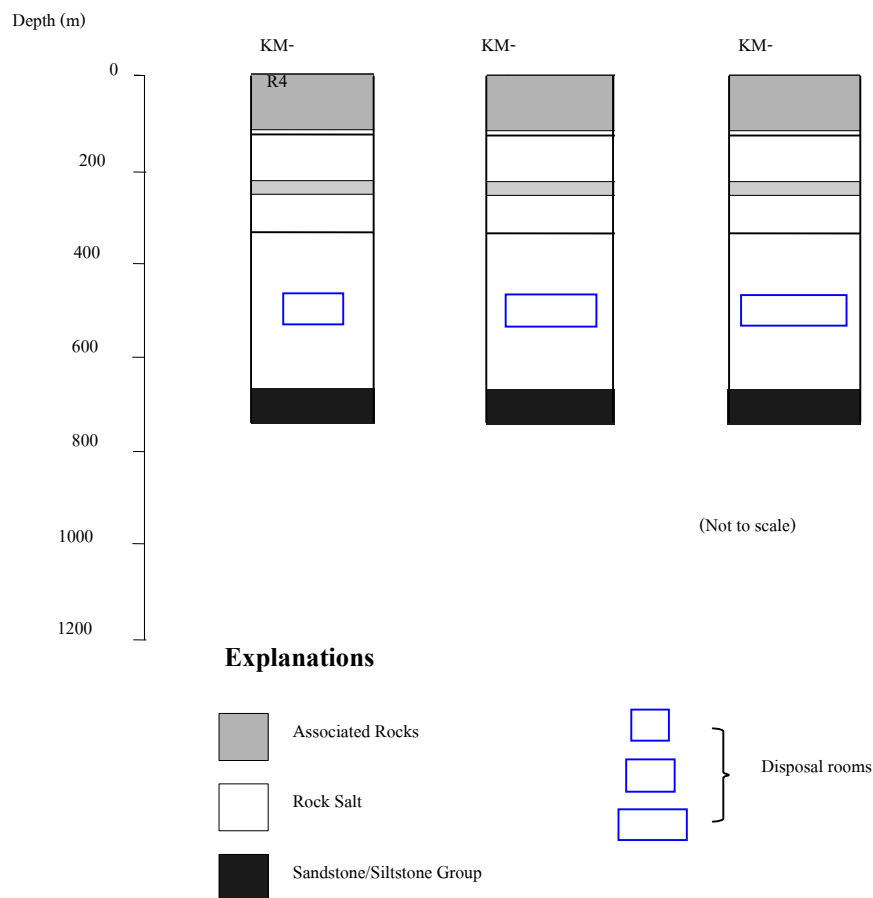


**Figure 5.6** Repository rooms in rock salt formation designed to study the effect of room width. Stratigraphy of salt and associated rocks in Ban Kao, Muang District, Udon Thani Province is used in the study. The room widths vary from 4, 6 to 8 meters.

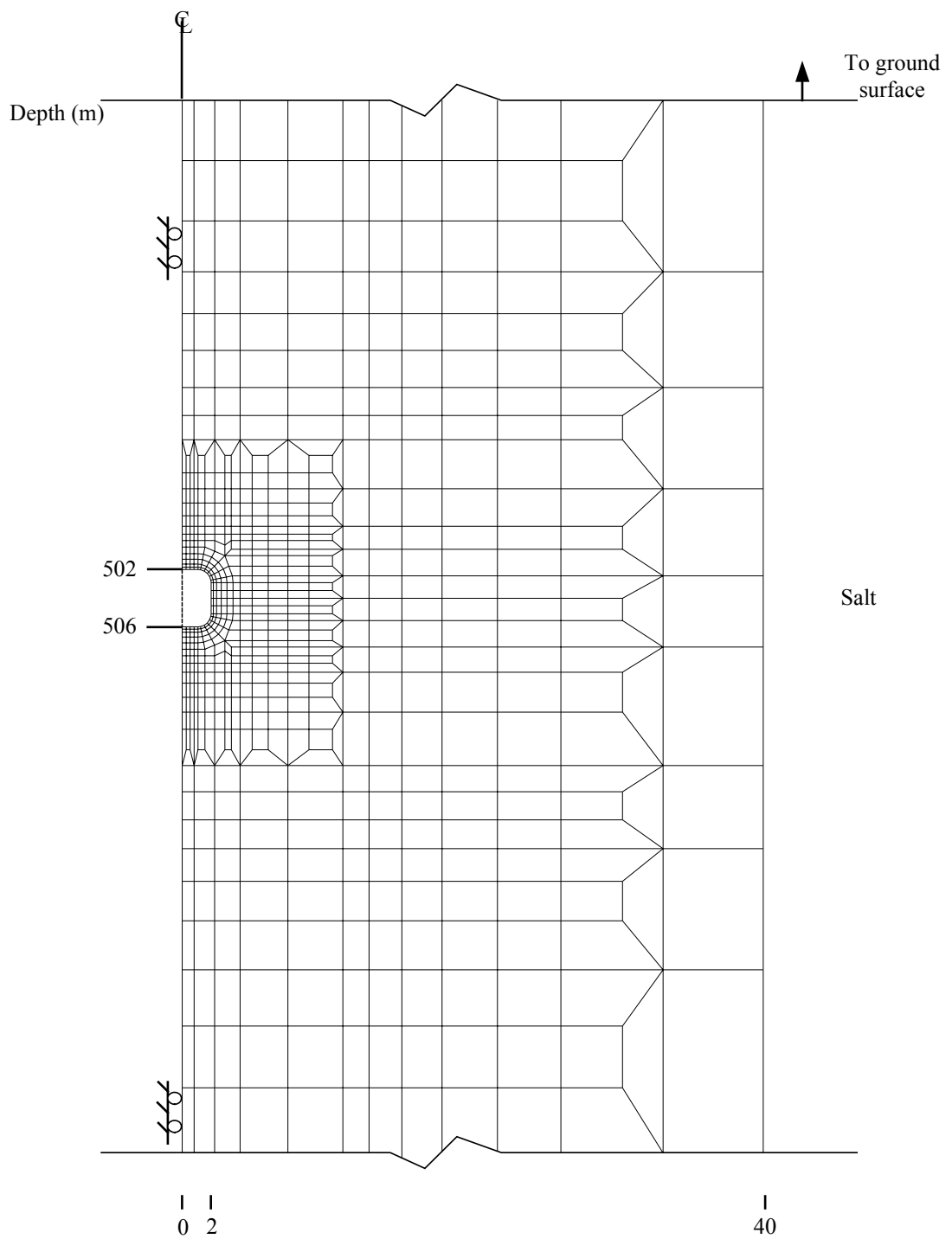


**Figure 5.7** Close-up finite element mesh for model KM-R4 at Ban Khao, Muang District, Udon Thani Province. Room width is 4 meters.

assumed to be a square opening with a room width of 4 meters and height of 4 meters. Small elements (0.5 meters  $\times$  0.5 meters) are used adjacent to and near the opening boundaries to capture the detailed distribution of the stresses and strains under high gradients. Larger elements are used in the overburden (far from the salt roof), as its behavior does not impact the opening stability. The overburden is included in the analysis in order to provide the gravitational force on the salt opening, and to allow an assessment of the ground surface subsidence. Figures 5.8 and 5.9 show the close-up finite element mesh of models KM-R6 and KM-P8. The model characteristics (the mesh construction, the analysis method and the opening depth) are similar to those of the model KM-R4. They are assumed to be rectangle opening with room width of 6 meters and 8 meters. Small elements (0.5 meters  $\times$  0.6 meters) are close to the opening boundaries.

### **5.5.2 Study on the Effect of Pillar Widths**

The study area at Ban Kao, Muang District, Udon Thani Province is selected for studying the effect of pillar widths. Six finite element models (models KM-P1, KM-P2, KM-P3, KM-P4, KM-P5 and KM-P9) are constructed to represent the repository rooms that have the pillar widths varying from 4, 8, 12, 16, 20 to 36 meters. The geometry and locations of the repository rooms in rock salt formation for these models are show in Figure 5.10. The room width and height of all finite element models are 4 meters. Figures 5.11 – 5.16 show the close-up finite element mesh of models KM-P1, KM-P2, KM-P3, KM-P4, KM-P5 and KM-P9. The model characteristics (the mesh construction, the analysis method and the opening depth) are similar to those of the model KM-R4. They are assumed to be square opening with

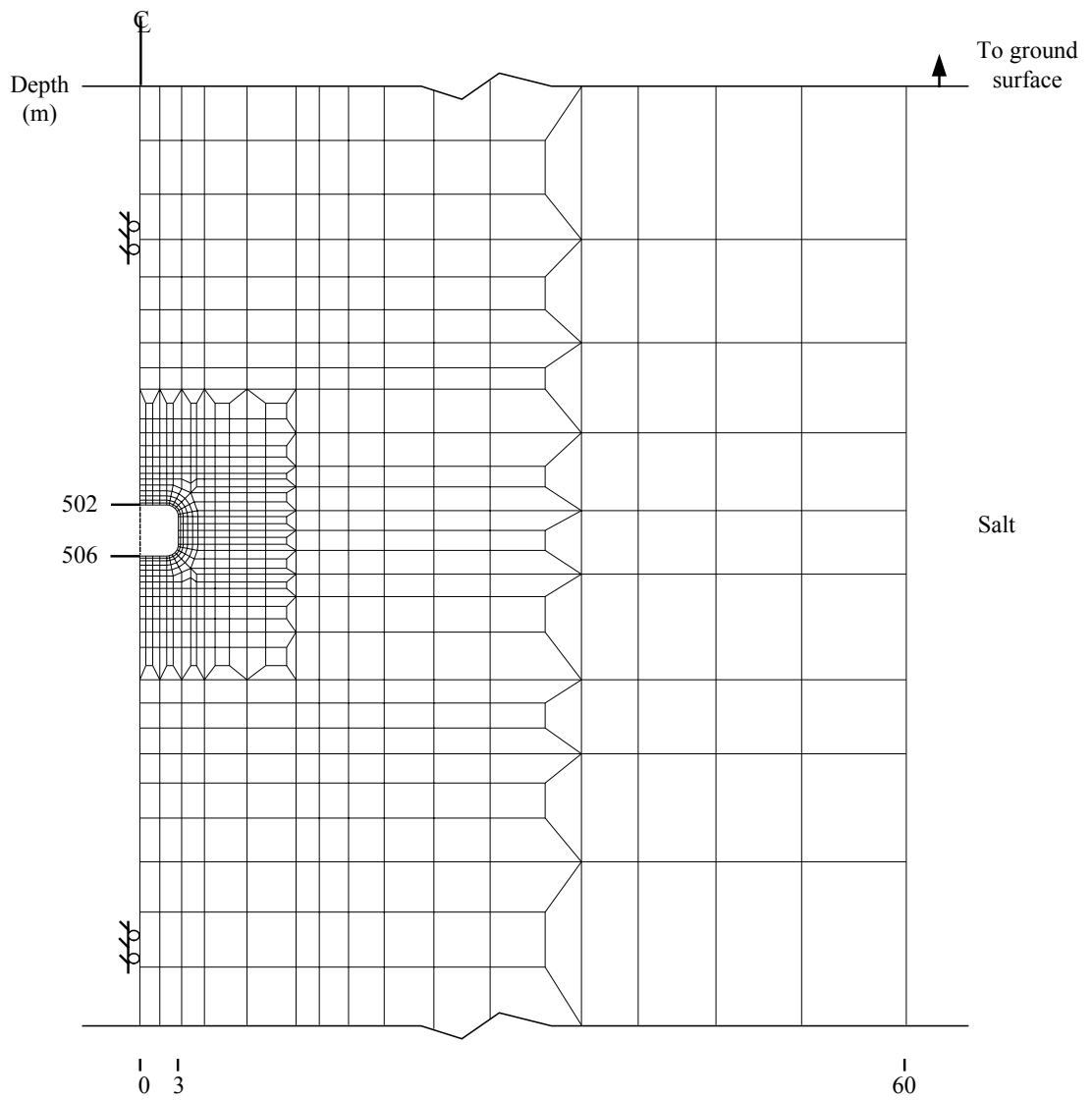


**Figure 5.8** Close-up finite element mesh for model KM-R6 at Ban Khao, Muang District, Udon Thani Province. Room width is 6 meters.

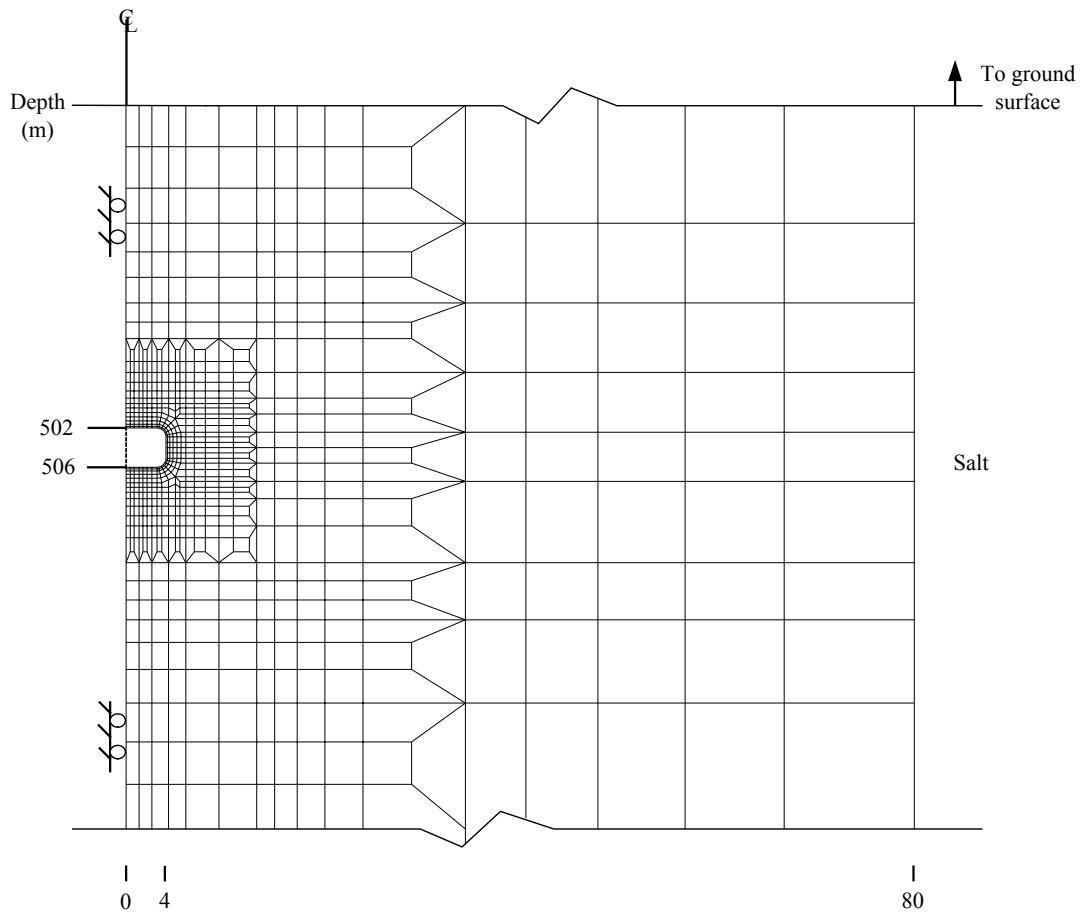


**Figure 5.9** Close-up finite element mesh for model KM-R8 at Ban Khao, Muang District, Udon Thani Province. Room width is 8 meters.

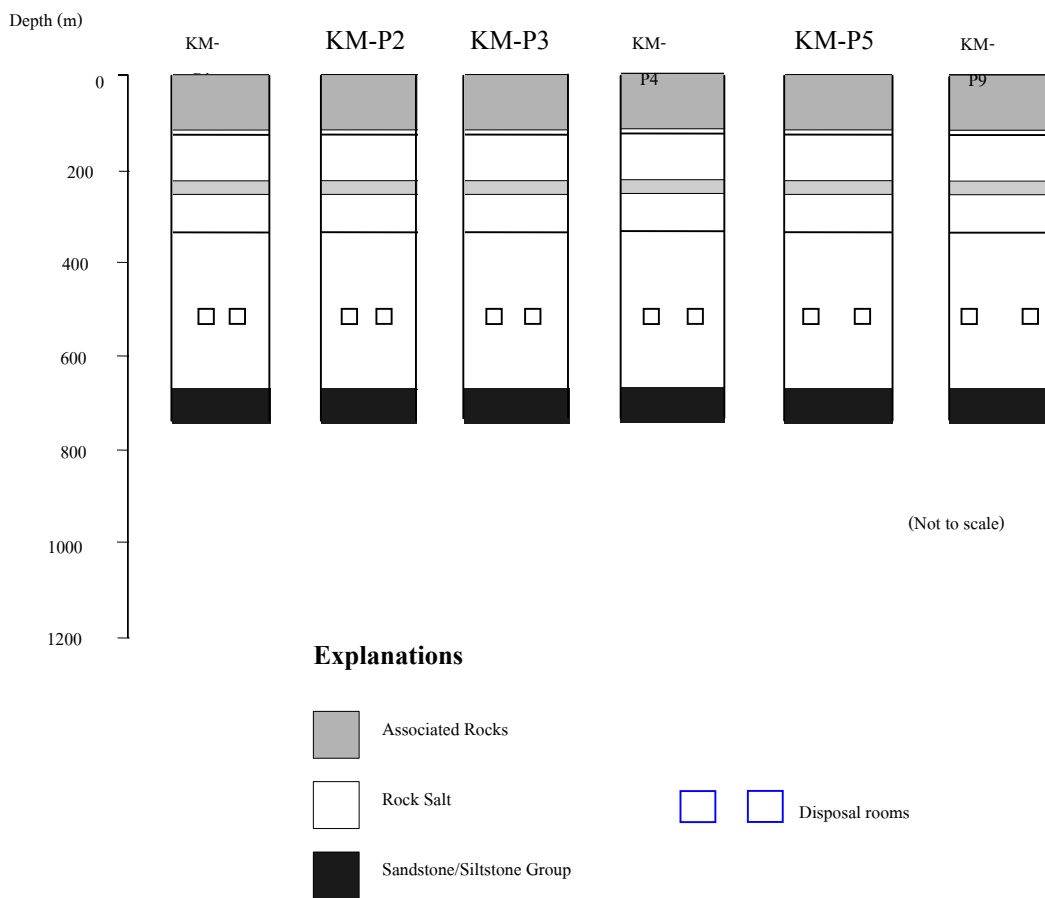


**Figure 5.10** Repository rooms in rock salt formation defined to study the effect of pillar width. Stratigraphy of salt and associated rocks in Ban Kao, Muang District, Udon Thani Province is used in the study. The pillar widths vary from 4, 8, 12, 16, 20 to 36 meters.



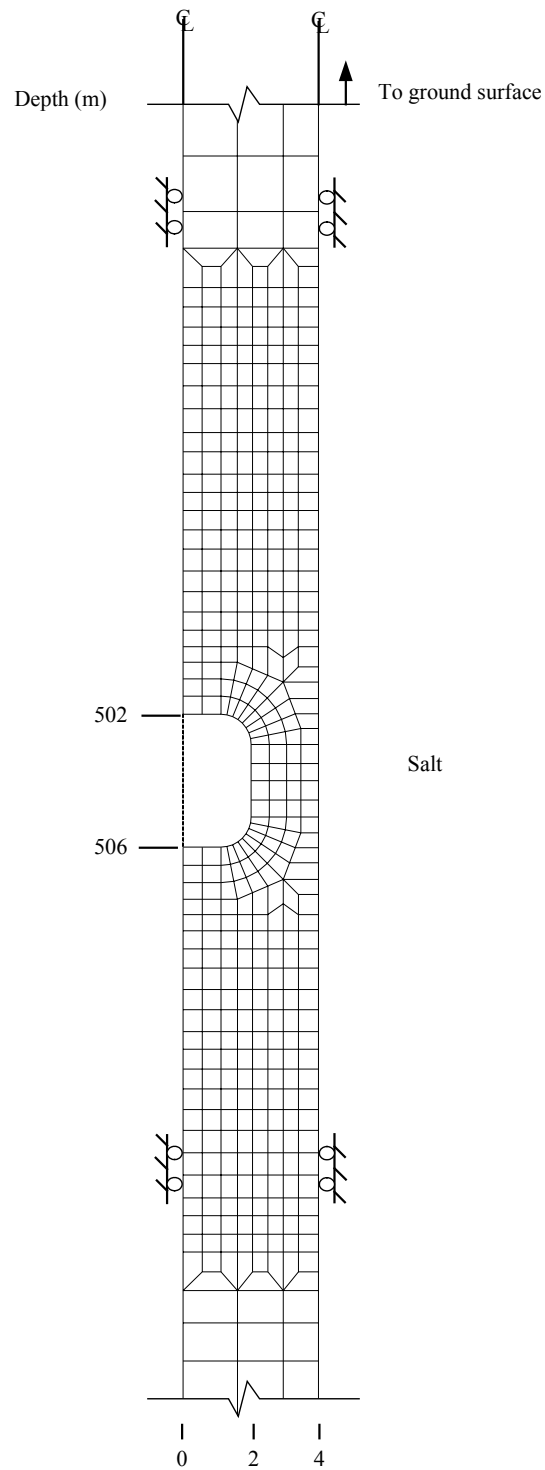


**Figure 5.11** Close-up finite element mesh for model KM-P1 at Ban Khao, Muang District, Udon Thani Province. Room and pillar widths are 4 meters.

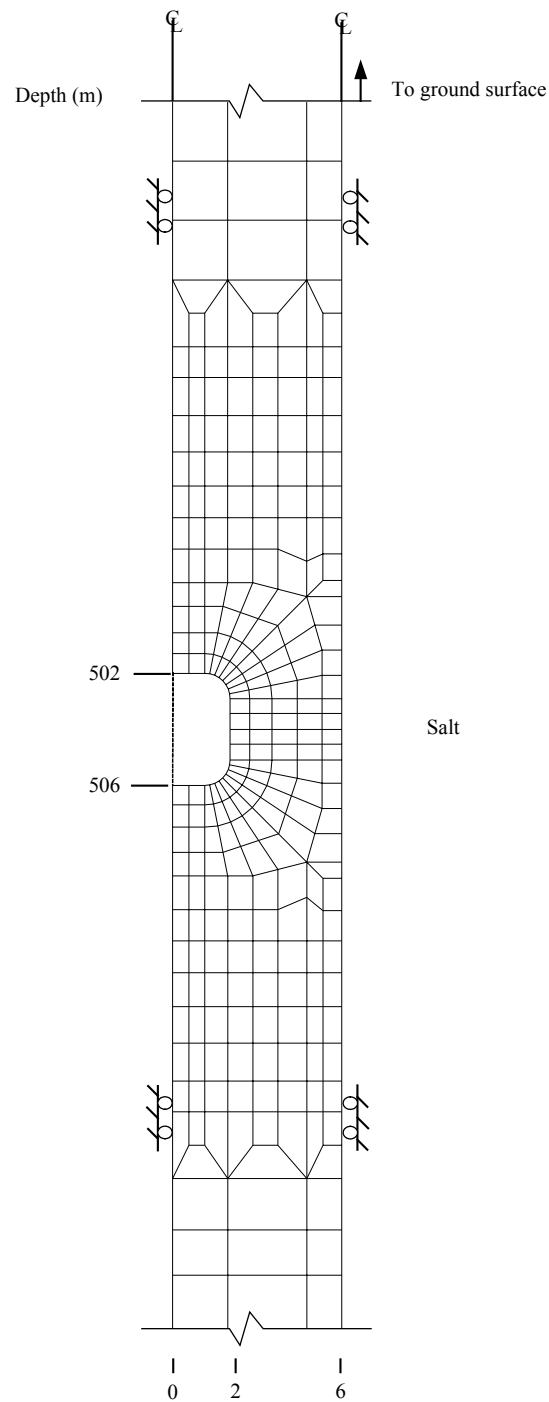


**Figure 5.12** Close-up finite element mesh for model KM-P2 at Ban Khao, Muang District, Udon Thani Province. Room and pillar widths are 4 and 8 meters, respectively.

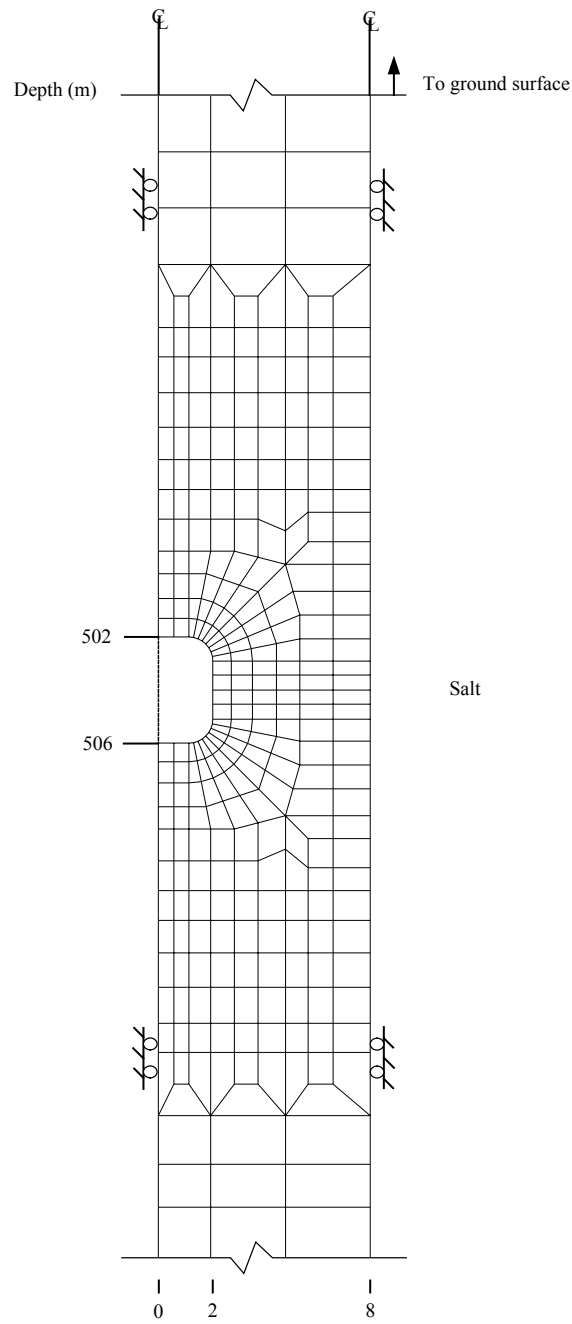


**Figure 5.13** Close-up finite element mesh for model KM-P3 at Ban Khao, Muang District, Udon Thani Province. Room and pillar widths are 4 and 12 meters, respectively.

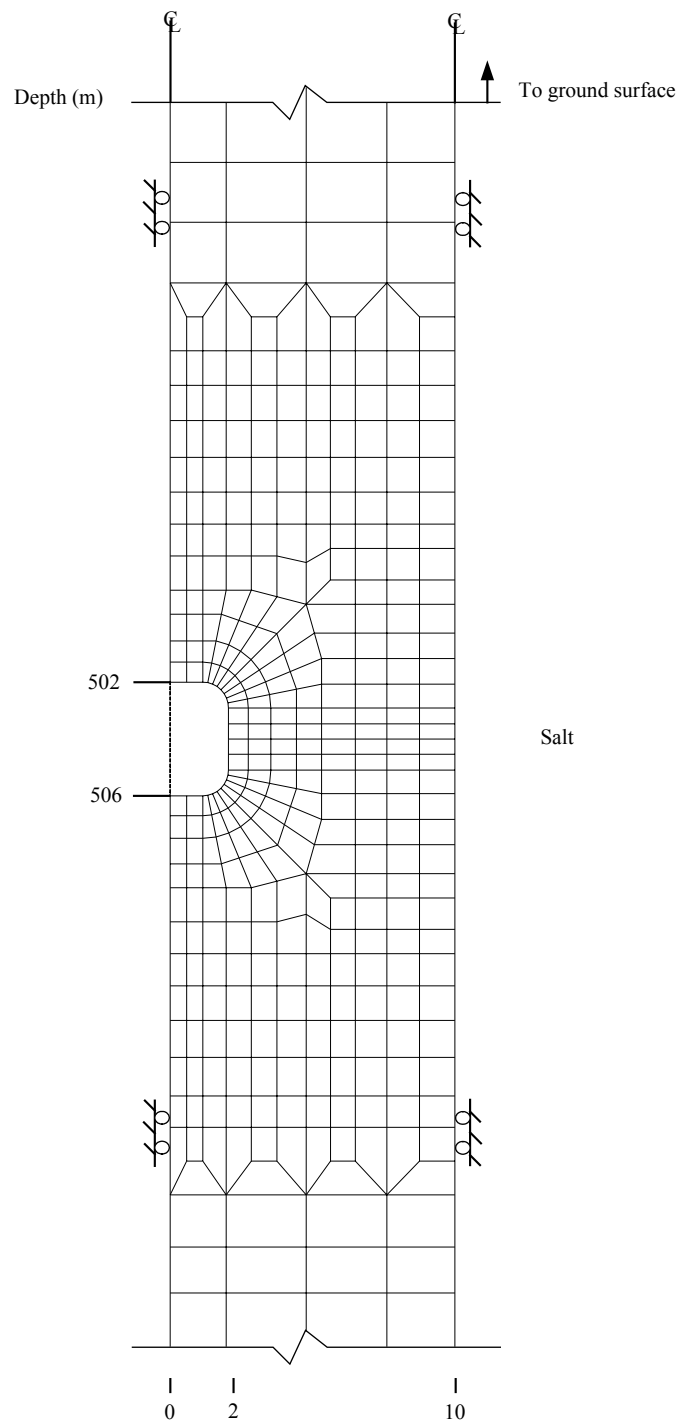


**Figure 5.14** Close-up finite element mesh for model KM-P4 at Ban Khao, Muang District, Udon Thani Province. Room and pillar widths are 4 and 16 meters, respectively.

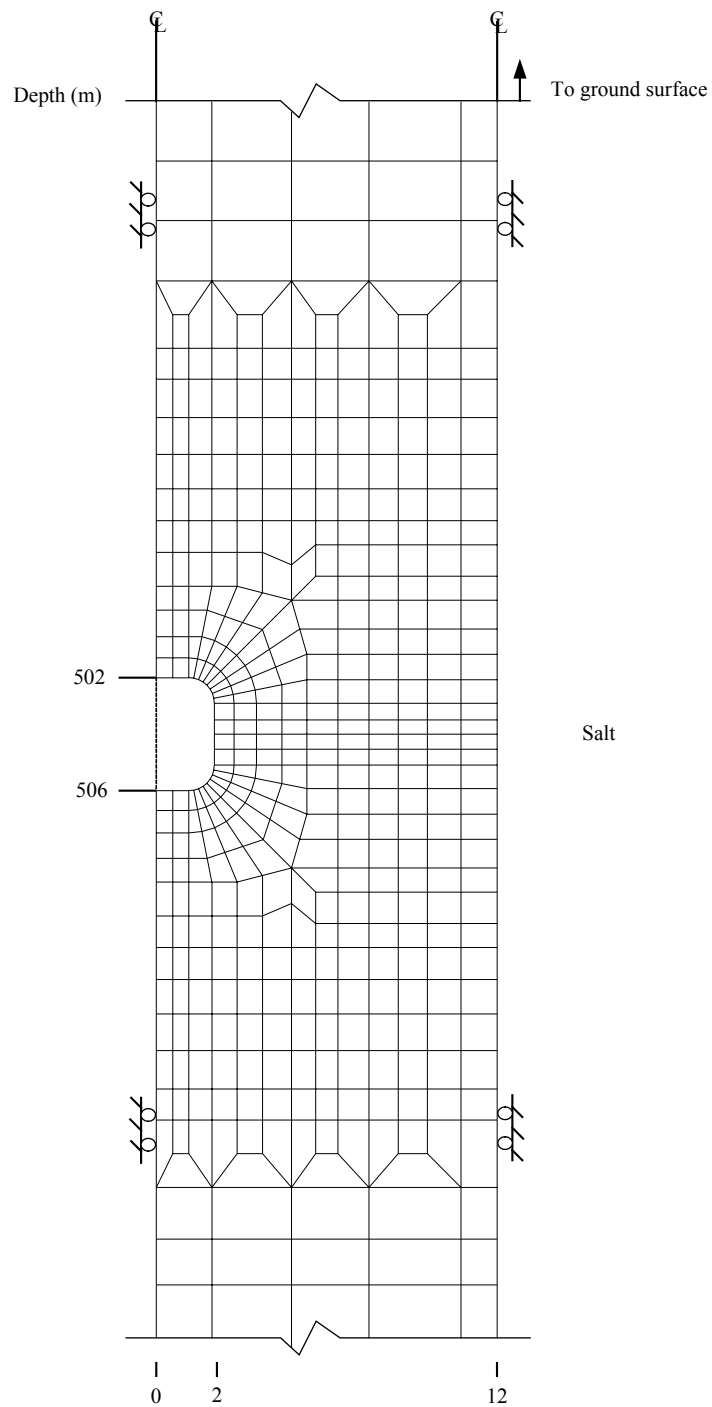


**Figure 5.15** Close-up finite element mesh for model KM-P5 at Ban Khao, Muang District, Udon Thani Province. Room and pillar widths are 4 and 20 meters, respectively.

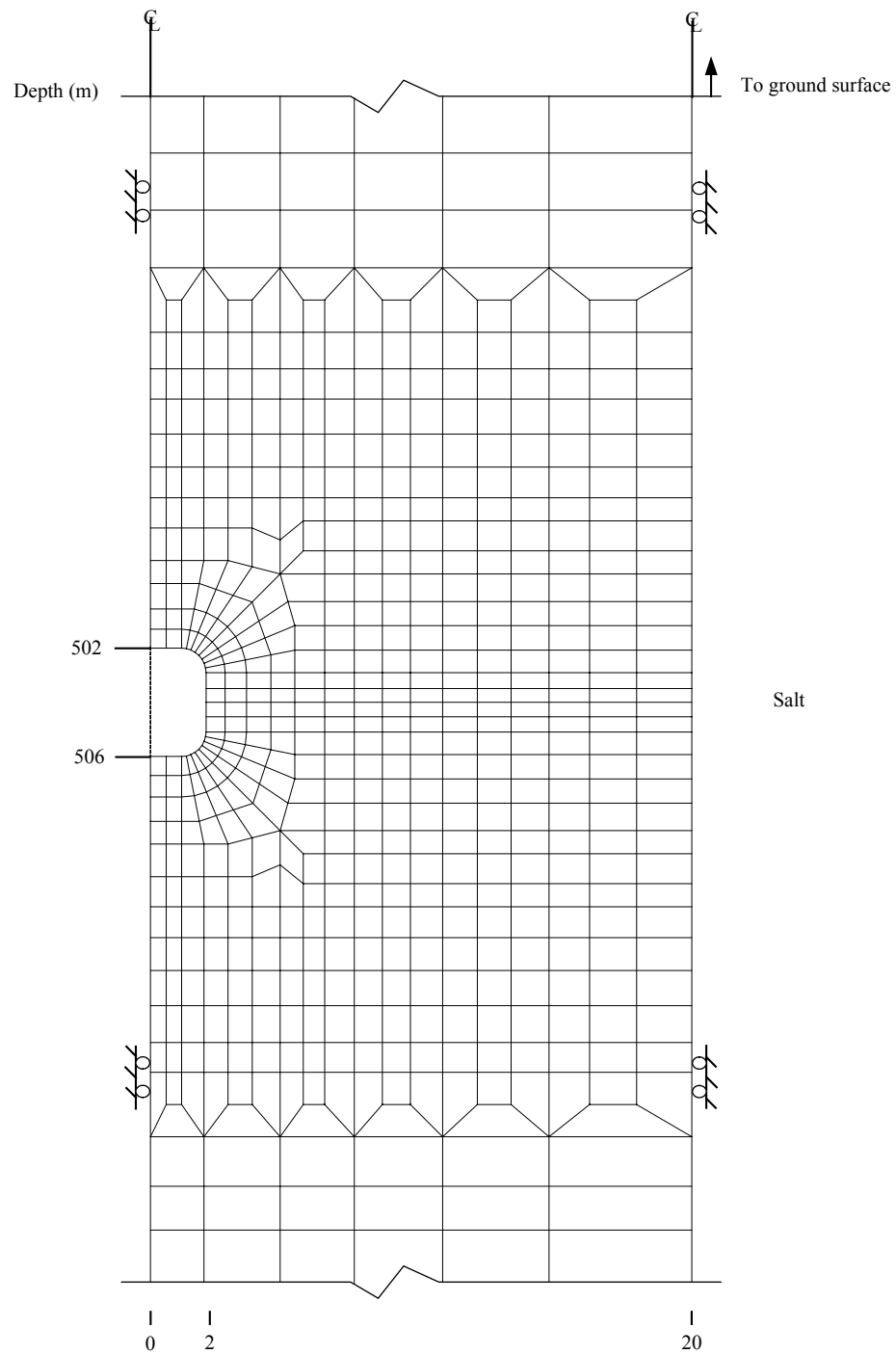


**Figure 5.16** Close-up finite element mesh for model KM-P9 at Ban Khao, Muang District, Udon Thani Province. Room and pillar widths are 4 and 36 meters, respectively.

pillar widths varying from 4, 8, 12, 16, 20 to 36 meters. Small elements (0.5 meters  $\times$  0.5 meters) are close to the opening boundaries.

### 5.5.3 Study on the Effect of Room Depth

Three finite element models (models KM-P4, KW-P4 and NB-P4) are constructed to represent the repository rooms. The study area at Ban Kao, Muang District, Udon Thani Province (model KW-P4), Ban Kudjig, Wanon Niwat District, Sakon Nakhon Province (model KW-P4) and Ban Nong Plue, Borabue District, Maha Sarakham Province (model NB-P4) are used to study the effect of room depths. Figure 5.17 shows the geometry and locations of the repository rooms in rock salt formation for these models. The room width and height of all finite element models are 4 meters and the pillar width of 16 meters. The finite element mesh of model KM-P4 is shown in Figure 5.13. Figures 5.18 and 5.19 show the finite element mesh of models KW-P4 and NB-P4. The model characteristics (the mesh construction and the analysis method) are similar to those of the model KM-R4. They are assumed to be square opening. The top and bottom of the opening are located at depths of 603 and 607 meters (model KW-P4) and 817 and 821 meters (model NB-P4). Small elements (0.5 meters  $\times$  0.5 meters) are close to the opening boundaries.

Summary of the shapes and dimensions of repository rooms used in the modeling are listed in Table 5.3. Table 5.4 summarizes numbers of nodes and elements for all finite element models. The stress field at the sites is assumed to be hydrostatic. The vertical stress at any point in the model is calculated from the depth and density of the overburden. Table 5.2 lists the density gradients of all rock formations. The internal pressure in the repository room is taken to be zero. All modeling is assumed to have not support for conservative condition. The analysis of

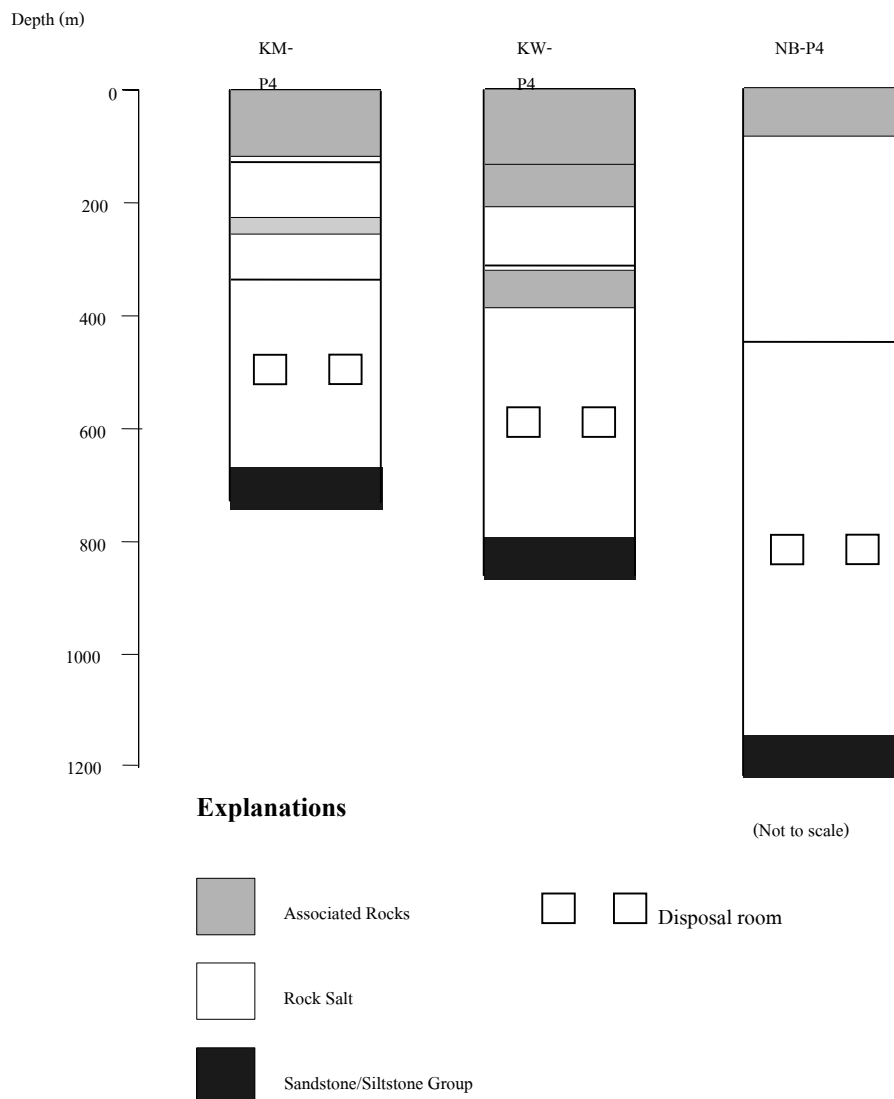


**Figure 5.17** Comparisons of the disposal rooms located in rock salt formation to study the effect of room depth. Stratigraphy of salt and associated rocks in 1). Ban Kao, Muang District, Udon Thani Province (model KM-P4), 2) Ban Kudjig, Wanon Niwat District, Sakon Nakhon Province (model KW-P4) and, 3) Ban Nong Plue, Borabue District, Mahasarakham Province (model NB-P4) are used in the study. The room height and width are 4 meters and 16 meters of pillar width.



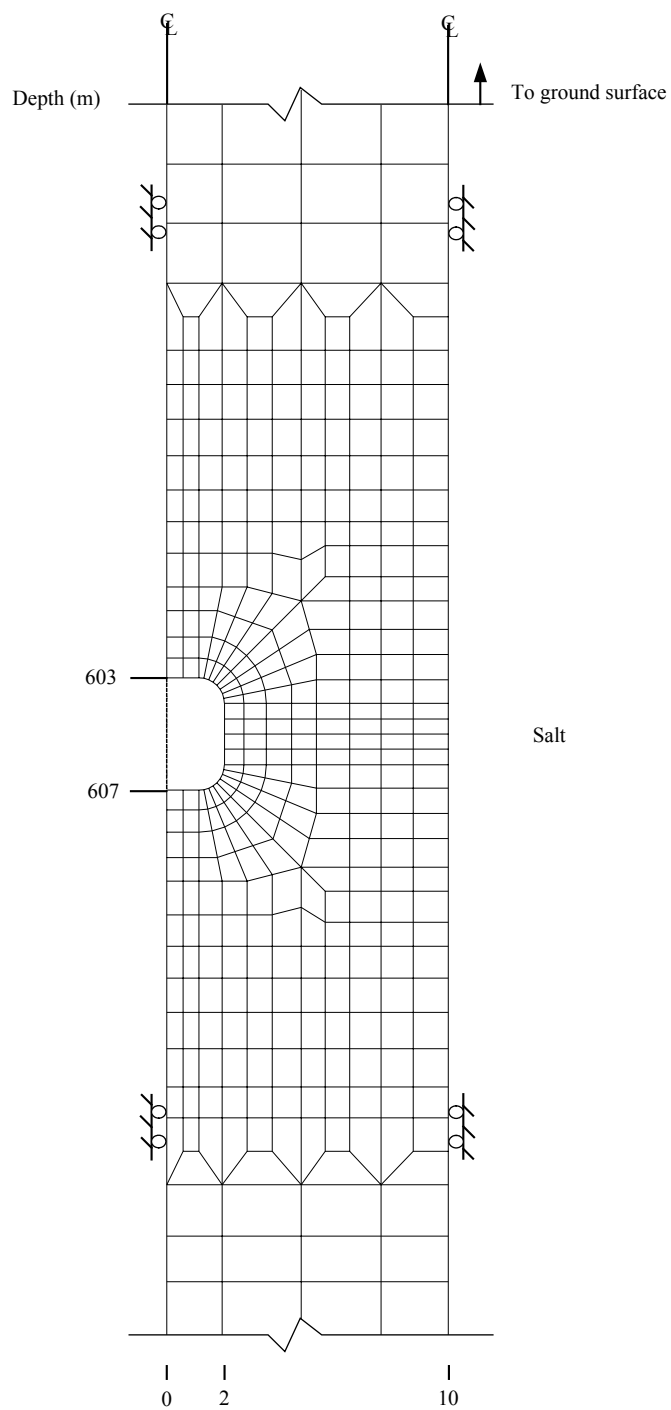


**Figure 5.18** Close-up finite element mesh for model KW-P4 at Ban Kudjig, Wanon Niwat District, Sakon Nakhon Province. Room and pillar widths are 4 and 16 meters, respectively.

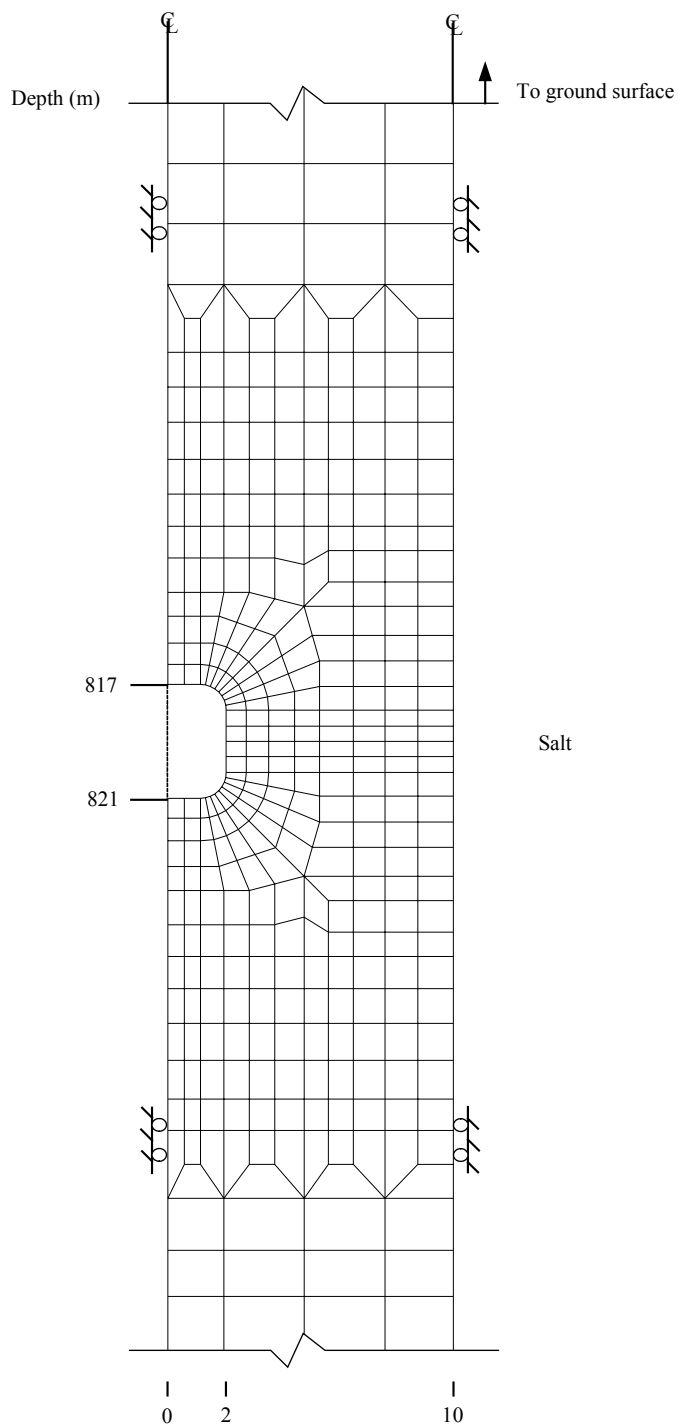


**Figure 5.19** Close-up finite element mesh for model KW-P4 at Ban Nong Plue, Borabue District, Mahasarakham Province. Room and pillar widths are 4 and 16 meters, respectively.

**Table 5.3** Shape and size of salt openings used in the modeling.

Model	Room Width/Pillar Width Ratio	Room Width (m)	Room Width/Height Ratio	Depth to the Roof (m)	Remarks
KM-R4	1:20	4	1:1	502	Study the effect of room width
KM-R6	1:20	6	3:2	502	
KM-R8	1:20	8	2:1	502	
KM-P1	1:1	4	1:1	502	Study the effect of pillar width
KM-P2	1:2	4	1:1	502	
KM-P3	1:3	4	1:1	502	
KM-P5	1:5	4	1:1	502	
KM-P9	1:9	4	1:1	502	
KM-P4	1:4	4	1:1	502	Study the effect of depth
KW-P4	1:4	4	1:1	603	
NB-P4	1:4	4	1:1	817	

**Note:** 1) All models are square openings shaped, except models KM-R6 and KM-R8

are rectangle openings shaped.

2) The room height is defined to be 4 meters to satisfied the available equipment.

**Table 5.4** Number of nodes and elements in finite element models.

<b>Models</b>	<b>Number of Nodes</b>	<b>Number of Elements</b>
KM-P1	784	628
KM-P2	528	424
KM-P3	567	459
KM-P5	786	680
KM-P9	969	864
KM-R4	988	918
KM-R6	1097	1024
KM-R8	1194	1124
KM-P4	710	598
KW-P4	764	634
NB-P4	776	642

computer modeling is plane strain. The openings are assumed to construct at the same time.

## **5.6 Modeling Results**

The results of computer simulation are evaluated in terms of the mechanical stability at 500 years after waste emplacement. Considerations are specifically given on the ground surface subsidence through 500 years, the vertical opening closure, the salt pillar, roof and floor deformations, the octahedral shear stress and strain and the principal stresses and strains around the salt opening through 50 years. The effect of the opening width, pillar width and the room depths among the three study areas are assessed.

### **5.6.1 The Results of Study on the Effect of Room Width**

The results of study on the effect of room width are show in Appendix B. Figure B.1 compares the surface subsidence at the centerline of the opening for various geometries (square and rectangular shapes). The square (model KM-R4) and the rectangular shapes (models KM-R6 and KM-R8) show surface subsidence equal 0.4, 0.5, and 0.6 centimeters, respectively. The surface subsidence of all shapes is rapidly increased during the first 10 years after the waste emplacement and remains constant through the next 500 years. The vertical opening closures at the centerline of the opening for various geometries are compared in Figure B.2. The models KM-R4, KM-R6 and KM-R8 show vertical closures about 6.7, 8.6, and 10.4 centimeters, respectively. Figure B.3 compares the salt roof deformation at the centerline of opening for various geometries. The square (model KM-R4) and the rectangular shapes (models KM-R6 and KM-R8) show salt roof deformation equal 3.3, 4.3 and

5.3 centimeters, respectively. Figure B.4 compares the salt floor deformation at the centerline of opening for various geometries. The square (model KM-R4) and the rectangular shapes (models KM-R6 and KM-R8) show salt floor deformation equal 3.4, 4.3 and 5.2 centimeters, respectively. The vertical closures, the salt roof and floor deformations of all shapes are rapidly increased during the first 10 years after the waste emplacement and remain constant through the next 50 years.

The contours of octahedral shears stresses near the salt opening are shown in Figures B.5 - B.7. The octahedral shear stresses concentrate at the opening top and bottom corners for the all shapes. The model KM-R8 shows the highest value of octahedral shear stress about 3.4 MPa. The models KM-R4 and KM-R6 show the same octahedral shear stress about 3.1 MPa. Figures B.8 - B.10 show the contours of octahedral shears strains near the salt opening. The octahedral shear strains concentrate at the opening top and bottom corners for all shapes. The model KM-R4 shows the lowest value of octahedral shears strains about  $27 \times 10^{-3} \%$ . The models KM-R6 and KM-R8 show the octahedral shear strains about  $33 \times 10^{-3} \%$  and  $39 \times 10^{-3} \%$ . The distributions of the stress vectors are shown in Figures B.11 - B.13. It is found that all models show similar the maximum stresses about 7.8 MPa. The largest stresses concentrate at the opening top and bottom corners for all shapes. The distributions of the strain vectors are shown in Figures B.14 - B.16. The model KM-R8 shows the maximum strains about 2.61 %. The models KM-R4 and KM-R6 show the maximum strain equal 1.81 and 2.16 %, respectively. The strains of all shapes concentrate at the opening top and bottom corners.

### 5.6.2 Results of Study on the Effect of Pillar Width

The results of study on the effect of pillar width are summarized in Appendix C. The comparison of the surface subsidence under the effect of different pillar widths is shown in Figures C.1 and C.2. It is found that the models KM-P1, KM-P2, KM-P3, KM-P4, KM-P5 and KM-P9 show surface subsidence about 108.3, 18.2, 4.6, 1.9, 1.5 and 0.8 centimeters, respectively. The surface subsidence of these models are rapidly increased during the first 10 years after the waste emplacement and remain constant through the next 500 years. Figures C.3 and C.4 compare the vertical closures at the centerline of the opening under the effect of different pillar widths. The models KM-P1, KM-P2, KM-P3, KM-P4, KM-P5 and KM-P9 show the vertical closure about 127.3, 27.1, 9.4, 6.1, 5.9 and 5.9 centimeters, respectively. The comparisons of the salt roof deformations under the effect of different pillar widths are shown in Figures C.5 and C.6. It is found that the models KM-P1, KM-P2, KM-P3, KM-P4, KM-P5 and KM-P9 show the salt roof deformation about 64.6, 13.6, 4.6, 3.0, 3.0 and 2.9 centimeters, respectively. Figures C.7 and C.8 compare the salt floor deformations under the effect of different pillar widths. The results indicated that the models KM-P1, KM-P2, KM-P3, KM-P4, KM-P5 and KM-P9 show the salt floor deformation about 62.7, 13.5, 4.6, 3.0, 3.0 and 3.0 centimeters, respectively. Figures C.9 and C.10 compare the pillar yielding at the centerline of pillar under the effect of different pillar widths. It is found that the models KM-P1, KM-P2, KM-P3, KM-P4, KM-P5 and KM-P9 show the pillar yielding about 85.8, 13.3, 2.6, 0.5, 0.3 and 0.1 centimeters, respectively. The vertical closures, the salt roof and floor deformations and the pillar yielding of these models are rapidly increased during the first 10 years after the waste emplacement and remain constant through the next 50 years.

The contours of octahedral shears stresses near the salt opening are shown in Figures C.11 - C.16. The octahedral shear stresses concentrate at the opening top and bottom corners for the all models. All models show similar the octahedral shear stress about 3.4 MPa. Figures C.17 - C.22 show the contours of octahedral shears strains near the salt opening. The octahedral shear strains concentrate at the opening top and bottom corners for all models. These models show the octahedral shears strains ranging from 1.8 -  $55 \times 10^{-2}\%$ . The distributions of the stress vectors are shown in Figures C.23 - C.28. It is found that these models show the maximum stresses ranging from 17.8 to 17.9 MPa. The largest stresses concentrate at the opening top and bottom corners for all models. The distributions of the strain vectors are shown in Figures C.29 - C.34. These models show the maximum strains ranging from 1.23% to 34.32 %. The strains of all models concentrate at the opening top and bottom corners.

### **5.6.3 Results of Study on the Effect of Room Depth**

Summaries of the study results on the effect of room depth are show in Appendix D. The comparison of the surface subsidence at the centerline of the opening for various depths (at 502, 603 and 817 meters) is shown in Figure D.1. It is found that the models KM-P4 (502 meters room depth), KW-P4 (603 meters room depth) and NB-P4 (817 meters room depth) show surface subsidence about 1.9, 6.4 and 27.1 centimeters, respectively. The surface subsidences of these models are rapidly increased during the first 10 years after the waste emplacement and remain constant through the next 500 years. Figure D.2 compares the vertical closures at the centerline of the opening under the effect of different room depths. It is found that the models KM-P4, KW-P4 and NB-P4 show the vertical closure about 6.1, 17.2 and 74.2



centimeters, respectively. The comparison of the salt roof deformations at the centerline of opening for various depths is shown in Figure D.3. The models KM-P4, KW-P4 and NB-P4 show salt roof deformation about 3.0, 5.4 and 36.9 centimeters, respectively. Figure D.4 compares the salt floor deformations under the effect of different room depths. It is found that the models KM-P4, KW-P4 and NB-P4 show the salt floor deformation about 3.0, 11.8 and 37.3 centimeters, respectively. Figure D.5 compares the pillar yielding at the centerline of pillar for various depths. The models KM-P4, KW-P4 and NB-P4 show pillar yielding about 0.5, 3.2 and 15.1 centimeters, respectively. The vertical closures, the salt roof and floor deformations and the pillar yielding of these models are rapidly increased during the first 10 years after the waste emplacement and remain constant through the next 50 years.

The contours of octahedral shears stresses near the salt opening are shown in Figures D.6 - D.8. The octahedral shear stresses concentrate at the opening top and bottom corners for the all models. All models show similar the octahedral shear stress about 3.4 MPa. Figures D.9 - D.11 show the contours of octahedral shears strains near the salt opening. The octahedral shear strains concentrate at the opening top and bottom corners for all models. These models show the octahedral shears strains ranging from 2.4 -  $24 \times 10^{-2}$  %. The distributions of the stress vectors are shown in Figures D.12 - D.14. It is found that these models show the maximum stresses ranging from 17.8 to 29.6 MPa. The largest stresses concentrate at the opening top and bottom corners for all models. The distributions of the strain vectors are shown in Figures D.15 - D.17. These models show the maximum strains ranging from 1.57 to 16.18 %. The strains of all models concentrate at the opening top and bottom corners.

## 5.7 Design of Underground Layout

The objective of this task is to design the underground layout of the disposal. It can be divided into three main groups; repository room, main entry and barrier pillars (see Figure 5.20). The repository rooms are 4 m wide, 4 m high and 50 m long, separated by 16 m wide pillar. It requires 25 rooms to accommodate the nuclear waste amount of 33,000 m<sup>3</sup> and increasing in next 50 years.

The main entry is 4.5 m high, 5 m wide and 50 m long, separated by 20 m wide pillar. Figure 5.21 shows the finite element mesh of main entry. The mesh is constructed to represent a vertical cross-section of the double opening. The surrounding rocks are discretized from the ground surface to the depth of 800 meters. The mesh is designed for plane strain analysis using the opening and pillar axes as centerlines. It covers a horizontal distance of 400 meters. The left boundary represents the opening centerline and is laterally constrained. The right boundary represents the pillar centerline. In order to show the opening boundaries, the elements inside the room are not drawn in the Figure. The top and bottom of the opening are located at depths of 502 meters and 506.5 meters. The opening is assumed to be a square opening with a room width of 5 meters and height of 4.5 meters. Small elements (0.5 meters × 0.5 meters) are used adjacent to and near the opening boundaries to capture the detailed distribution of the stresses and strains under high gradients. Larger elements are used in the overburden, as its behavior does not impact the opening stability. The overburden is included in the analysis in order to provide the gravitational force on the salt opening and to allow an assessment of the ground surface subsidence.

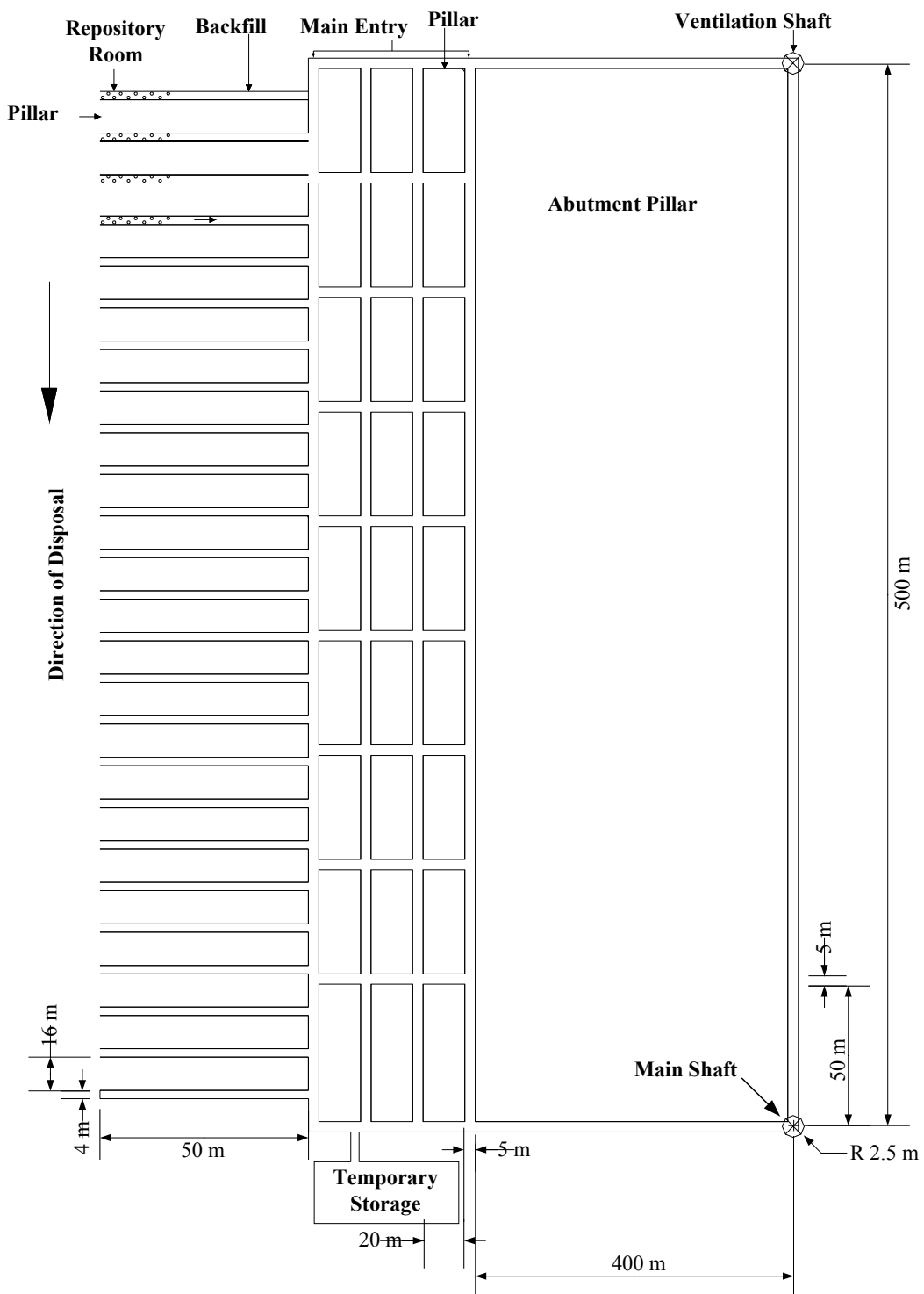


**Figure 5.20** Underground layout for the repository at Ban Kao, Muang District, Udon Thani

Province.

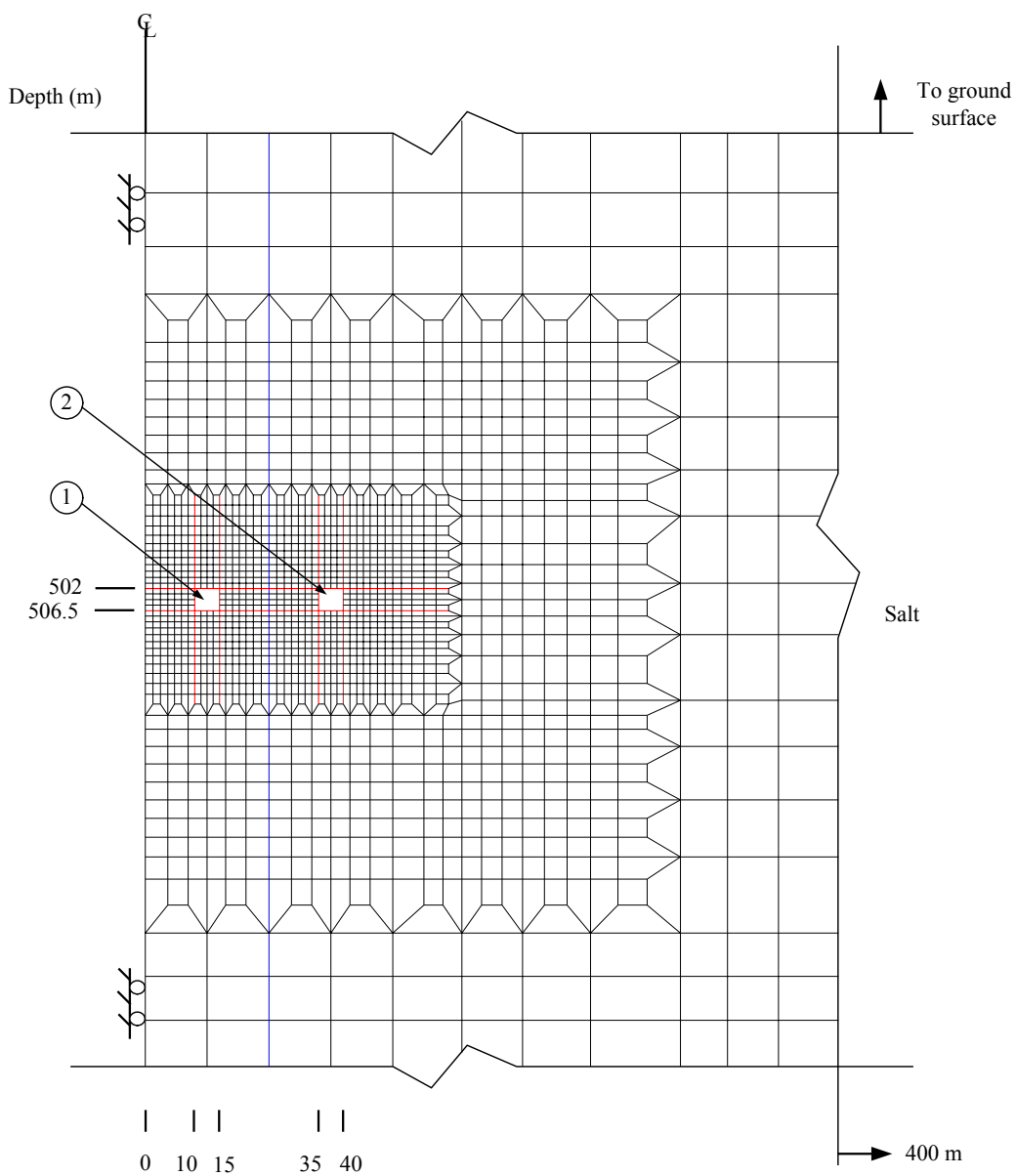


**Figure 5.21** Finite element mesh for model main entry at Ban Kao, Muang District, Udon Thani Province. The main entry is 5 m wide and 4.5 m high, separated by 20 m wide pillar.

The results of computer simulation as show in Appendix E are evaluated in terms of the mechanical stability at 500 years after waste emplacement. Figure E.1 shows the surface subsidence at the left centerline of finite element mesh equals 0.3 centimeters. It is rapidly increased during the first 10 years after the waste emplacement and remains constant through the next 500 years. The comparisons of vertical opening closures at the centerline between room no.1 (inner) and room no.2 (outer) are similarly about 7 centimeters (Figure E.2). Figure E.3 compares the salt roof deformation at the centerline between room no. 1 and room no. 2 equal 1.8 and 1.9 centimeters. Comparison of the salt floor deformation at the centerline of room no. 1 and room no. 2 is shown in Figure E.4. They are about 1.8 and 1.9 centimeters. Figure E.5 compares the pillar yielding at the centerline of room no. 1 and room no.2. It is found that the room no. 1 and room no. 2 show similar pillar yielding about 0.4 centimeters. The vertical opening closure, the salt pillar, roof and floor deformation of both rooms are rapidly increased during the first 10 years after the emplacement and remains constant to the next 50 years.

The contour of octahedral shears stresses near the main entry is shown in Figures E.6. The octahedral shear stresses concentrate at the opening top and bottom corners. The octahedral shear stress value is about 3.4 MPa. Figure E.7 shows the contour of octahedral shears strains near the main entry. The octahedral shear strains concentrate at the opening top and bottom corners. The value of octahedral shears strains about  $14 \times 10^{-3} \%$ . The distributions of the stress vectors are shown in Figures E.8. It is found that the maximum stresses about 17.7 MPa. The largest stresses concentrate at the opening top and bottom corners. The distribution of the strain

vector is shown in Figures E.9. The maximum strains about 1.0 %. The strains concentrate at the opening top and bottom corners.

## 5.8 Discussions

The time-dependent vertical closures, salt roof and floor deformations, pillar yielding and surface subsidence are considered in the analysis for the long-term geomechanical stability. This also conforms to the approach used by several researchers (Nguyen-Minh et al., 1996; Rolfs, 1996; Frayne, 1996; Kwon and Miller, 1998; De Menezes and Nguyen-Minh, 1998; Pudewills, 1998). Studying the effect of opening geometries includes the square and rectangular shapes with room widths varying from 4, 6 to 8 meters. The area at Ban Khao, Muang District, Udon Thani Province has been used. The computer simulation suggests that the square shaped openings show the lowest vertical closure of about 6.7 centimeters. The salt roof and floor deformations are less than 3 centimeters. The surface subsidence is about 0.4 centimeter at 500 years after emplacement. Studying the effect of pillar widths includes the models of square shaped rooms with different pillar widths varying from 4, 8, 12, 16, 20 to 36 meters. The area at Ban Khao, Muang District, Udon Thani Province has been used. The modeling results indicate that the square shaped room with 16 to 36 meters of pillar width shows the lowest vertical closures of about 6.1 centimeters. The salt roof and floor deformations are about 3 centimeters. The pillar yielding is about 0.5 centimeter. The surface subsidence is less than 2 centimeters at 500 years after emplacement. Studying the effect of different room depths includes three areas on the Khorat Plateau. The three areas are Ban Khao, Muang District, Udon Thani Province (model KM-P4), Ban Kudjig, Wanon Niwat District, Sakon

Nakhon Province (model KW-P4) and Ban Nong Plue, Borabue District, Maha Sarakham Province (model NB-P4). The modeling results indicate that the square shaped room with 16 meters pillar width and 502 meters room depth shows the lowest vertical closures of about 6.1 centimeters. The salt roof and floor deformations are about 3 centimeters. The pillar yielding is about 0.5 centimeter. The surface subsidence is less than 2 centimeters at 500 years after emplacement.

The main entry is 4.5 m high, 5 m wide and 50 m long, separated by 20 m wide pillar. The minimum width for the barrier and protective pillars is 400 meters.

# **CHAPTER VI**

## **DISCUSSIONS, CONCLUSIONS AND RECOMMENDATIONS**

### **6.1 Discussions**

Research discussions provided in this chapter emphasize the sufficiency and suitability of test methods and results, constitutive laws, computer program, and the advantages and disadvantages of the proposed disposal concept.

#### **6.1.1 Sufficiency and Suitability of Test Results**

The results from the tests indicate that rock salt in the northeast of Thailand have a relatively high intrinsic variability, as suggested by the high standard deviation of the calibrated parameters. The amounts of salt core specimens are limited, and hence may not provide a representative result for the actual in-situ condition. This research however assumes that the mechanical properties of the salt in northeastern Thailand are similar for all areas.

The borehole data also concentrate in small areas. They may not represent the entire Sakon Nakhon and Khorat basins. The borehole logs indicate that the depths and thickness of salt beds in both basins vary significantly. The creep properties of rock salt are also affected by inclusions. For the final design after site selection, a more site-specific study is deemed necessary.



### 6.1.2 Experimental Methods

The diameter of the salt specimens used in this research is relatively small compared to those recommended by the ASTM and ISRM standard practices. The salt core specimens that donated by Asia Pacific Potash Corporation are 6 cm in diameter, while the average salt grain size is about one centimeter. As a result the rock salt deformation in steady-state creep phase from small specimens may be lower than that from the larger specimens. The visco-plastic coefficient of the salt in this research may therefore be high as compared with those from other sites.

### 6.1.3 Suitability of Constitutive Law

Researchers have purposed numerous constitutive equations to describe the mechanical behavior of the salt (described in Chapter II). Each constitutive equation has specific advantages and disadvantages. In the design and analysis of engineering structures in rock salt the constitutive equation that suitable to the specific objectives should be used. The constitutive law used in this study is developed by Fuenkajorn and Serata (1992, 1993, 1994) and Serata and Fuenkajorn (1992). The rheological constitutive model used here is capable of simulating the elastic, viscoelastic, viscoplastic, strain-softening and dilation behavior of time-dependent materials, such as rock salt. These equations have been incorporated into a finite element code, named GEO. A brief discussion identifying its unique derivation of the constitutive equations is given in Chapter II. A limitation of this equation is that it can not calculate the deformation under elevated temperatures. This does not affect the outcome of this research because the nuclear waste studied here is classified as low-level and low-

temperature waste. The constitutive law used in this study is still considered suitable for the analysis and design of the repository in rock salt.

#### **6.1.4 Advantages and Disadvantages of Proposed Concept**

It is proposed here that the underground repository should invoke the long-wall pillar concept. This concept is being used to design the nuclear waste repository at the WIPP site in New Mexico (Matalucci and Munson, 1988). A comparison between the dry salt mining and solution mining concepts is summarized in Table 6.1 (Fuenkajorn, 2003). The table shows the advantages and disadvantages of the two concepts.

## **6.2 Conclusions**

The objective of this research is to assess the mechanical performance of the rock salt formations in northeastern Thailand for nuclear waste disposal. The sequences of rock salt in Khorat Plateau have been reclassified in this research into three main geomechanics groups: associated rocks, rock salt and sandstone/siltstone groups. One of the difficulties in selecting a suitable repository area is that the salt formations in Thailand are relatively thin and shallow. The selected criteria used here are the thickness and depth of the rock salt formations. Three areas in the region have been taken into consideration, including 1) Ban Khao, Muang District, Udon Thani Province, 2) Ban Kudjig, Wanorn Niwat District, Sakon Nakorn Province, and 3) Ban Nong Plue, Borabue District, Mahasarakham Province.

Rock salt samples used in the laboratory experiments are obtained from Udon Thani Province (in Sakon Nakorn Basin). The core specimens are collected from the Middle and the Lower Salt members at depths ranging between 250 meters and 400

meters. The core specimens are in cylindrical shapes with 60 millimeters in diameter.

**Table 6.1** Comparison the advantages and disadvantages of disposal concepts between dry salt mining and solution mining (Fuenkajorn, 2003).

<b>Criteria</b>	<b>Dry salt mining</b>	<b>Solution mining</b>
Construction cost	3,000 - 5,000 MM Bath	Less than 500 MM Bath
Stability monitoring	Direct measurement	Indirect measurement
Waste emplacement	Convenient, safety and reliability	Complicated
Retrievability	Simple	Difficult
Containment monitoring	Direct measurement	Indirect measurement
Backfill installation	Complicated and high cost	Simple and low cost
Mechanical stability	High	Fairly high
Surface subsidence	Relatively high	Low
Mine tailing / waste	Used as backfill	Disposed
Construction duration	Long	Short

They contain more than 99 percent of halite (NaCl). The rock salt is coarsely crystallized. The crystal size varies from 1 to 10 mm. The average density is 2,170 kg/m<sup>3</sup>. The color is clear or white, but sometimes pink and gray can be found.

The sample preparations follow the ASTM standards practice (ASTM D4543) as much as practical. The procedures for the triaxial creep test also follow the ASTM standards (ASTM D4341, D4405 and D4406). The creep tests are divided into 2 groups, uniaxial and triaxial creep tests. The results from the tests are used to calibrate the visco-plastic parameter (plastoviscosity) of the rock. The computer program used to calibrate the plastoviscosity is called GEO. The average plastoviscosity is about 33.6 GPa·day.

Eleven finite element models are constructed to represent the geologic sequences of the three study areas in two-dimensional. The studies are divided into three groups. The first group is to assess the effect of the opening geometry. The excavation is assumed to be square and rectangular shape with different room widths. The area at Ban Kao, Muang District, Udon Thani Province (Sakon Nakhon Basin) is selected to assess the opening stability. The second group is designed to determine the optimum pillar width. The last group is to assess the effect of different depths of salt. The simulation results suggest that the repository rooms should be 4 m wide and 4 m high, separated by 16 m wide pillar. The excavations should be at approximately 502 meters depth. The main entries are 4.5 m high, 5 m wide, 50 m long and are separated by 20 m wide pillar. The minimum width for the barrier and protective pillars is 400 meters. Under these design parameters, the predicted vertical and horizontal closures are about 0.5 %. The surface subsidence is calculated to be less than 0.22 meter through the next 500 years.

### **6.3 Recommendations for Future Research Study**

For an actual site-selection more salt specimens are needed for the determination of the salt constitutive parameters (properties). The specimens should be obtained from both Khorat and Sakon Nakhon basins. They should be collected from only the Lower Salt Member at various depths because the suitable rock salt formation used for nuclear waste repository is Lower Salt Bed. Larger core specimens (at least 102 inches in diameter) are required to ensure the representativeness of the results. The creep testing under a wider range of loading and test period (more than one month) is also desirable to obtain a more representative result. GEO program may not adequately describe the salt behavior, particularly for short-term prediction. Different creep laws and computer codes should be used to confirm the correctness of the calculation and prediction. Other constitutive laws, such as FLAC program (Itasca, 1992; 1994) may be used in the simulations and for the redundant analyzes. For the final design after site selection, a more site-specific study will be necessary. The investigation should include core logging, geophysical exploration, hydrogeology and chemical studies for true site-specific design.

## REFERENCES

- ASTM D4341-93. Standard test method for creep of cylindrical hard rock core specimens in uniaxial compression. In **Annual Book of ASTM Standards** (Vol. 04.08). Philadelphia: American Society for Testing and Materials.
- ASTM D4405-93. Standard test method for creep of cylindrical soft rock core specimens in uniaxial compressions. In **Annual Book of ASTM Standards** (Vol. 04.08). Philadelphia: American Society for Testing and Materials.
- ASTM D4406-93. Standard test method for creep of cylindrical rock core specimens in triaxial compression. In **Annual Book of ASTM Standards** (Vol. 04.08). Philadelphia: American Society for Testing and Materials.
- ASTM D4543-85. Standard practice for preparing rock core specimens and determining dimensional and shape tolerances. In **Annual Book of ASTM Standards** (Vol. 04.08). Philadelphia: American Society for Testing and Materials.
- Albers, G. (1983). MAUS–A computer code for modeling thermo-mechanical stresses in rock salt. In **Proceedings of Technology Session EUR9355 EN, Computer Modeling of Stresses in Rock Salt**. Brussels.
- Allemandou, X. and Dusseault, M. B. (1996). Procedures for cyclic creep testing of salt rock, results and discussions. In **Proceedings of the Third Conference on the Mechanical Behavior of Salt** (pp. 207-218). Clausthal-Zellerfeld, Germany: Trans Tech Publications.

- Aubertin, M. (1996). On the physical origin and modeling of kinematics and isotropic hardening of salt. In **Proceedings of the Third Conference on the Mechanical Behavior of Salt** (pp. 1-18). Clausthal-Zellerfeld, Germany: Trans Tech Publications.
- Aubertin, M., Gill, D. E. and Ladanyi, B. (1991). A unified visco-plastic model for the inelastic flow of alkali halides. **Mechanics of Materials**. 11: 63-82.
- Aubertin, M., Gill, D. E. and Ladanyi, B. (1992). Modeling the transient inelastic flow of rocksalt. In **the Seventh Symposium on Salt** (vol. 1, pp. 93-104). Amsterdam: Elsevier Science Publishers.
- Aubertin, M., Julien M. R., Servant, S. and Gill, D. E. (1999). A rate-dependent model for the ductile behavior of salt rocks. **Canadian Geotechnical Journal**. 36(4): 660-674.
- Aubertin, M., Sgaoula, J. and Gill, D. E. (1992). A damage model for rock salt: Application to tertiary creep. In **the Seventh Symposium on Salt** (vol. 1, pp. 117-125). Amsterdam: Elsevier Science Publishers.
- Aubertin, M., Sgaoula, J. and Gill, D. E. (1993). Constitutive modeling of rock salt: Basic considerations for semi-brittle behavior. In **Proceedings of the Fourth International Symposium on Plasticity and It's Current Applications** (pp. 92). Baltimore.
- Aubertin, M., Sgaoula, J., Servant, S., Julien, M. R., Gill, D. E. and Ladanyi, B. (1998). An up-to-date version of SUVIC-D for modeling the behavior of salt. In **Proceedings of the Fourth Conference on the Mechanical Behavior of Salt** (pp. 205-220). Clausthal-Zellerfeld, Germany: Trans Tech Publications.

- Barber, D. J. (1990). Regimes of plastic deformation processes and microstructure. In **An Overview, Deformation Processes in Minerals, Ceramics and Rocks** (pp. 138-178). Unwin Hyman.
- Bechthold, W., Rothfuchs, T., Huertas, F., Poley, A., Ghoreychi, M., Heusermann, S. and Gens, A. (1999). Back-filling and sealing of repositories in rock salt - The BAMBUS project. In **the Fifth International Conference, Radioactive Waste Management Strategies and Issues** (pp. 366-369). Luxembourg: Euradwaste.
- Beddoes, R. J. (1994). **Analyses of bench test area at Goderich mine**. Internal Report for Sifto Canada Inc., Prepared by Golder Associate Ltd., Calgary, AB, Canada.
- Berest, P. (1993). General report: Mining and civil engineering in rock salt. In **Proceedings of the Seventh International Congress on Rock Mechanics**. (Vol. 3, pp. 1847-1851). Balkema.
- Berest, P., Brouard, B. and Durup, G. (1998). Behavior of sealed solution-mined caverns. In **Proceedings of the Fourth Conference on the Mechanical Behavior of Salt** (pp. 511-524). Clausthal-Zellerfeld, Germany: Trans Tech Publications.
- Biffle, J. H. (1984). **JAC-A two-dimensional finite element computer program for the non-linear quasistatic response of solids with the conjugate gradient method**. SAND81-0998, Sandia National Laboratories, Albuquerque, NM.



- Billiotte, J., Guen, L. C., Deveughele, M and Brulhet, J. (1996). On laboratory measurements of porosity and permeability of salt rocks (Bressa basis-France). In **Proceedings of the Third Conference on the Mechanical Behavior of Salt** (pp. 221-230). Clausthal-Zellerfeld, Germany: Trans Tech Publications.
- Blanquer-Fernandez, S. (1991). **Interaction des cavities souterraines**. Project de Fin d'Etudes, EPF, LMS. French Ecole: Polytechnique.
- Boontongloan, C. (2000). **Engineering properties of the evaporitic and clastic rocks of Maha Sarakam formation, Sakon Nakhon evaporite basin**. M.S. thesis, Asian Institute of Technology, Thailand.
- Brodsky, N. S., Hansen, F. D. and Pfeifle, T. W. (1998). Properties of dynamically compacted WIPP salt. In **Proceedings of the Fourth Conference on the Mechanical Behavior of Salt** (pp. 303-316). Clausthal-Zellerfeld, Germany: Trans Tech Publications.
- Broek, W. M. G. T. and Heilbron, H. C. (1997). Influence of salt behavior on the retrievability of radioactive waste. In **Proceedings of the Fourth Conference on the Mechanical Behavior of Salt** (pp. 561-573). Clausthal-Zellerfeld, Germany: Trans Tech Publications.
- Callahan, G. D., Fossum, A. F. and Svalstad, D. K. (1989). **Documentation of SPECTROM-32: A finite element thermo-mechanical stress analyses program**. DOE/CH10378-2, prepared by RE/SPEC, Inc., Rapid City, SD, RSI-0269, for US Department of Energy, Chicago Operations Office, Vol.1 and 2, February.

- Callahan, G. D., Loken, M. C., Hurtads, L. D. and Hansen, F. D. (1998). Evaluation of constitutive models for crushed salt. In **Proceedings of the Fourth Conference on the Mechanical Behavior of Salt** (pp. 317-330). Clausthal-Zellerfeld, Germany: Trans Tech Publications.
- Carter, N. L., Horseman, S. T., Russell, J. E. and Handin, J. (1993). Rheology of rocksalt. **Structural Geology** 15(10): 1257-1272.
- Chen, Z., Wang, M. L. and Lu, T. (1997). Study of Tertiary Creep of Rock Salt. **Journal of Engineering Mechanics** 123 (1): 77.
- Chokski, A. H. and Langdon, T. G. (1991). Characteristics of creep deformation in ceramics. **Materials Science and Technology** 7: 577-584.
- Cleach, J. M. L., Ghazali, A., Deveughele, H., and Brulhet, J. (1996). Experimental study of the role of humidity on the thermomechanical behavior of various halitic rocks. In **Proceedings of the Third Conference on the Mechanical Behavior of Salt** (pp. 231-236). Clausthal-Zellerfeld, Germany: Trans Tech Publications.
- Cristescu, N. D. (1991). Non-associated elastic/visco-plastic constitutive equations for sand. **International Journal of Plasticity** 7: 41-64.
- Cristescu, N. D. (1992). Rock rheology. **Comprehensive Rock Engineering**, Chapter 21. Pergamon Press.
- Cristescu, N. and Hunsche, U. (1996). A comprehensive constitutive equation for rock salt determination and application. In **Proceedings of the Third Conference on the Mechanical Behavior of Salt** (pp. 191-205). Clausthal-Zellerfeld, Germany: Trans Tech Publications.

- Cristescu, N. D. (1993a). Constitutive equation for rock salt and mining applications. In **Proceedings of the Seventh Symposium on Salt** (Vol. 1, pp. 105-115). Amsterdam: Elsevier Science Publishers.
- Cristescu, N. D. (1993b). Constitutive equation for rock salt and mining applications. In **Proceedings of the Seventh Symposium on Salt** (Vol. 1, pp. 105-115). Amsterdam: Elsevier Science Publishers.
- Cristescu, N. D. (1993c). A general constitutive equation for transient and stationary creep of rock salt. **International Journal of Rock Mechanics, Sciences and Geomechanics Abstracts**. 30 (2): 125-140.
- Cristescu, N. D. (1996). Stability of large underground caverns in rock salt. In **Proceedings of the Second Symposium North American Rock Mechanics** (pp. 101-108). Canada: A. A. Balkema.
- Davidson, B. C. and Dusseault, M. B. (1998). Granular halite backfill as a structural and disposal medium. In **Proceedings of the Fourth Conference on the Mechanical Behavior of Salt** (pp. 341-352). Clausthal-Zellerfeld, Germany: Trans Tech Publications.
- De Menezes, J. E. Q. and Nguyen-Minh, D. (1998). Numerical modeling of leached cavern fields using mixed BEM-FEM method. In **Proceedings of the Fourth Conference on the Mechanical Behavior of Salt** (pp. 417-426). Clausthal-Zellerfeld, Germany: Trans Tech Publications.
- Dreyer, W. (1982). **Underground storage in salt deposits and other non-hard rocks**. (pp. 147-176). New York: Halsted Press.

- Durup, G. and Xu, J. (1996). Comparative study of certain constitutive laws used to describe the rheological deformation of salts. In **Proceedings of the Third Conference on the Mechanical Behavior of Salt** (pp. 75-84). Clausthal-Zellerfeld, Germany: Trans Tech Publications.
- Dusseault, M.B. and Fordham, C.J. (1993). Time-dependent behavior of rocks. **Comprehensive Rock Engineering Principles, Practice and Project: Rock Testing and Site Characterization** (Vol. 3, pp. 119-149). London, Pergamon.
- Eduardo, J., Menezes, Q. D. and Ngugen-Minh, D. (1996). **Numerical modeling of leached cavern fields using mixed BEM-FEM method** (pp. 417-426).
- Farmer, I. W. and Gilbert, M. J. (1984). Time dependent strength reduction of rock salt. In **Proceedings of the First Conference on the Mechanical Behavior of Salt** (pp. 3-18). Clausthal-Zellerfeld, Germany: Trans Tech Publications.
- Fokker, P. A. (1995). **The behavior of salt and salt caverns**. Ph.D Thesis, Delft University of Technology.
- Fokker, P. A. (1998). The micro-mechanics of creep in rock salt. In **Proceedings of the Fourth Conference on the Mechanical Behavior of Salt** (pp. 49-61). Clausthal-Zellerfeld, Germany: Trans Tech Publications.
- Fokker, P. A. and Kenter, C. J. (1994). The micro mechanical description of rock salt plasticity. In **Eurock'94** (pp. 705-713). Rotterdam: Balkema.
- Franssen, R. C. M. (1998). Mechanical anisotropy of synthetic polycrystalline rock salt. In **Proceedings of the Fourth Conference on the Mechanical Behavior of Salt** (pp. 63-75). Clausthal-Zellerfeld, Germany: Trans Tech Publications.

- Franssen, R. C. M. and Spiers, C. J. (1990). Deformation of polycrystalline salt in compression and in shear at 250-350°C. **Deformation Mechanisms, Rheology and Tectonics, Geological Society Special Publication 45**: 201-213.
- Frayne, M. A. (1996). Four cases study in salt rock: Determination of material parameters for numerical modeling. In **Proceedings of the Third Conference on the Mechanical Behavior of Salt** (pp. 471-482). Clausthal-Zellerfeld, Germany: Trans Tech Publications.
- Frayne, M. A. (1998). The goderich salt mine: past, present and future. In **Proceedings of the Fourth Conference on the Mechanical Behavior of Salt** (pp. 445-458). Clausthal-Zellerfeld, Germany: Trans Tech Publications.
- Fuenkajorn, K. (2000). Geohydrological integrity of storage caverns in salt formation. **Symposium on Mineral, Energy, and Water Resources of Thailand** (pp. 270-275). Bangkok, Thailand.
- Fuenkajorn, K. (2003). **Mechanical performance assessment of rock salt for nuclear waste disposal in northeastern Thailand**. Suranaree University of Technology (417p), Thailand.
- Fuenkajorn, K. and Daemen, J. J. K. (1988). **Boreholes closure in salt**. Technical Report Prepared for The U.S. Nuclear Regulatory Commission. Report No. NUREG/CR-5243 RW. University of Arizona.
- Fuenkajorn, K. and Serata, S. (1992). Geohydrological integrity of CAES in rock salt. In **Compressed-Air Energy Storage: Proceedings of the Second International Conference** (pp. 4.1-4.21). San Francisco, CA: Electric Power Research Institute.

- Fuenkajorn, K. and Serata, S. (1994). Dilation-induced permeability increase around caverns in rock salt. In **Proceedings of the First North American Rock Mechanics Symposium** (pp. 648-656). Rotterdam: A. A. Balkema.
- Gartling, D.K. (1981a). **COYOTE- A finite element computer program for nonlinear heat conduction problems.** SAND77-0463. Sandia National Laboratories, Albuquerque, NM.
- Gartling, D.K. (1981b). **MERLIN- A computer program to transfer data between finite element meshes.** SAND81-0463. Sandia National Laboratories, Albuquerque, NM.
- Gevantman, L. H. (1981). **Physical properties data for rock salt.** National Bureau of Standards Monograph 167 (282 pp.). Washington: U.S. Government Printing Office.
- Goodman, R. E. (1989). **Introduction to rock mechanics (2<sup>nd</sup> ed.).** Canada: John Wiley and Sons.
- Habib, P. and Berest, P. (1993). Rock mechanics for underground nuclear waste disposal in France: Developments and case studies. **Comprehensive Rock Engineering, Geothermal Energy and Radioactive Waste Disposal** (Vol. 5, pp. 547-563). Great Britain: Pergamon.
- Hamami, M., Tijani, S. M. and Vouille, G. (1996). A methodology for the identification of rock salt behavior using multi-step creep tests. In **Proceedings of the Third Conference on the Mechanical Behavior of Salt** (pp. 53-66). Clausthal-Zellerfeld, Germany: Trans Tech Publications.

- Hampel, A., Hunsche, U., Weidinger, P. and Blum, W. (1998). Description of the creep of rock salt with the composite model – II: Steady-state creep. In **Proceedings of the Fourth Conference on the Mechanical behavior of salt, Series on soil and rock mechanics** (Vol. 22, pp. 287-300). Montreal, Canada: Trans Tech Publications.
- Hansen, F. D. Mellegard, K. D. and Senseny, P. E. (1984). Elasticity and strength of ten natural rock salts. In **Proceedings of the First Conference on the Mechanical Behavior of Salt**, (pp. 71-83). Clausthal-Zellerfeld, Federal Republic of Germany: Trans Tech Publications.
- Hansen, F. D., Callahan, G. D. and van Sambeek, L. L. (1996). Reconsolidating of salt as applied to permanent seals for the waste isolation pilot plant. In **Proceedings of the Third Conference on the Mechanical Behavior of Salt** (pp. 232-336). Clausthal-Zellerfeld, Germany: Trans Tech Publications.
- Hardy, H. R. (1996). Application of the Kaiser effect for the evaluation of in-situ stress in salt. In **Proceedings of the Third Conference on the Mechanical Behavior of Salt**, (pp. 85-100). Clausthal-Zellerfeld, Germany: Trans Tech Publications.
- Harrington, T. J., Chabannes, C. R. and Shukla, K. (1991). Rock mechanics consolidations in the WIPP room design. In **Proceedings of the First Conference on the Mechanical Behavior of Rock Salt** (pp. 681- 696). Clausthal-Zellerfeld, Germany: Trans Tech Publications.
- Heusermann, S. (1996). Measurement of initial rock stress at the Asse salt mine. In **Proceedings of the Third Conference on the Mechanical Behavior of Salt** (pp. 101-114). Clausthal-Zellerfeld, Germany: Trans Tech Publications.

- Heusermann, S., Koss, S. and Sonnke, J. (1996). Analysis of stress measurements in the TSDE at the Asse salt mine. In **Proceedings of the Third Conference on the Mechanical Behavior of Salt** (pp. 17-29). Clausthal-Zellerfeld, Germany: Trans Tech Publications.
- Hoek, E., Kaiser, P. K. and Bawden, W. E. (1995). **Support of underground excavations in hard rock** (215 pp.). Rotherdam: A. A. Balkema.
- Hofmann, R. (1976). **STEALTH, a lagrange explicit finite-difference code for solid, structural, and themohydraulic analysis**. User's manual, EPRI NP-260, Vol. 1. Electric Power Research Institute, Palo Alto, California, August 1976, Prepared by Science Applications, Inc. San Leandro, California.
- Honecker, A. and Wulf, A. (1988). The FE-system ANSALT a dedicated tool for rock and salt-mechanics. In **Proceedings of the Second Conference on the Mechanical Behavior of Rock Salt** (pp. 4409-4520). Clausthal-Zellerfeld, Germany: Trans Tech Publications.
- Hou, Z. and Lux, K. H. (1999). Some new developments in the design of pillars in salt mining. **The Ninth International Congress on Rock Mechanics, International Society for Rock Mechanics** (pp. 297-300). Balkema.
- Hunsche, U. (1993). Failure behaviour of rock salt around underground cavities. In **Proceedings of the Seventh Symposium on Salt** (Vol. 1, pp. 59-65). Amsterdam: Elsevier Science Publishers.
- Hunsche, U. and Schulze, O. (1996). Effect of humidity and confining pressure on creep of rock salt. In **Mechanical Behavior of salt, Series on Soil and Rock Mechanics** (Vol. 20, pp. 237-248). Trans Tech Publications.



- Itasca (1992). **User manual for FLAC–fast Lagrangian analysis of continua, version 3.0**. Itasca Consulting Group Inc., Minneapolis, MN.
- Itasca (1994). **User manual for FLAC–fast Lagrangian analysis of continua in 3 dimensions, version 1.0**. Itasca Consulting Group Inc., Minneapolis, MN.
- Japakasetr, T. (1985). Review on rock salt and potash exploration in Northeast of Thailand. In **Conference on Geology and Mineral Resources Development of the Northeast of Thailand**. Khon Kaen University, Thailand.
- Japakasetr, T. and Suwanich, P. (1977). **Potash and rock salt in Thailand** (pp. A1-A252). Bangkok: Economic Geology Division, Department of Mineral Resources.
- Japakasetr, T. and Workman, D. R. (1981). **Evaporite deposits of Northeast of Thailand**. Circum-Pacific Conferences (pp. 179-187). Hawaii.
- Japakasetr, T. (1985). Review on rock salt and potash exploration in Northeast Thailand. In **Conference on Geology and Mineral Resources Development of the Northeast of Thailand** (pp. 135-147). Khon Kaen University, Thailand.
- Japan International Cooperation Agency. (1981). **Evaluation study report for ASEAN rock salt-soda ash project in the kingdom of Thailand**. Tokyo, Japan.
- Jeremic, M. L. (1994). **Rock mechanics in salt mining** (530 pp.). Rotherdam: A. A. Balkema.
- Jin, J. and Cristescu, N. D. (1998). An elastic/visco-plastic model for transient creep of rock salt. **International Journal of Plasticity** 14 (1-3): 85.

- Julien, M. R., Foerch, R., Aubertin, M. and Cailletaud, G. (1998). Some aspects of numerical implementation of SUVIC-D. In **Proceedings of the Fourth Conference on the Mechanical Behavior of Salt** (pp. 389-402). Clausthal-Zellerfeld, Germany: Trans Tech Publications.
- Knowles, M. K., Borns, D., Fredrich, J., Holcomb, D., Price, R. and Zeuch, D. (1998). Testing the disturbed zone around a rigid inclusion in salt. In **Proceedings of the Fourth Conference on the Mechanical Behavior of Salt** (pp. 175-188). Clausthal-Zellerfeld, Germany: Trans Tech Publications.
- Korthaus, E. (1996). Measurement of crushed salt consolidation under hydrostatic and deviatoric stress conditions. In **Proceedings of the Third Conference on the Mechanical Behavior of Salt** (pp. 311-322). Clausthal-Zellerfeld, Germany: Trans Tech Publications.
- Korthaus, E. (1998). Consolidation and deviatoric deformation behavior of dry crushed salt at temperatures up to 150 °C. In **Proceedings of the Fourth Conference on the Mechanical Behavior of Salt** (pp. 365-378). Clausthal-Zellerfeld, Germany: Trans Tech Publications.
- Krieg, R. D., Morgan, H. S. and Stone C. M. (1988). Structural analyses overview on the WIPP project. In **Proceedings of the Second Conference on the Mechanical Behavior of Rock Salt** (pp. 533-549). Clausthal-Zellerfeld, Germany: Trans Tech Publications.
- Kwon, S. and Miller, H. (1998). Using a neural network to the deformation of underground excavations in rock salt. In **Proceedings of the Fourth Conference on the Mechanical Behavior of Salt** (pp. 405-416). Clausthal-Zellerfeld, Germany: Trans Tech Publications.

- Langer, M. (1993). Geoscientific evaluation of geological and geotechnical barriers with respect to waste disposal projects. In **Proceedings of the Seventh International IAEG Congress**. (pp. 2827-2935). Rotterdam, Balkema.
- Langer, M. (1996). Underground disposal of wastes requiring special monitoring in salt rock masses. In **Proceedings of the Third Conference on the Mechanical Behavior of Salt** (Vol. 20, pp. 583-603). Clausthal-Zellerfeld, Germany: Trans Tech Publications.
- Langer, M. and Rothemeyer, H. (1996). Geoscientific and rock mechanical activities for the radioactive waste repositories in Germany: Key issues, status and future plans. Chapter 11: Germany.
- Lux, K. H. and Schmidt, T. (1996). Optimizing underground gas storage operations in salt caverns, with special reference to the rock mechanics and thermodynamics involved. In **Proceedings of the Third Conference on the Mechanical Behavior of Salt** (pp. 445-458). Clausthal-Zellerfeld, Germany: Trans Tech Publications.
- Maleki, H. and Chaturvedi, L. (1997). Prediction of long-term closure and stability of underground workings in the waste isolation pilot plant. **International Journal of Rock Mechanics and Mining Sciences** 34 (3-4): 493.
- Massier, D. (1996). Rate type constitutive equations with applications to the calculus of the stress state and of the displacement field around cavities in rock salt. In **the Third Conference on Mechanical behavior of salt, Series on soil and rock mechanics** (Vol. 20, pp. 545-558). Trans Tech Publications.

- Matalucci, R.V. and Hunter, T.O. (1984). Geomechanical applications for the waste isolation pilot plant (WIPP) project. In **Proceedings of the First Conference on the Mechanical Behavior of Salt** (pp. 791-812). Clausthal-Zellerfeld, Germany: Trans Tech Publications.
- Matalucci, R.V. and Munson, D.E. (1988). Planning, developing, and organizing in situ tests for the waste isolation pilot plant (WIPP). In **Proceedings of the Second Conference on the Mechanical Behavior of Salt** (pp. 329-360). Clausthal-Zellerfeld, Germany: Trans Tech Publications.
- Munson, D. E. and Wawersik, W. R. (1993). Constitutive modeling of salt behavior – State of the technology. In **Proceedings of the Seventh International Congress on Rock Mechanics** (vol. 3, pp. 1797-1810). Balkema.
- Nguyen-Minh, D. and Quintanilha de Menezes, E. (1996). Incompressible numerical modeling for long term convergence evaluation of underground works in salt. In **Proceedings of the Third Conference on the Mechanical Behavior of Salt** (pp. 523-531). Clausthal-Zellerfeld, Germany: Trans Tech Publications.
- Nicolae, M. (1996). Research work concerning the characterization of the rheologic behavior of the salt massif in the Slanic-Prahova zone. In **Proceedings of the Third Conference on the Mechanical Behavior of Salt** (pp. 559-570). Clausthal-Zellerfeld, Germany: Trans Tech Publications.
- Ong, V. (1994). **Evaluation of 3D VISAGE finite element program**. Report submitted to SPPA.

- Ong, V., Unrau, J., Jones, J. Coode, A. and Mackintosh, D. (1998). Triaxial creep testing of saskatchewan potash samples. In **Proceedings of the Fourth Conference on the Mechanical Behavior of Salt** (pp. 469-480). Clausthal-Zellerfeld, Germany: Trans Tech Publications.
- Plookphol, T. (1987). **Engineering properties of the evaporite in the Khorat plateau**. M.S. thesis, Asian Institute of Technology, Thailand.
- Pudewills, A. (1998). Influence of anhydrite strata on a waste disposal drift. In **Proceedings of the Fourth Conference on the Mechanical Behavior of Salt** (pp. 551-560). Clausthal-Zellerfeld, Germany: Trans Tech Publications.
- Pudewills, A. and Hornberger, K. (1996). A unified visco-plastic model for rock salt. In **Proceedings of the Third Conference on the Mechanical Behavior of Salt** (pp. 45-52). Clausthal-Zellerfeld, Germany: Trans Tech Publications.
- Pudewills, A., Muller-Hoeppe, N. and Papp, R. (1995). Thermal and thermo-mechanical analyses for disposal in drifts of a repository in rock salt. **Nuclear Technology** 1: 79-88.
- Raj, S. V. and Pharr, G. M. (1992). Effect of temperature on the formation of creep substructure in sodium chloride single crystal. **American Ceramic Society** 75 (2): 347-352.
- Ratigan, J. L. and Vogt, T. J. (1993). LPG storage at Mont Belvieu, Texas: A case history. **SPE Advanced Technologies Series** 1 (1): 204-211.
- Rizkalla, M. (1991). **Comparison of three different geotechnical codes, using GEOROC**. Report Submitted to SPPA by Noranda Technology Centre.

- Rokahr, R. and Staudtmeister, K. (1996). The assessment of the stability of a cavern field in bedded salt with the help of the new Hannover dimensioning concept. In **Proceedings of the Third Conference on the Mechanical Behavior of Salt** (pp. 533-544). Clausthal-Zellerfeld, Germany: Trans Tech Publications.
- Rolnik, H. (1988). High-level waste repository in rock salt: Suitable rheological forms. In **Proceedings of the Second Conference on the Mechanical Behavior of Rock Salt** (pp. 625-643). Clausthal-Zellerfeld, Germany: Trans Tech Publications.
- Salzer, K. and Scheriner, W. (1998). Long-term safety of salt mines in flat bedding. In **Proceedings of the Fourth Conference on the Mechanical Behavior of Salt** (pp. 481-494) Clausthal-Zellerfeld, Germany: Trans Tech Publications.
- Sattayarak, N. (1985). Review on geology of Khorat plateau. In **Conference on Geology and Mineral Resources Development of the Northeast** (pp. 23-30). Thailand: Khon Kaen University.
- Senseny, P. E. and Fussum, A. F. (1998). Testing to estimate the Munson-Dawson parameters. In **Proceedings of the Fourth Conference on the Mechanical Behavior of Salt** (pp. 263-272). Clausthal-Zellerfeld, Germany: Trans Tech Publications.
- Senseny, P. E., Handin, J. W., Hansen, F. D. and Russell, J. E. (1992). Mechanical behavior of rock salt: phenomenology and micro-mechanisms. **International Journal of Rock Mechanics and Mining Sciences** 29 (4): 363-378.
- Serata (1991). **GEO/REM computer programs for Sifto Canada's Goderich salt mine**. Internal report prepared by Serata Geomechanics Inc., Goderich, ON, Canada.

- Serata, S. and Fuenkajorn, K. (1991). **Permeability studies in relation to stress state and cavern design: Phase I.** Research Project Report, Contract 1-91, prepared for Solution Mining Research Institute by Serata Geomechanics, Inc., Richmond, CA.
- Serata, S. and Fuenkajorn, K. (1992a). Formulation of a constitutive equation for salt. In **Proceedings of the Seventh International Symposium on Salt** (Vol. 1, pp. 483-488). Amsterdam: Eisevier Science.
- Serata, S. and Fuenkajorn, K. (1992b). **Finite element program "GEO" for modeling brittle-ductile deterioration of aging earth structures.** SMRI Paper, Presented at the Solution Mining Research Institute, Fall Meeting, October 19-22, Houston, Texas. (24 pp.).
- Serata, S. and Fuenkajorn, K. (1993). Formulation of a constitutive equation for salt. **The Seventh Symposium on Salt** (pp.483-488). Amsterdam: Eisevier Science Publications.
- Spiers, C. J. and Carter, N. L. (1998). Microphysics of rock salt flow in nature. In **Proceedings of the Fourth Conference on the Mechanical Behavior of Salt** (pp. 115-128). Clausthal-Zellerfeld, Germany: Trans Tech Publications.
- Stone, C. M., Krieg, R. D. and Beisinger, Z.E. (1985). **SANCHO, a finite element computer program for the quasistatic, large deformation, Inelastic response of two-dimensional solid**, SAND84-2618.
- Stormont, J. C. and Fuenkajorn, K. (1994). Dilation-induced permeability changes in rock salt. In **Proceedings of the Eighth International Conference on Computer Methods and Advances in Geomechanics.** (pp. 1296-1273). Morgantown, West Virginia.

- Stormont, J. C., Daemen J. J. K. and Desai, C. S. (1992). Prediction of dilation and permeability changes in rock salt. **International Journal for Numerical and Analytical Methods in Geomechanics** 16 (8): 545-569.
- Supajanya, T., Vichapan, K. and Sri-israporn, S. (1992). Surface expression of shallow salt dome in northeast Thailand. In **National conference on geologic resources of Thailand: Potential for future development** (pp. 89-95). Thailand: Department of Mineral Resources.
- Suwanich, P. (1978). Potash in northeastern of Thailand (in Thai). **Economic Geology Document No. 22**. Bangkok: Economic Geology, Division, Department of Mineral Resources.
- Suwanich, P. (1986). **Potash and Rock Salt in Thailand**: Nonmetallic Minerals Bulletin No.2. Economic Geology Division; Department of Mineral Resources; Bangkok, Thailand.
- Suwanich, P. and Ratanajaruraks, P. (1982). Sequences of rock salt and potash in Thailand. **Nonmetallic Minerals Bulletin No. 1**. Bangkok: Economic Geology, Division, Department of Mineral Resources.
- Suwanich, P., Ratanajaruraks, P. and Kunawat, P. (1982). **Core log Bamnet Narong area at Chaiyaphum province**. Bangkok: Economic Geology Division, Department of Mineral Resources.
- Tabakh, M. E., Utha-aroon, C., Coshell, L. and Warren, K. (1995). Cretaceous saline deposits of the Maha Sarakham Formation in the Khorat basin, Northeastern Thailand. In **International Conference on Geology, Geotechnology and Mineral Resources of Indochina (GEO-INDO'95)** 22-25 November 1995. Khon Kaen, Thailand: Khon Kaen University.



- The Office of Atomic Energy for Peace. (2000). **Nuclear review** (Thai). 15 (1).
- Therol, L. and Ghoreychi, M. (1996). Rock salt damage experimental results and interpretation. In **Proceedings of the Third Conference on the Mechanical Behavior of Salt** (pp. 175-189). Clausthal-Zellerfeld, Germany: Trans Tech Publications.
- Thoms, R. L. and Gehle, R. (1994). **Analysis of a solidified waste disposal cavern in gulf coast salt dome**. SMRI Fall Meeting (p. 637).
- Utha-aroon, C. (1993). Continental origin of the Maha Sarakham evaporites, northeastern Thailand. **Journal of Southeast Asian Earth Sciences**. 8 (1-4): 193-203.
- Van den Broek, W. M. G. T. (1989). **Aspects of underground disposal of radioactive waste in rock salt**. Ph.D thesis, Technical University Karlsruhe.
- Van den Broek, W. M. G. T. and Heilbron, H. C. (1998). Influence of salt behavior on the retrievability of radioactive waste. In **Proceedings of the Fourth Conference on the Mechanical Behavior of Salt** (pp. 469-480). Clausthal-Zellerfeld, Germany: Trans Tech Publications.
- Van den Broek, W. M. G. T., Menken, M. J. V. and Heilbron, H. C. (1994). Preliminary study on retrieval of radioactive waste from a salt-mine repository. In **Proceedings of Symposium on Waste Management** (Vol. 1, pp. 593-596). Tucson.
- Viboonsawat, P. (1998). Vision of energy: Quality of life and development. In **Vision Thailand in Science, Technology, Environmental, Telecommunication, Energy and Human Resources** (pp. 108-55). Bangkok: Office of the Civil Service Commission, Association of Thai Government Scholarships.

- Vogler, U. W. and Kovari, K. (1978). Suggested methods for determining the strength of rock materials in triaxial compression. **International Journal of Rock Mechanics and Mining Sciences and Geomechanics Abstracts**. 15 (2): 47-54.
- Vouille, G., Bergues, J., Durup, J. G. and You, T. (1996). Study of the stability of caverns in rock salt created by solution mining proposal for a new design criterion. In **Proceedings of the Third Conference on the Mechanical Behavior of Salt** (Vol. 20, pp. 427-444). Clausthal-Zellerfeld, Germany: Trans Tech Publications.
- Wallner, M. (1984). Analysis of thermo-mechanical problems related to the storage of heat producing radioactive waste in rock salt. In **Proceedings of the First Conference on the Mechanical Behavior of Salt** (pp. 739-763). Clausthal-Zellerfeld, Germany: Trans Tech Publications.
- Wallner, M. and Wulf, A. (1982). Thermomechanical calculations concerning the design of a radioactive waste repository in rock salt. In **ISRM Symposium**, 26-28 May 1982. (pp. 1003-1012). Aachen.
- Wanten, P. H., Spiers, C. J. and Peach, C. J. (1996). Deformation of NaCl single crystals at  $0.27T_m < T < 0.44T_m$ . In **Proceedings of the Third Conference on the Mechanical Behavior of Salt** (pp. 117-128). Clausthal-Zellerfeld, Germany: Trans Tech Publications.
- Warren, J. (1999). **Evaporites: Their evolution and economics** (pp. 235-239). Blackwell Science.
- Weidinger, P., Blum, W., Hampel, A. and Hunsche, U. (1998). Description of the creep of rock salt with the composite model - I. transient creep. In **Proceedings of the Fourth Conference on the Mechanical Behavior of Salt** (pp. 277-286). Clausthal-Zellerfeld, Germany: Trans Tech Publications.

- Wetchasat, K. (2002). **Assessment of mechanical performance of rock salt formations for nuclear waste repository in northeastern Thailand**, M.S. thesis, Suranaree University of Technology, Thailand.
- Whittaker, B. N. and Reddish, D. J. (1993). Subsidence behavior of rock structures. **Comprehensive Rock Engineering Principles, Practice and Project: Excavation, Support and Monitoring** (Vol. 4, pp. 751-780). London, Pergamon.
- Yumuang, S. (1983). **On the origin of evaporite deposits in the Maha Sarakham Formation in Bamnet Narong area, Changwat Chaiyaphum**. A Thesis Submitted in Partial Fulfillment of the Requirements for the Degrees of Master of Science, Department of Geology, Graduate School, Chulalongkorn University, Thailand.
- Yumuang, S. (1995). **Potash ore reserve evaluation of Bamnet Narong area, Northeast of Thailand**. Department of Geology, Faculty of Science, Chulalongkorn University.
- Yumuang, S., Khantaprab, C. and Taiyagupt, M. (1986). **The evaporite deposits in Bamnet Narong area, northeastern Thailand**. GEOSEA V Proceedings, August, 1986 (Bulletin 20, vol. 2, pp. 249-267). Geological Society of Malaysia.
- Zhang, C., Schmidt, M. M. and Staupendahl, G. (1996). Experimental and modeling results for compaction of crushed salt. In **Proceedings of the Third Conference on the Mechanical Behavior of Salt** (pp. 391-402). Clausthal-Zellerfeld, Germany: Trans Tech Publications.

**APPENDIX A**

**STRATIGRAPHIC COLUMN OF BOREHOLES USED  
IN THE MODELING**

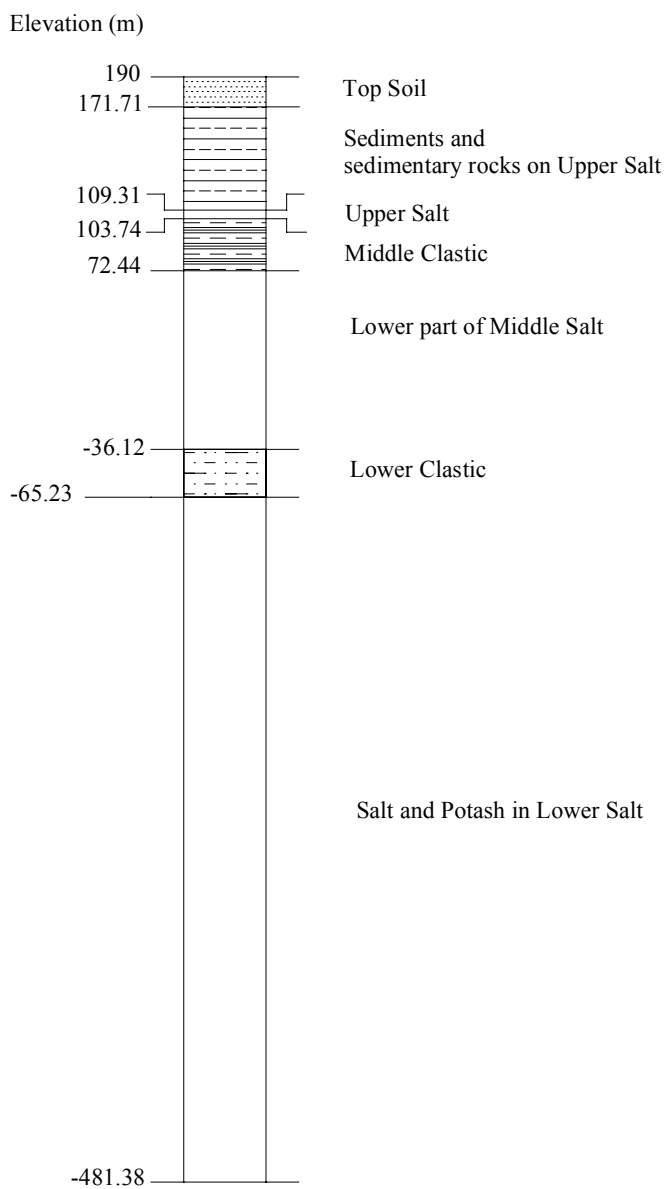


**Figure A.1** Stratigraphic column of rock salt and associated rocks at Ban Khao, Muang District, Udon Thani Province (borehole no. K-006).

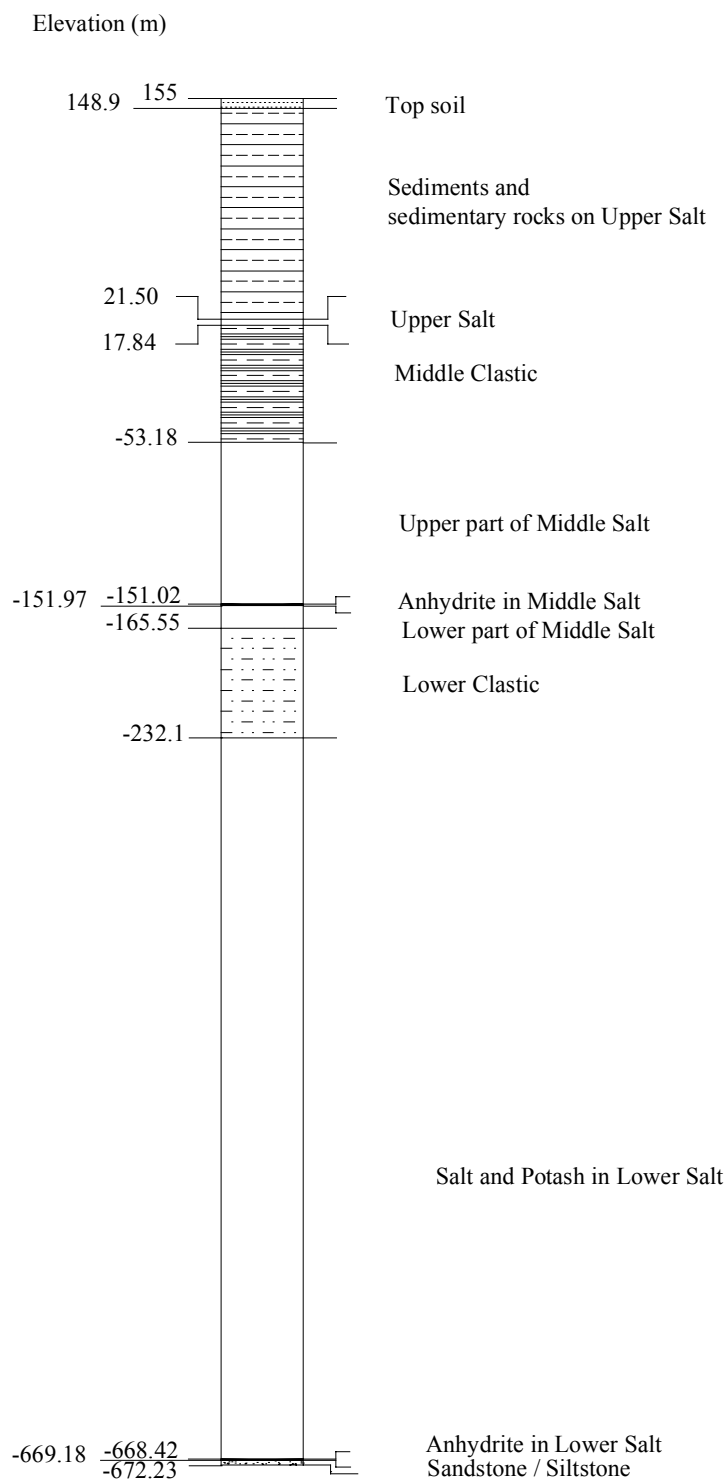


**Figure A.2** Stratigraphy column of rock salt and associated rocks at Ban Kudjig, Wanon Niwat District, Maha Sarakham Province (borehole no. K-055).

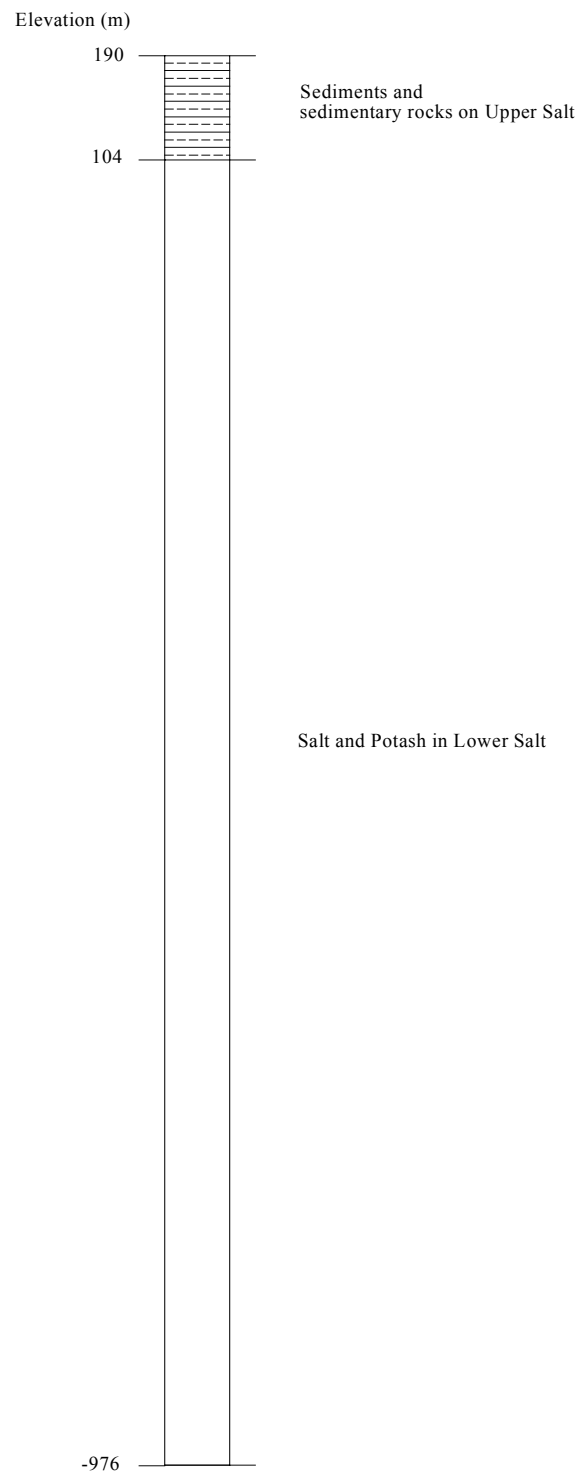


**Figure A.3** Stratigraphy column of rock salt and associated rocks at Ban Nong Plue, Borabue District, Maha Sarakham Province (borehole no. K-089).

**APPENDIX B**

**RESULTS FROM THE COMPUTER MODELING TO  
STUDY THE EFFECT OF ROOM WIDTH**



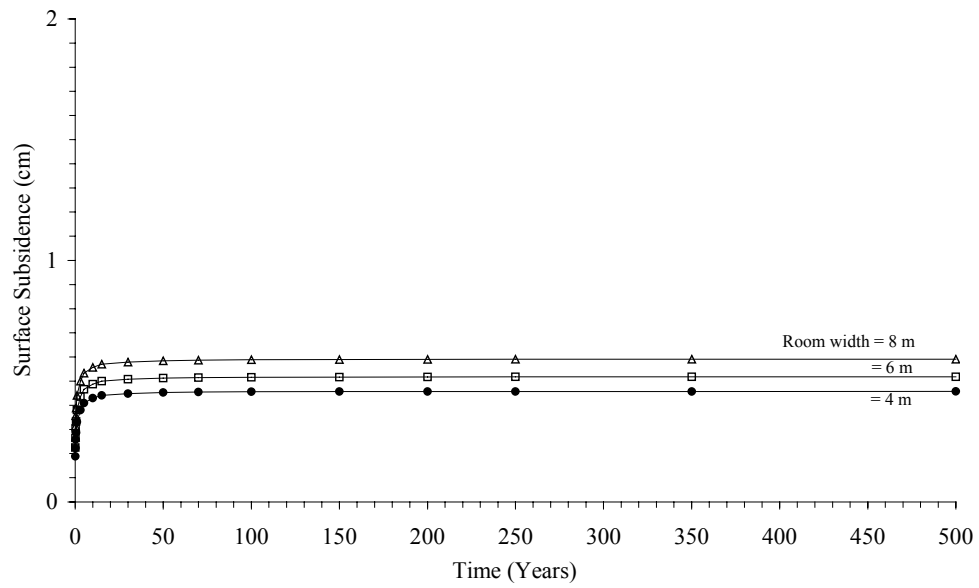


**Figure B.1** Predicted surface subsidence induced by repository rooms for various room widths. The room depth is 502 meters.

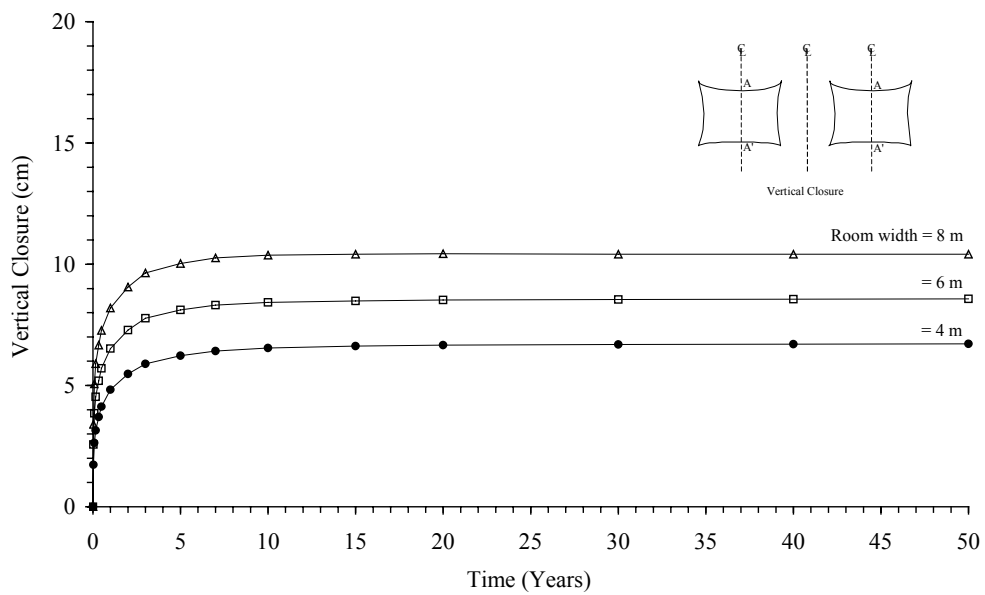


**Figure B.2** Predicted vertical closure of repository rooms for various room widths. The room depth is 502 meters.

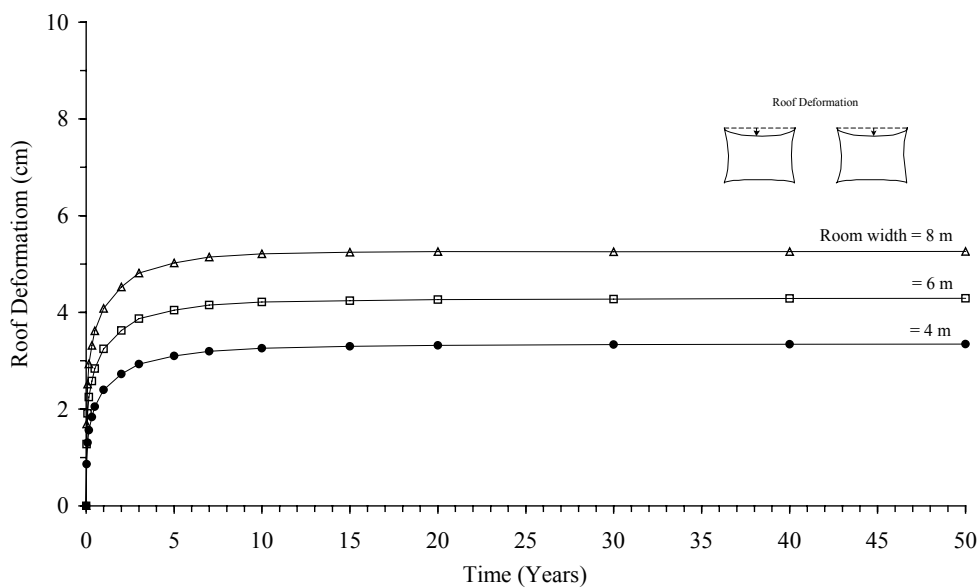


**Figure B.3** Predicted roof deformation of repository rooms for various room widths. The room depth is 502 meters.

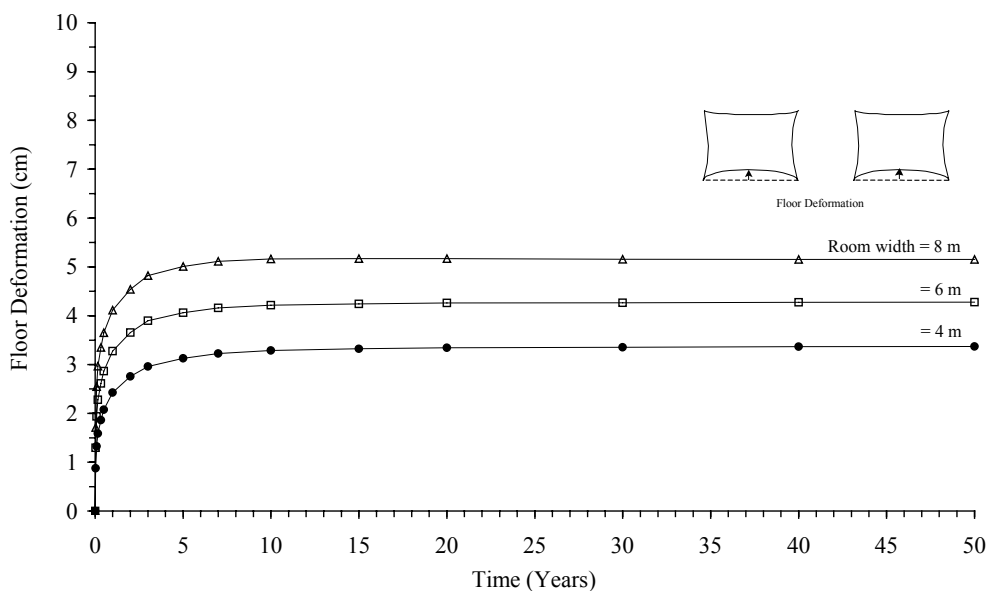


**Figure B.4** Predicted floor deformation of repository rooms for various room widths. The room depth is 502 meters.

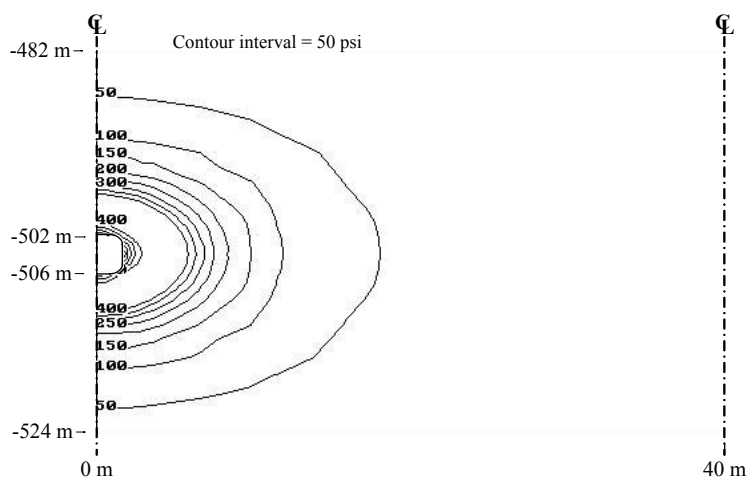


**Figure B.5** Contour of octahedral shear stress around repository room (model KM-R4) at 50 years after emplacement (the maximum octahedral shear stress = 450 psi). The room width is 4 meters.

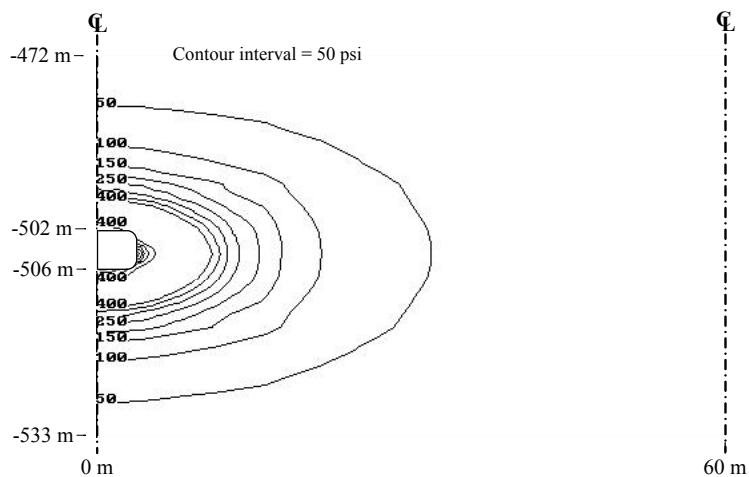


**Figure B.6** Contour of octahedral shear stress around repository room (model KM-R6) at 50 years after emplacement (the maximum octahedral shear stress = 450 psi). The room width is 6 meters.

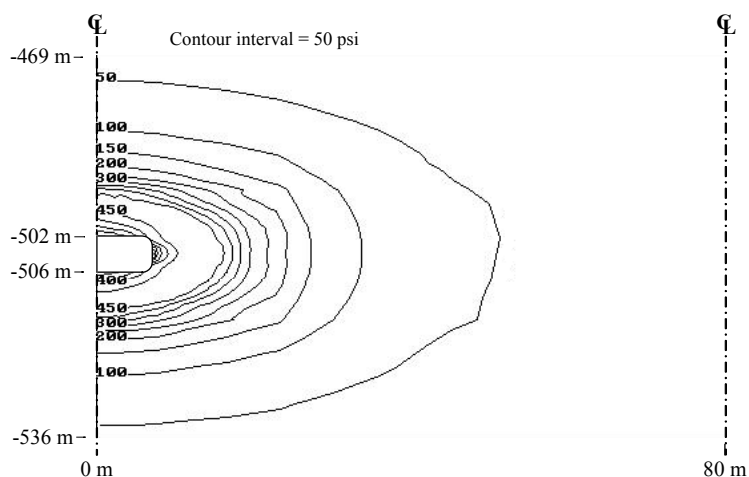


**Figure B.7** Contour of octahedral shear stress around repository room (model KM-R8) at 50 years after emplacement (the maximum octahedral shear stress = 500 psi). The room width is 8 meters.

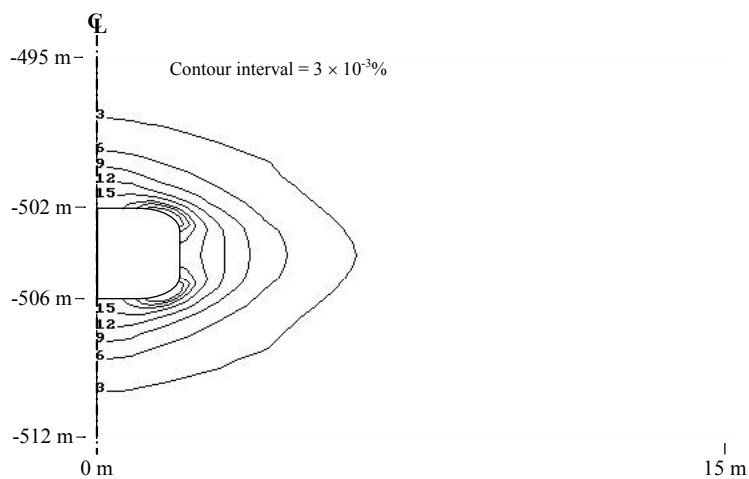


**Figure B.8** Contour of octahedral shear strain around repository room (model KM-R4) at 50 years after emplacement (the maximum octahedral shear strain =  $27 \times 10^{-3}\%$ ). The room width is 4 meters.

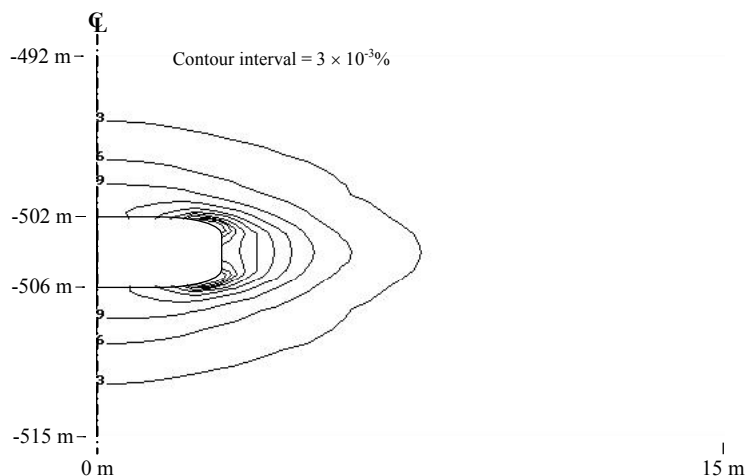


**Figure B.9** Contour of octahedral shear strain around repository room (model KM-R6) at 50 years after emplacement (the maximum octahedral shear strain =  $33 \times 10^{-3}\%$ ). The room width is 6 meters.

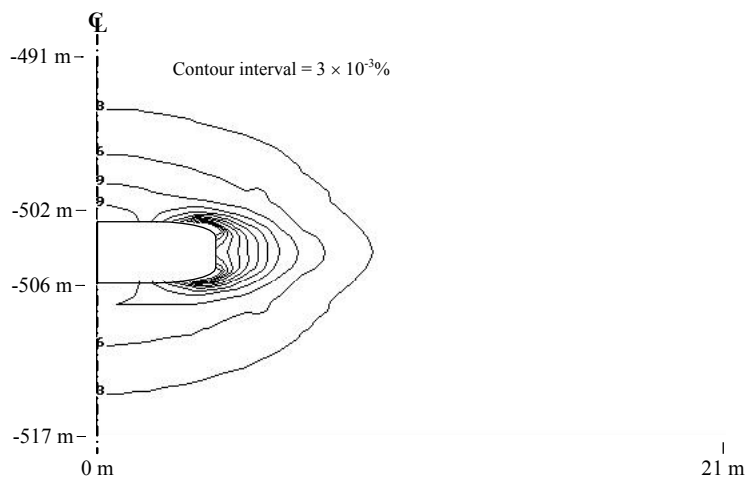


**Figure B.10** Contour of octahedral shear strain around repository room (model KM-R8) at 50 years after emplacement (the maximum octahedral shear strain =  $39 \times 10^{-3}\%$ ). The room width is 8 meters.

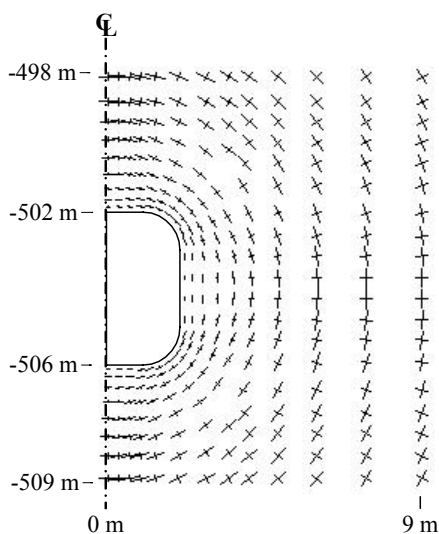


**Figure B.11** Principal stress vectors around repository room (model KM-R4) at 50 years after emplacement (the maximum stress = 2,575 psi). Scale is 10,000 psi/inch. The room width is 4 meters.

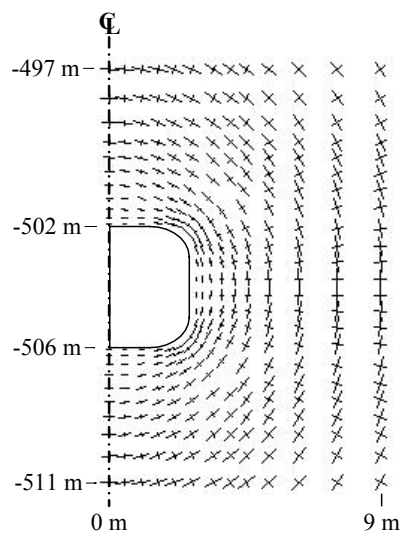


**Figure B.12** Principal stress vectors around repository room (model KM-R6) at 50 years after emplacement (the maximum stress = 2,575 psi). Scale is 10,000 psi/inch. The room width is 6 meters.

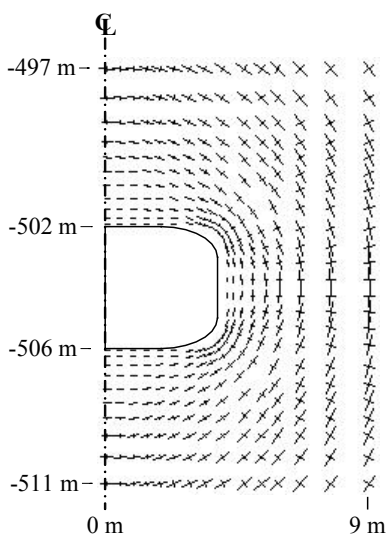


**Figure B.13** Principal stress vectors around repository room (model KM-R8) at 50 years after emplacement (the maximum stress = 2,575 psi). Scale is 10,000 psi/inch. The room width is 8 meters.

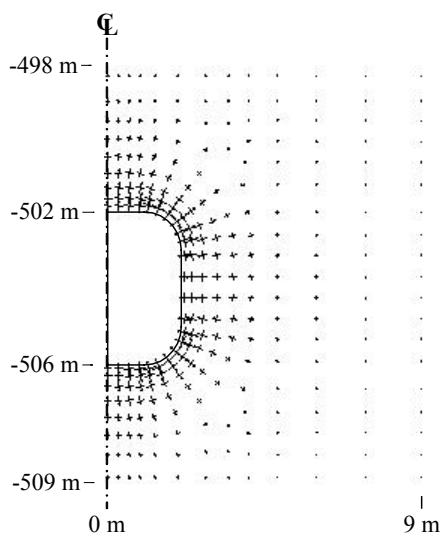


**Figure B.14** Principal strain vectors around repository room (model KM-R4) at 50 years after emplacement (the maximum strain = 1.81%). Scale is 10% /inch. The room width is 4 meters.

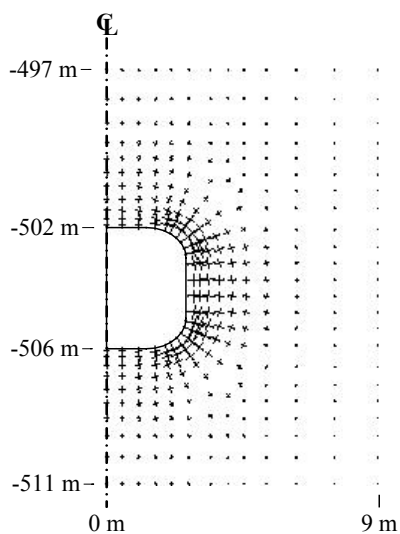


**Figure B.15** Principal strain vectors around repository room (model KM-R6) at 50 years after emplacement (the maximum strain = 2.16%). Scale is 10% /inch. The room width is 6 meters.

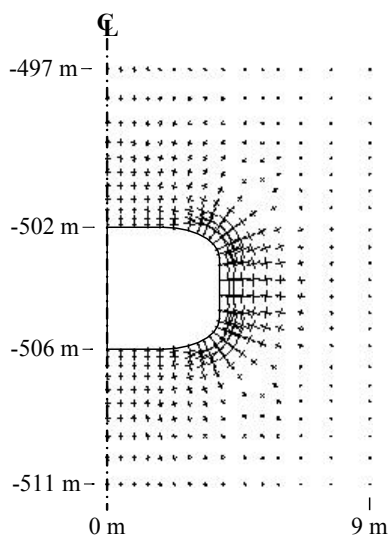


**Figure B.16** Principal strain vectors around repository room (model KM-R8) at 50 years after emplacement (the maximum strain = 2.61%). Scale is 10% /inch. The room width is 8 meters.



## **APPENDIX C**

### **RESULTS FROM THE COMPUTER MODELING TO STUDY THE EFFECT OF PILLAR WIDTH**

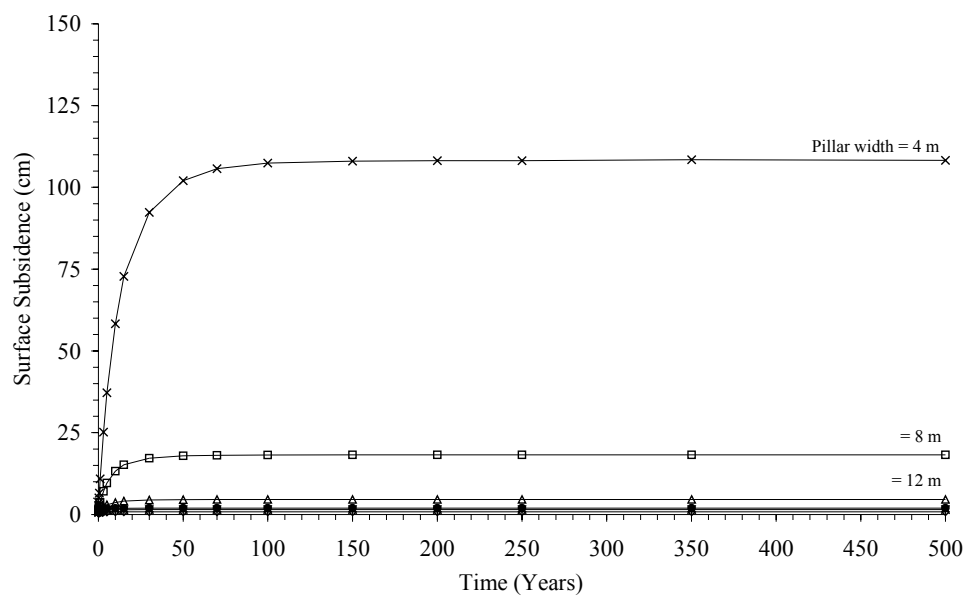


**Figure C.1** Predicted surface subsidence induced by repository rooms for various pillar widths. The room depth is 502 meters.

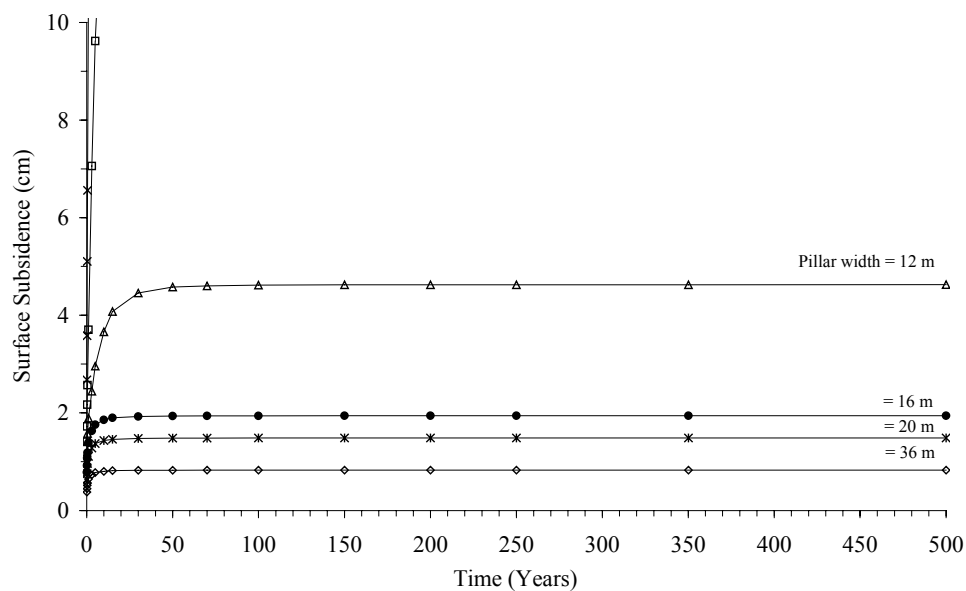


**Figure C.2** Close-up predicted surface subsidence induced by repository rooms for various pillar widths. The room depth is 502 meters.

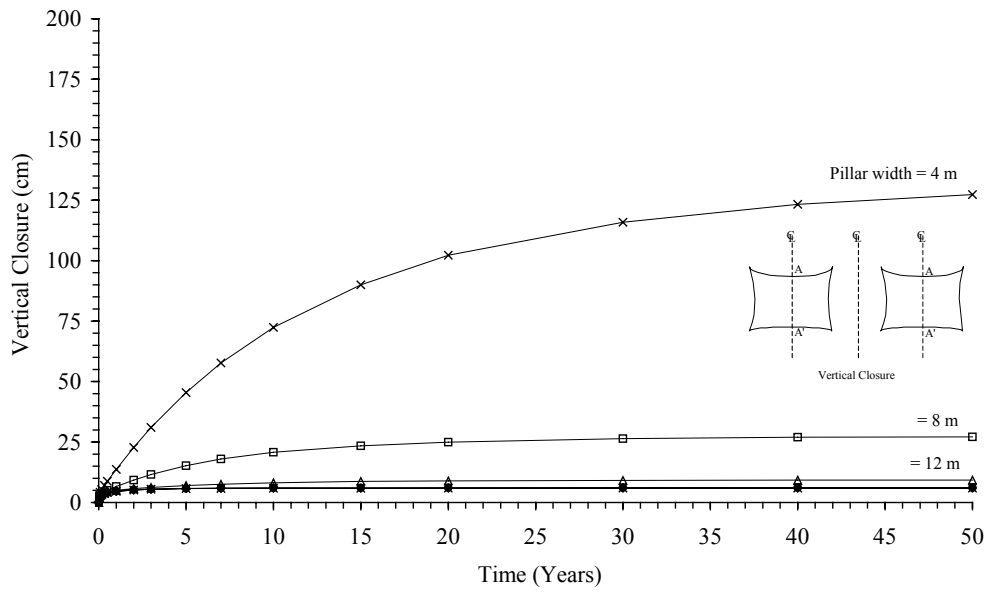


**Figure C.3** Predicted vertical closure of repository rooms for various pillar widths.

The room depth is 502 meters.

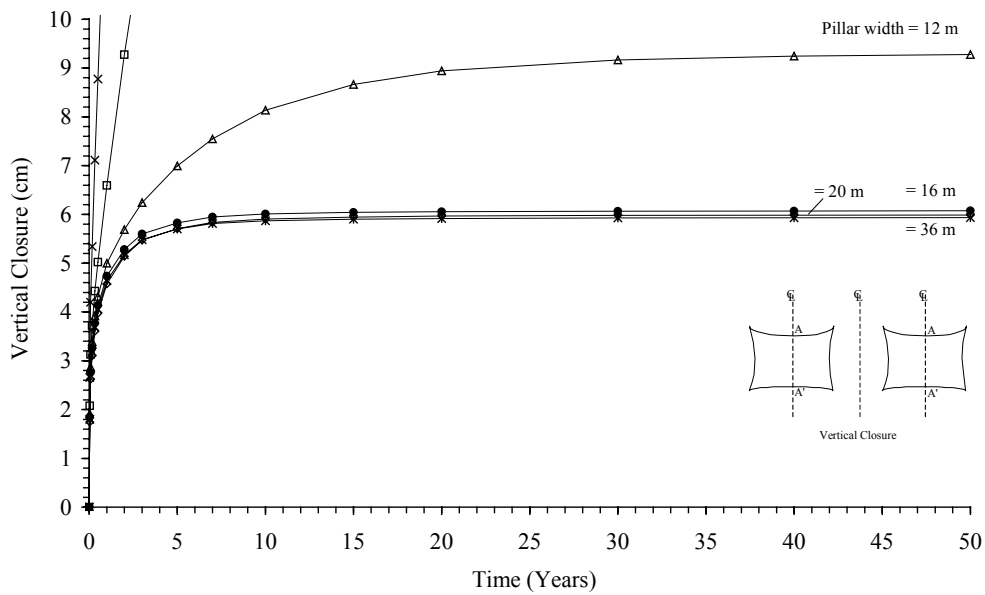


**Figure C.4** Closure-up predicted vertical closure of repository rooms for various

pillar widths. The room depth is 502 meters.

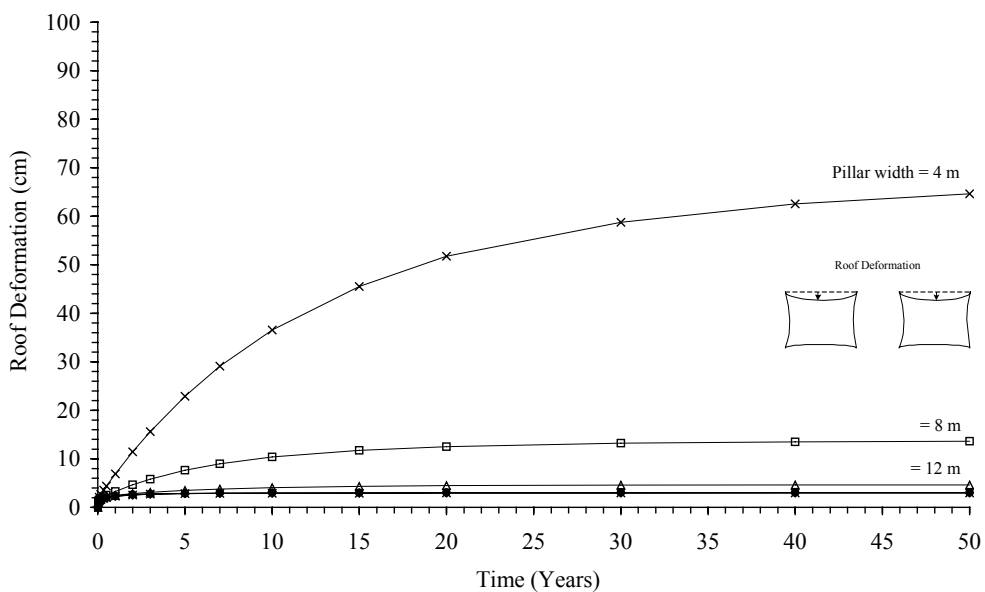


**Figure C.5** Predicted roof deformation of repository rooms for various pillar widths.

The room depth is 502 meters.

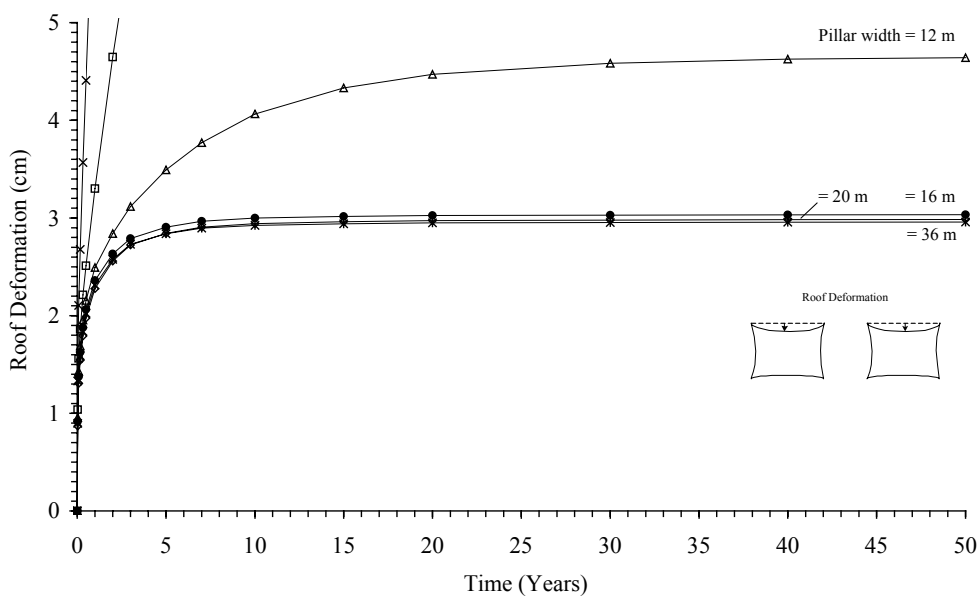


**Figure C.6** Closure-up predicted roof deformation of repository rooms for various pillar widths. The room depth is 502 meters.

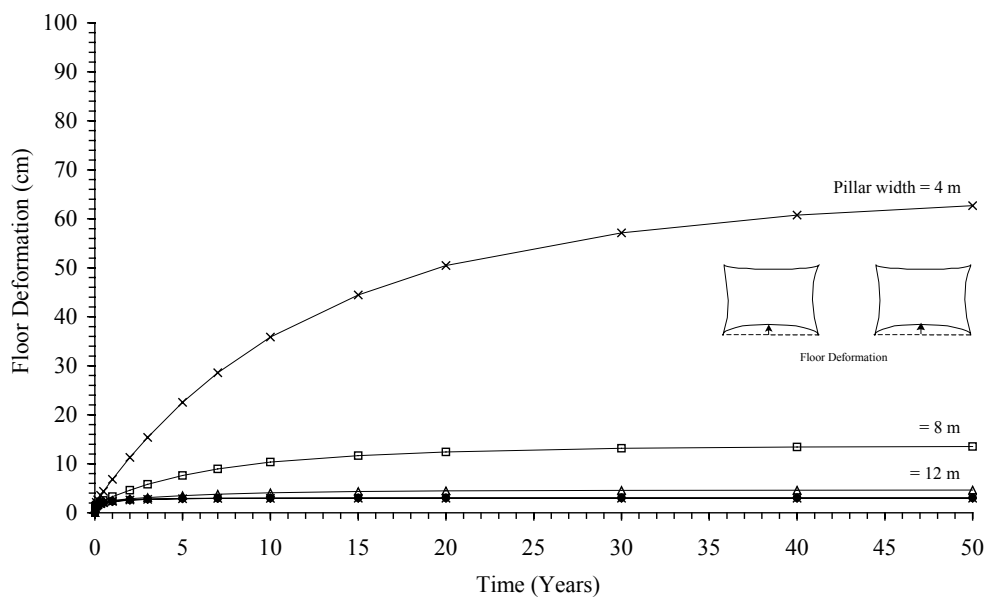


**Figure C.7** Predicted floor deformation of repository rooms for various pillar widths.

The room depth is 502 meters.

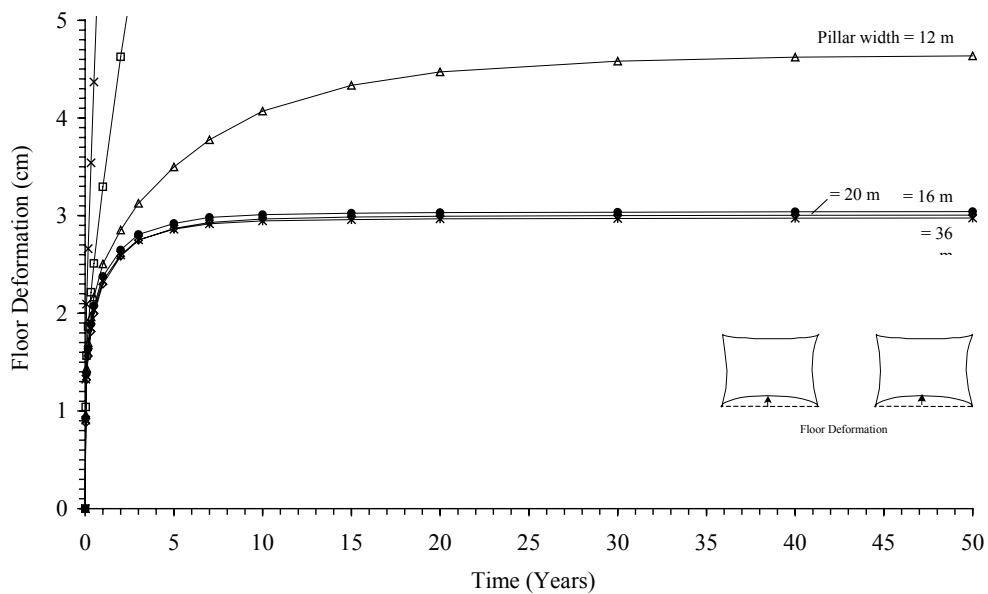


**Figure C.8** Closure-up predicted floor deformation of repository rooms for various

pillar widths. The room depth is 502 meters.

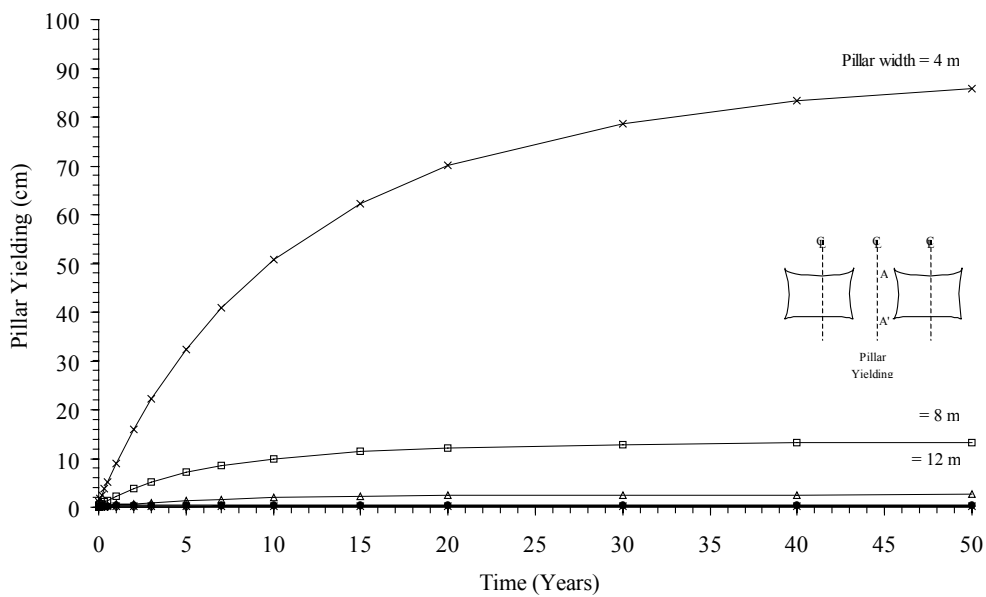


**Figure C.9** Predicted pillar yielding of repository rooms for various pillar widths.

The room depth is 502 meters.

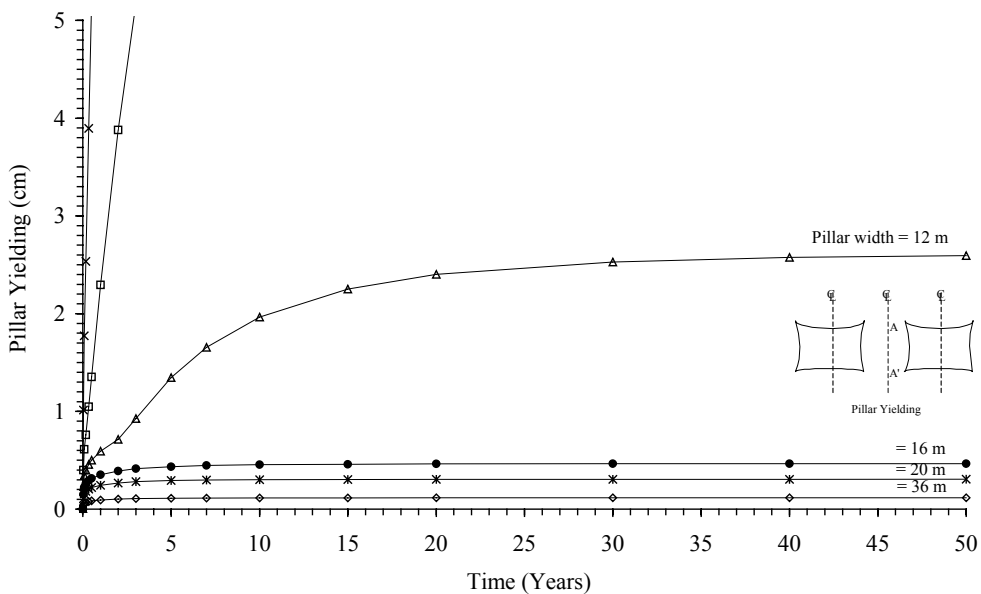


**Figure C.10** Closure-up predicted pillar yielding of repository rooms for various

pillar widths. The room depth is 502 meters.

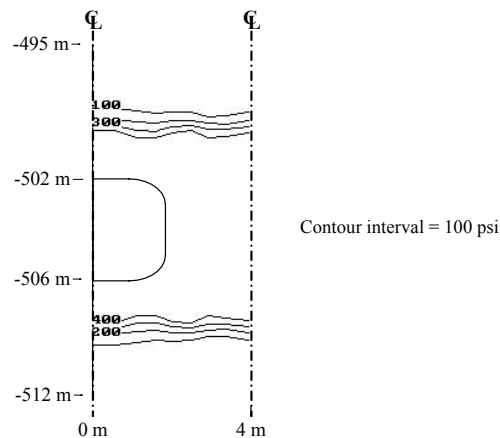


**Figure C.11** Contour of octahedral shear stress around repository room (model KM-P1) at 50 years after emplacement (the maximum octahedral shear stress = 500 psi). The room is 4 m wide and 4 m high, separated by 4 m wide pillar.

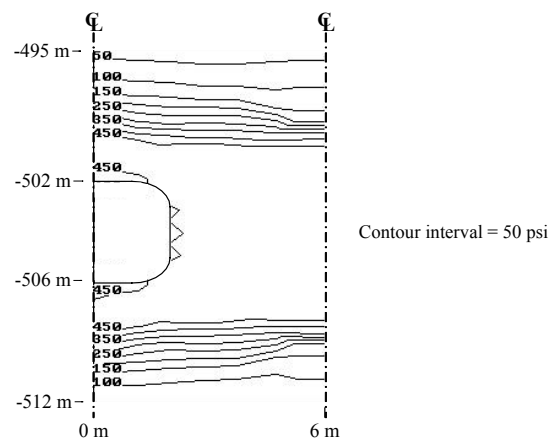


**Figure C.12** Contour of octahedral shear stress around repository room (model KM-P2) at 50 years after emplacement (the maximum octahedral shear stress = 500 psi). The room is 4 m wide and 4 m high, separated by 8 m wide pillar.

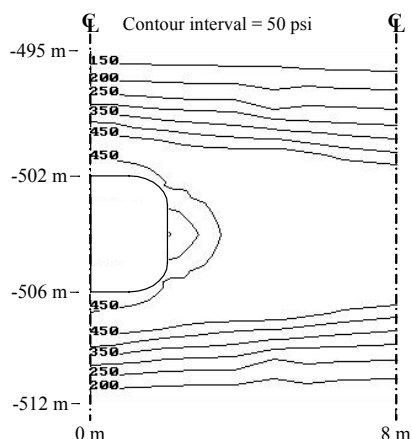


**Figure C.13** Contour of octahedral shear stress around repository room (model KM-P3) at 50 years after emplacement (the maximum octahedral shear stress = 500 psi). The room is 4 m wide and 4 m high, separated by 12 m wide pillar.

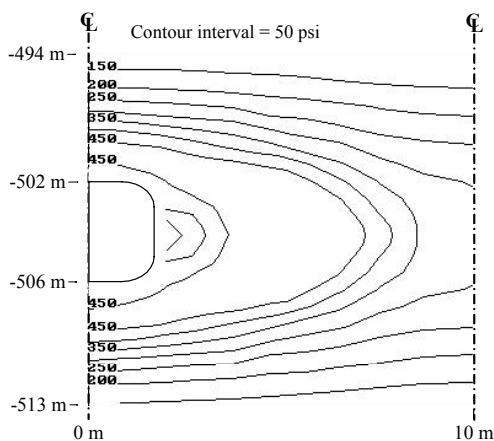


**Figure C.14** Contour of octahedral shear stress around repository room (model KM-P4) at 50 years after emplacement (the maximum octahedral shear stress = 500 psi). The room is 4 m wide and 4 m high, separated by 16 m wide pillar.



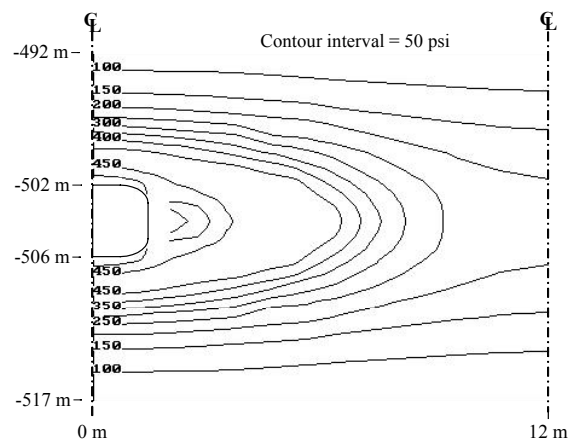


**Figure C.15** Contour of octahedral shear stress around repository room (model KM-P5) at 50 years after emplacement (the maximum octahedral shear stress = 500 psi). The room is 4 m wide and 4 m high, separated by 20 m wide pillar.

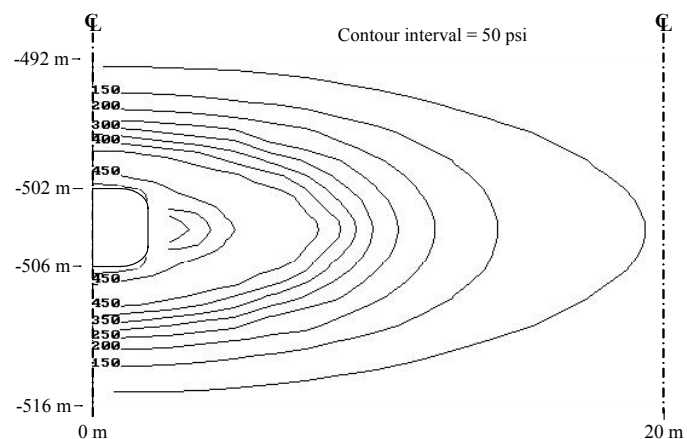


**Figure C.16** Contour of octahedral shear stress around repository room (model KM-P9) at 50 years after emplacement (the maximum octahedral shear stress = 500 psi). The room is 4 m wide and 4 m high, separated by 36 m wide pillar.

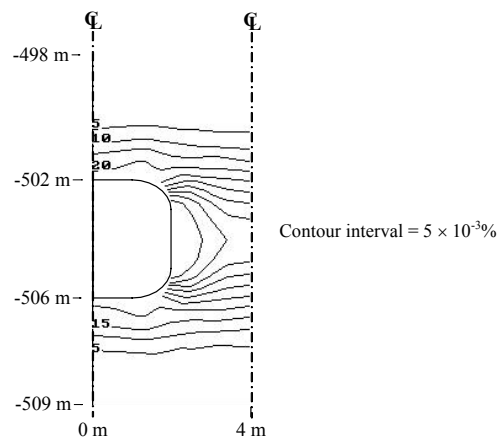


**Figure C.17** Contour of octahedral shear strain around repository room (model KM-P1) at 50 years after emplacement (the maximum octahedral shear strain =  $55 \times 10^{-2}$  %). The room is 4 m wide and 4 m high, separated by 4 m wide pillar.

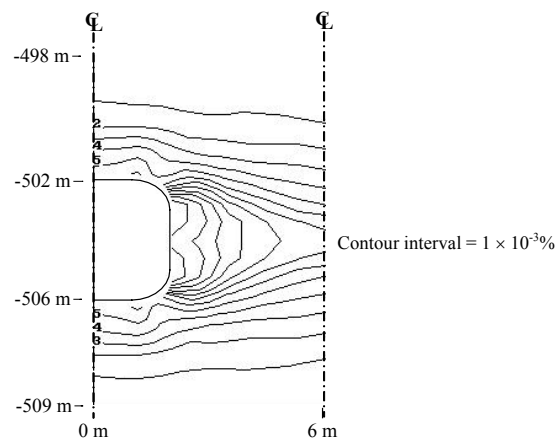


**Figure C.18** Contour of octahedral shear strain around repository room (model KM-P2) at 50 years after emplacement (the maximum octahedral shear strain =  $13 \times 10^{-2}$  %). The room is 4 m wide and 4 m high, separated by 8 m wide pillar.

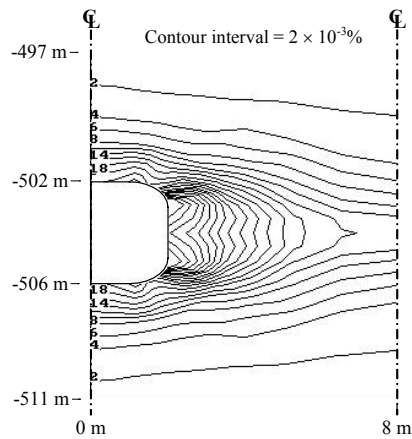


**Figure C.19** Contour of octahedral shear strain around repository room (model KM-P3) at 50 years after emplacement (the maximum octahedral shear strain =  $42 \times 10^{-3}\%$ ). The room is 4 m wide and 4 m high, separated by 12 m wide pillar.

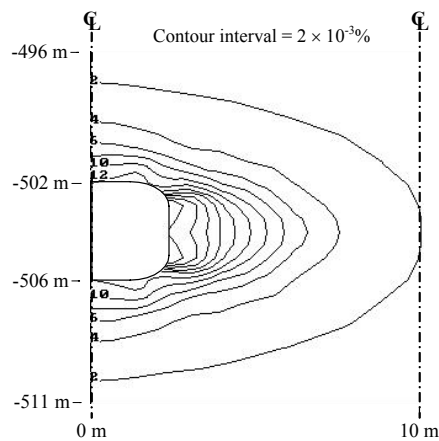


**Figure C.20** Contour of octahedral shear strain around repository room (model KM-P4) at 50 years after emplacement (the maximum octahedral shear strain =  $24 \times 10^{-3}\%$ ). The room is 4 m wide and 4 m high, separated by 16 m wide pillar.

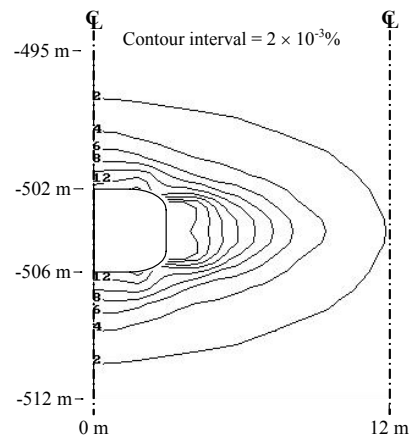


**Figure C.21** Contour of octahedral shear strain around repository room (model KM-P5) at 50 years after emplacement (the maximum octahedral shear strain =  $20 \times 10^{-3}\%$ ). The room is 4 m wide and 4 m high, separated by 20 m wide pillar.

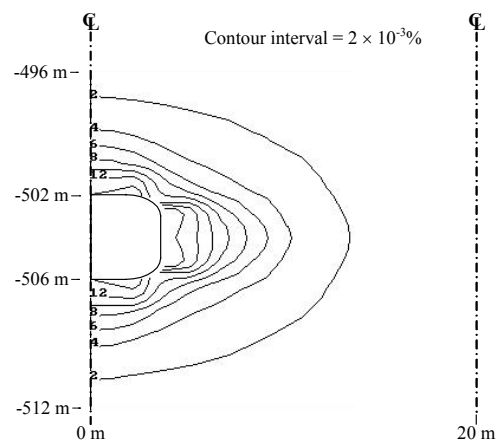


**Figure C.22** Contour of octahedral shear strain around repository room (model KM-P9) at 50 years after emplacement (the maximum octahedral shear strain =  $18 \times 10^{-3}\%$ ). The room is 4 m wide and 4 m high, separated by 36 m wide pillar.

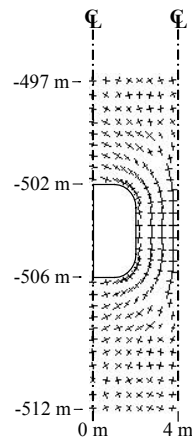


**Figure C.23** Principal stress vectors around repository room (model KM-P1) at 50 years after emplacement (the maximum stress = 2,603 psi). Scale is 20,000 psi/inch. The room is 4 m wide and 4 m high, separated by 4 m wide pillar.

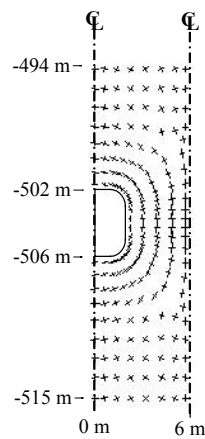


**Figure C.24** Principal stress vectors around repository room (model KM-P2) at 50 years after emplacement (the maximum stress = 2,579 psi). Scale is 20,000 psi/inch. The room is 4 m wide and 4 m high, separated by 8 m wide pillar.

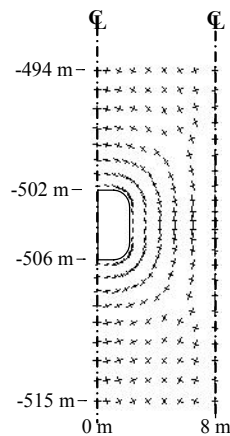


**Figure C.25** Principal stress vectors around repository room (model KM-P3) at 50 years after emplacement (the maximum stress = 2,594 psi). Scale is 20,000 psi/inch. The room is 4 m wide and 4 m high, separated by 12 m wide pillar.

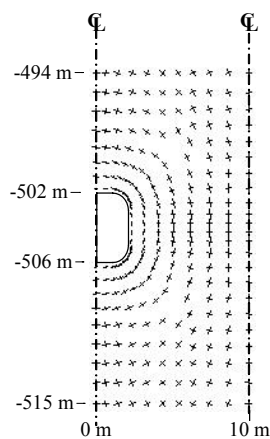


**Figure C.26** Principal stress vectors around repository room (model KM-P4) at 50 years after emplacement (the maximum stress = 2,594 psi). Scale is 20,000 psi/inch. The room is 4 m wide and 4 m high, separated by 16 m wide pillar.

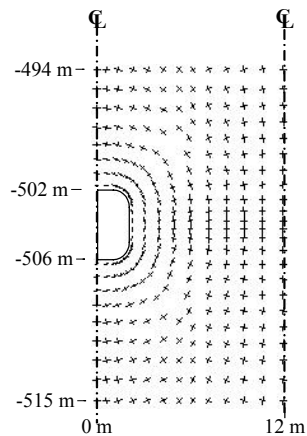


**Figure C.27** Principal stress vectors around repository room (model KM-P5) at 50 years after emplacement (the maximum stress = 2,583 psi). Scale is 20,000 psi/inch. The room is 4 m wide and 4 m high, separated by 20 m wide pillar.

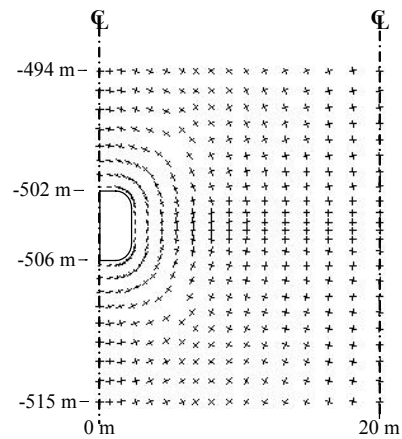


**Figure C.28** Principal stress vectors around repository room (model KM-P9) at 50 years after emplacement (the maximum stress = 2,583 psi). Scale is 20,000 psi/inch. The room is 4 m wide and 4 m high, separated by 36 m wide pillar.

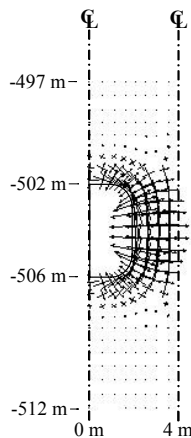


**Figure C.29** Principal strain vectors around repository room (model KM-P1) at 50 years after emplacement (the maximum strain = 34.32%). Scale is 50% /inch. The room is 4 m wide and 4 m high, separated by 4 m wide pillar.

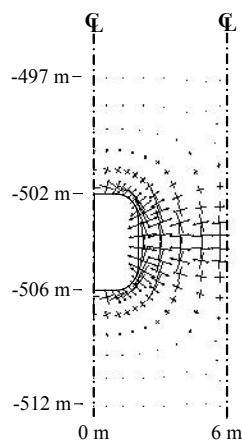


**Figure C.30** Principal strain vectors around repository room (model KM-P2) at 50 years after emplacement (the maximum strain = 8.42%). Scale is 20% /inch. The room is 4 m wide and 4 m high, separated by 8 m wide pillar.



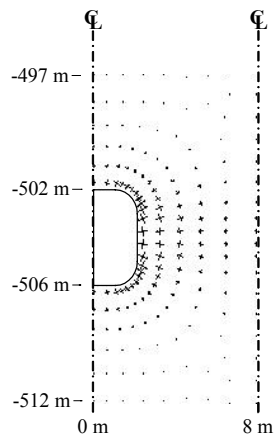


**Figure C.31** Principal strain vectors around repository room (model KM-P3) at 50 years after emplacement (the maximum strain = 2.77%). Scale is 20% /inch. The room is 4 m wide and 4 m high, separated by 12 m wide pillar.

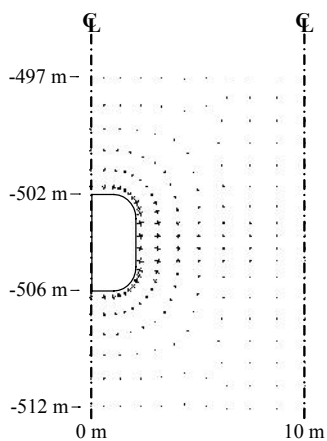


**Figure C.32** Principal strain vectors around repository room (model KM-P4) at 50 years after emplacement (the maximum strain = 1.57%). Scale is 20% /inch. The room is 4 m wide and 4 m high, separated by 16 m wide pillar.

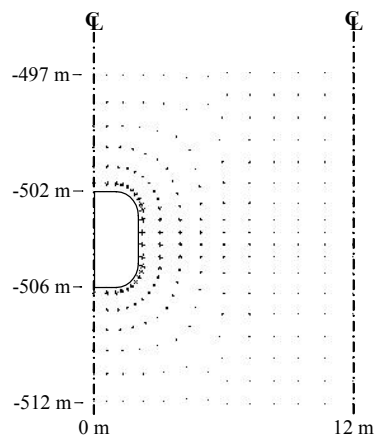


**Figure C.33** Principal strain vectors around repository room (model KM-P5) at 50 years after emplacement (the maximum strain = 1.42%). Scale is 20% /inch. The room is 4 m wide and 4 m high, separated by 20 m wide pillar.

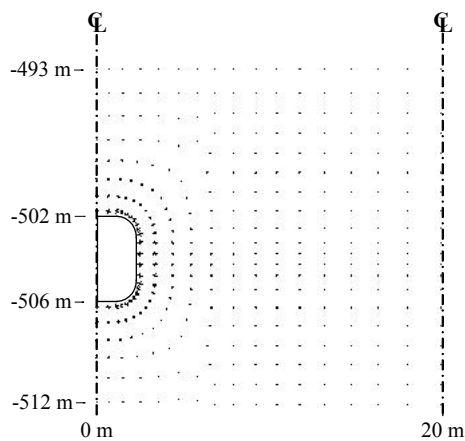


**Figure C.34** Principal strain vectors around repository room (model KM-P9) at 50 years after emplacement (the maximum strain = 1.23%). Scale is 20% /inch. The room is 4 m wide and 4 m high, separated by 36 m wide pillar.

## **APPENDIX D**

### **RESULTS FROM THE COMPUTER MODELING TO STUDY THE EFFECT OF ROOM DEPTH**

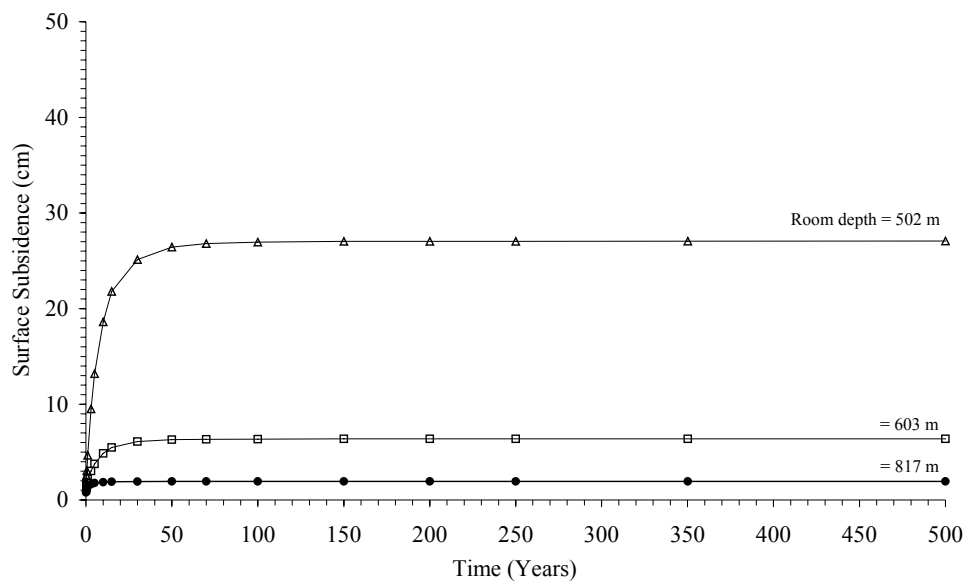


**Figure D.1** Predicted surface subsidence induced by repository rooms for various depths. The room depths vary from 502, 603 to 817 meters.

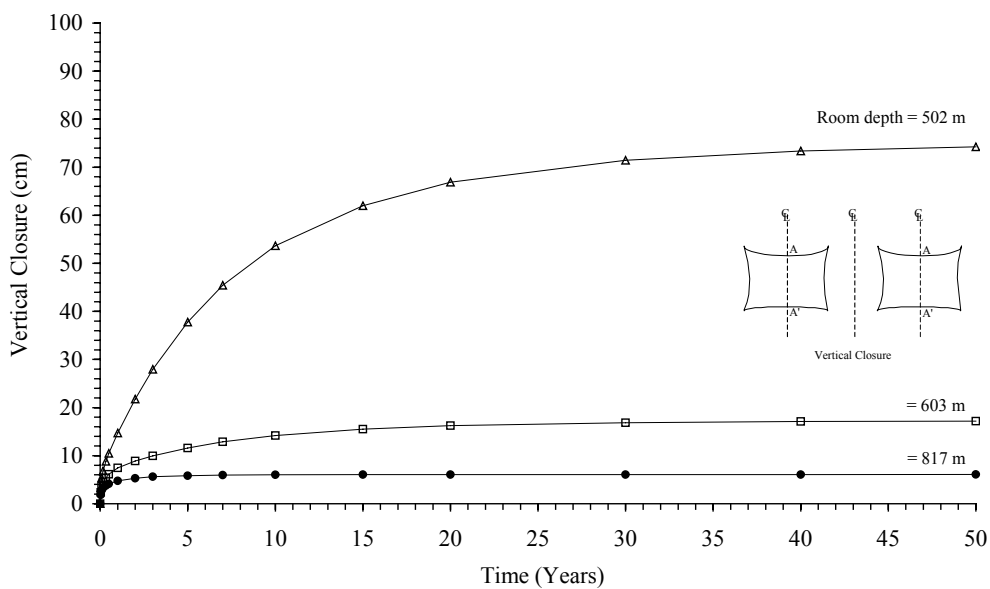


**Figure D.2** Predicted vertical closure of repository rooms for various depths. The room depths vary from 502, 603 to 817 meters.

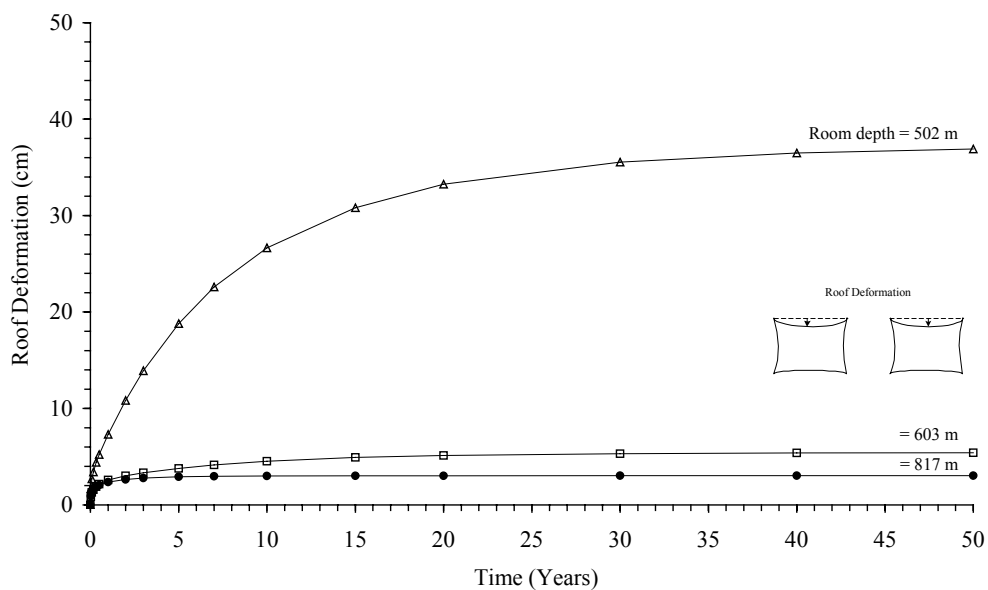


**Figure D.3** Predicted roof deformation of repository rooms for various depths.

The room depths vary from 502, 603 to 817 meters.

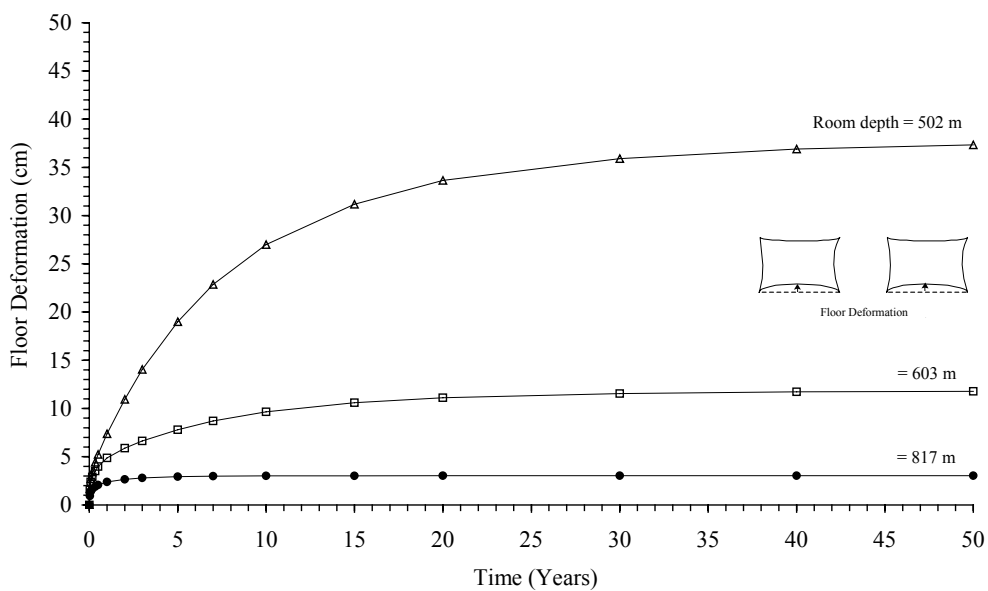


**Figure D.4** Predicted floor deformation of repository rooms for various depths.

The room depths vary from 502, 603 to 817 meters.

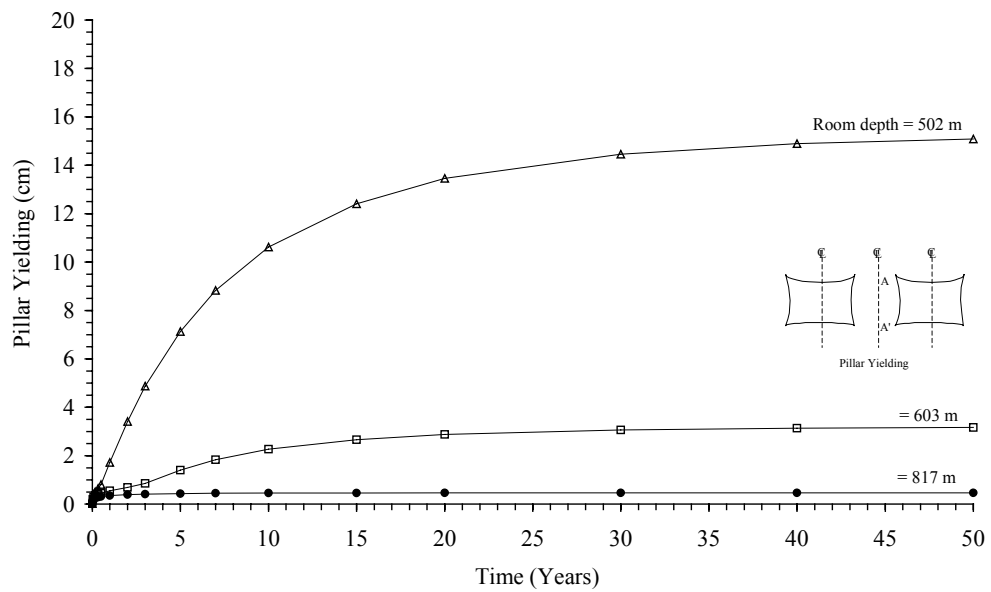


**Figure D.5** Predicted pillar yielding of repository rooms for various depths.

The room depths vary from 502, 603 to 817 meters.

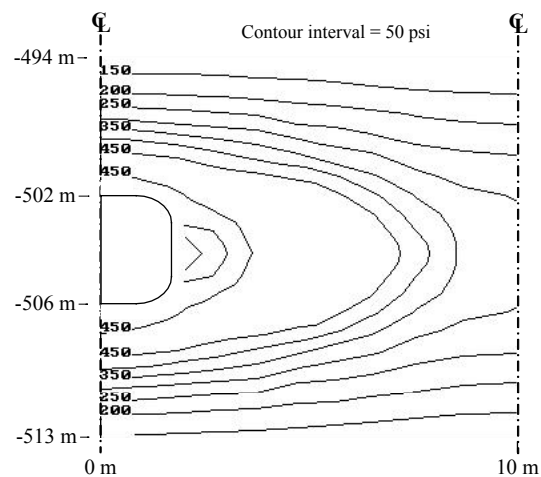


**Figure D.6** Contour of octahedral shear stress around repository room (model

KM-P4) at 50 years after emplacement (the maximum octahedral shear stress = 500 psi). The room depth is 502 meters.

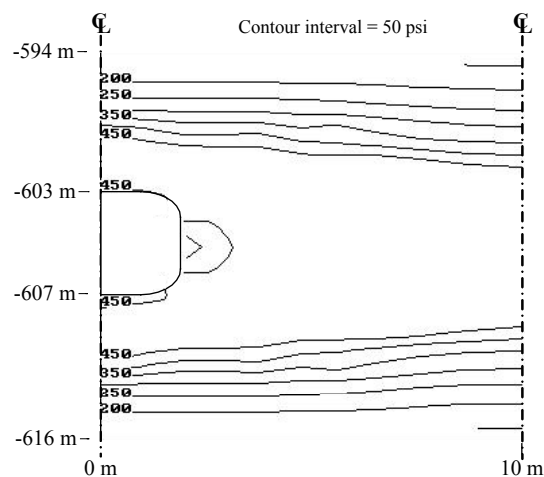


**Figure D.7** Contour of octahedral shear stress around repository room (model KW-P4) at 50 years after emplacement (the maximum octahedral shear stress = 500 psi). The room depth is 603 meters.

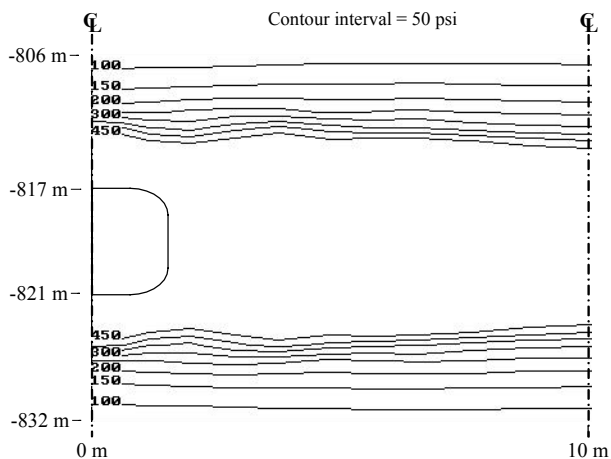


**Figure D.8** Contour of octahedral shear stress around repository room (model NB-P4) at 50 years after emplacement (the maximum octahedral shear stress = 500 psi). The room depth is 817 meters.

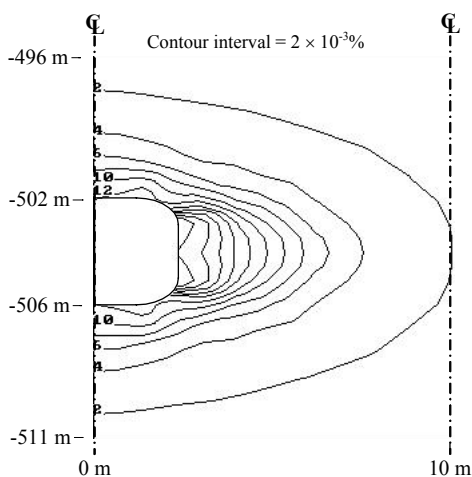


**Figure D.9** Contour of octahedral shear strain around repository room (model KM-P4) at 50 years after emplacement (the maximum octahedral shear strain =  $24 \times 10^{-3}\%$ ). The room depth is 502 meters.

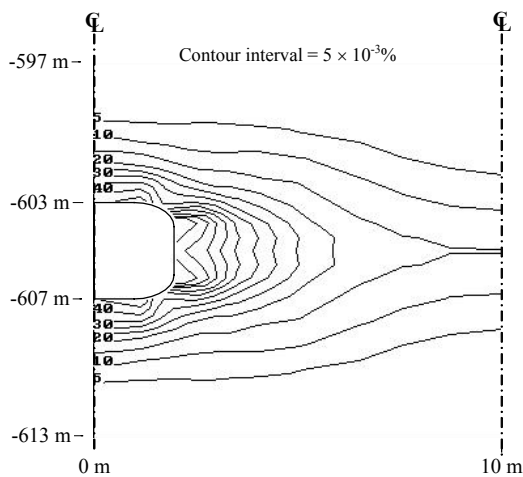


**Figure D.10** Contour of octahedral shear strain around repository room (model KW-P4) at 50 years after emplacement (the maximum octahedral shear strain =  $64 \times 10^{-3}\%$ ). The room depth is 603 meters.



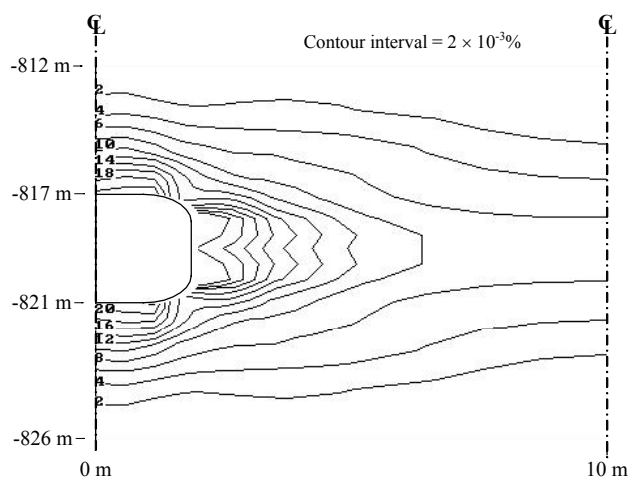


**Figure D.11** Contour of octahedral shear strain around repository room (model NB-P4) at 50 years after emplacement (the maximum octahedral shear strain =  $24 \times 10^{-2}$  %). The room depth is 817 meters.

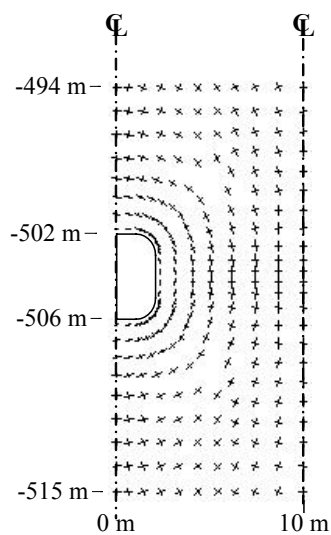


**Figure D.12** Principal stress vectors around repository room (model KM-P4) at 50 years after emplacement (the maximum stress = 2,594 psi). Scale is 20,000 psi/inch. The room depth is 502 meters.

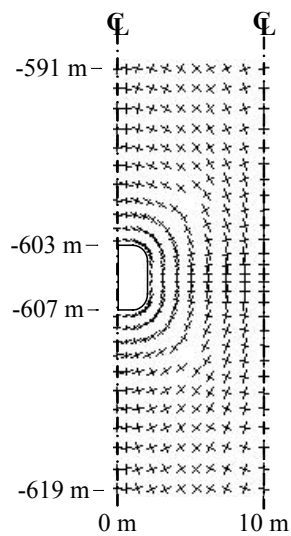


**Figure D.13** Principal stress vectors around repository room (model KW-P4) at 50 years after emplacement (the maximum stress = 3,360 psi). Scale is 20,000 psi/inch. The room depth is 603 meters.

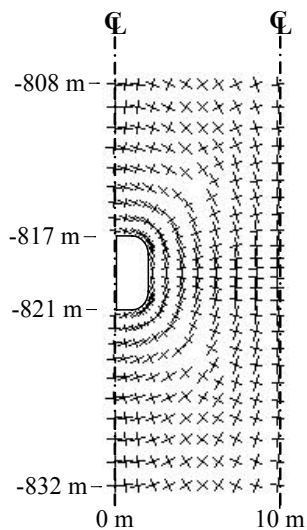


**Figure D.14** Principal stress vectors around repository room (model NB-P4) at 50 years after emplacement (the maximum stress = 4,289 psi). Scale is 20,000 psi/inch. The room depth is 817 meters.

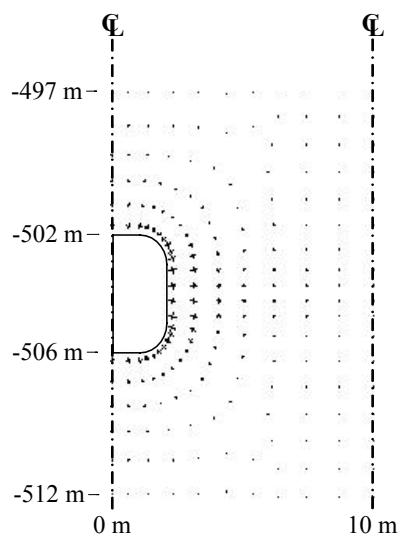


**Figure D.15** Principal strain vectors around repository room (model KM-P4) at 50 years after emplacement (the maximum strain = 1.57%). Scale is 20% /inch. The room depth is 502 meters.

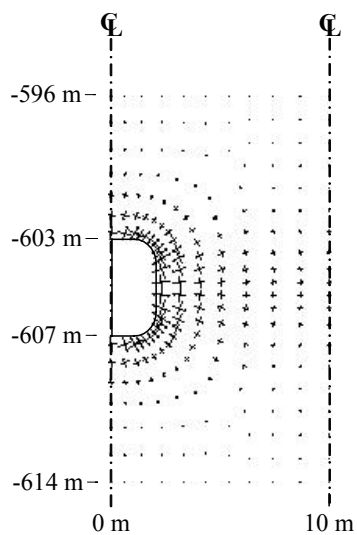


**Figure D.16** Principal strain vectors around repository room (model KW-P4) at 50 years after emplacement (the maximum strain = 4.44%). Scale is 20% /inch. The room depth is 603 meters.

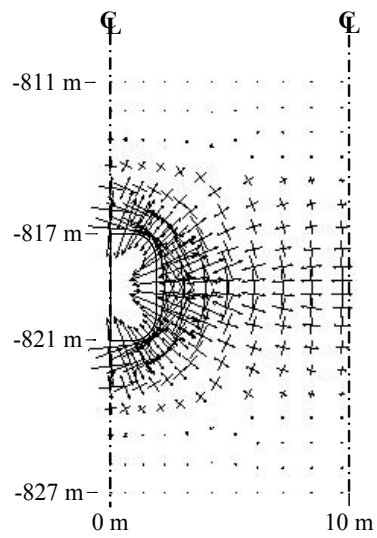


**Figure D.17** Principal strain vectors around repository room (model NB-P4) at 50 years after emplacement (the maximum strain = 16.18%). Scale is 20% /inch. The room depth is 817 meters.

## **APPENDIX E**

# **RESULTS FROM THE COMPUTER MODELING OF THE MAIN ENTRY**

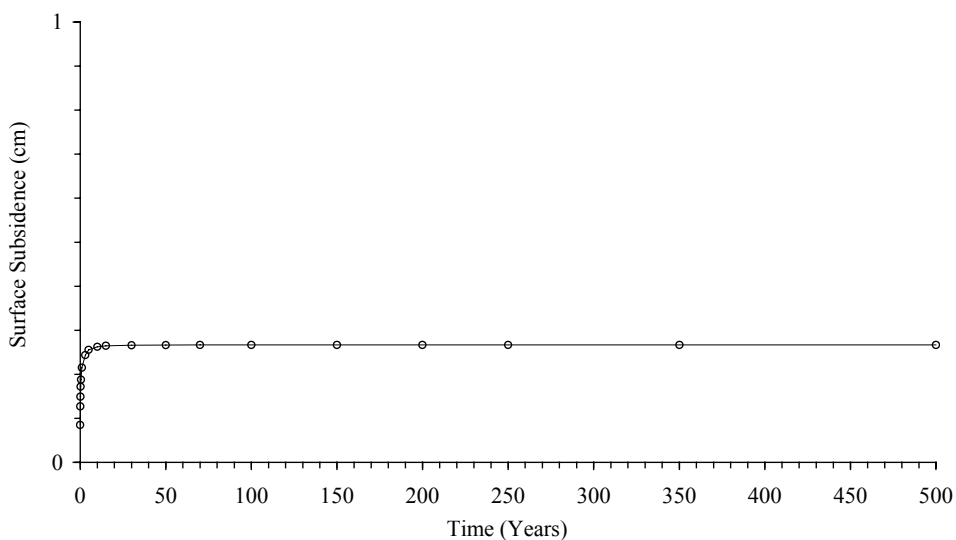


**Figure E.1** Predicted surface subsidence of the main entry at the center line.

The room is 5 m wide, 4.5 m high and 502 m deep, separated by 20 m wide pillar.

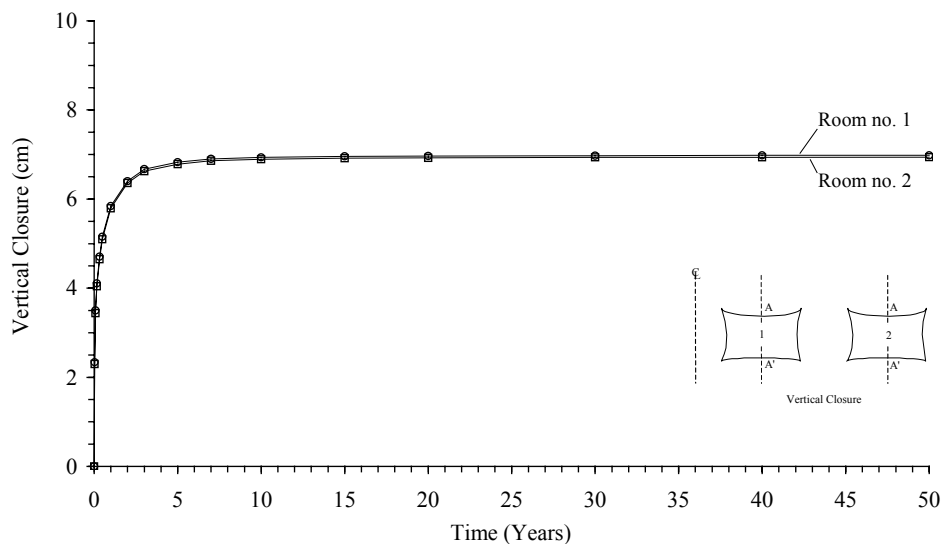


**Figure E.2** Predicted vertical closure of the main entry for room 1 (inner) and room 2 (outer). The room is 5 m wide, 4.5 m high and 502 m deep, separated by 20 m wide pillar.

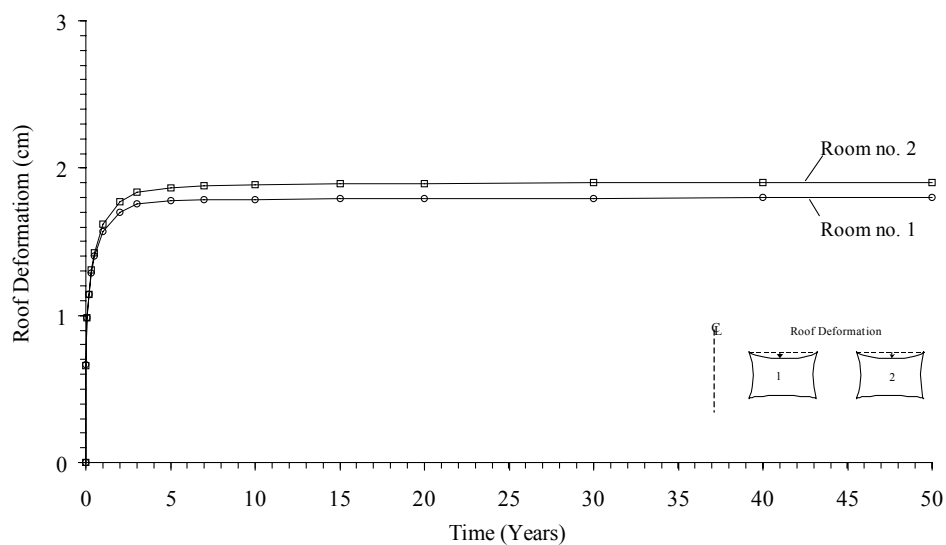


**Figure E.3** Predicted roof deformation of the main entry for room 1 (inner) and room 2 (outer). The room is 5 m wide, 4.5 m high and 502 m deep, separated by 20 m wide pillar.

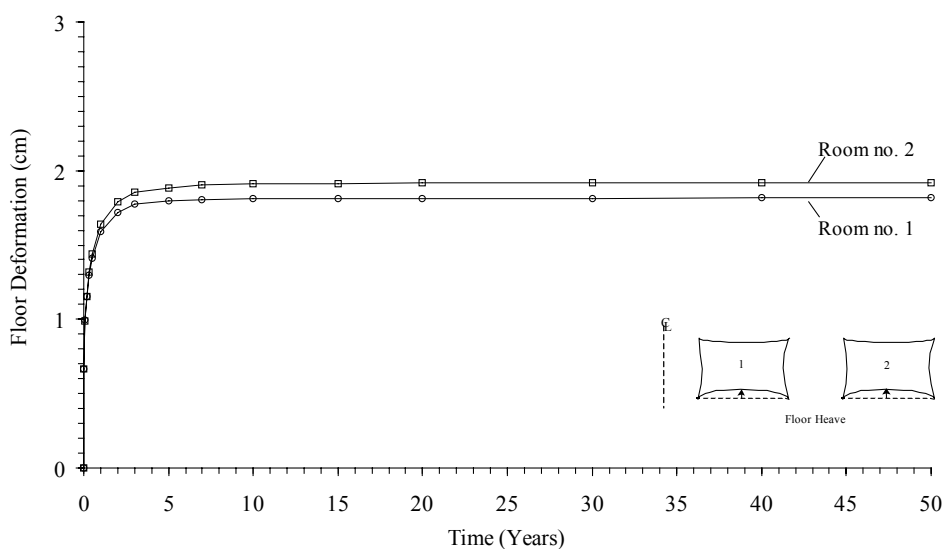


**Figure E.4** Predicted floor deformation of the main entry for room 1 (inner) and room 2 (outer). The room is 5 m wide, 4.5 m high and 502 m deep, separated by 20 m wide pillar.

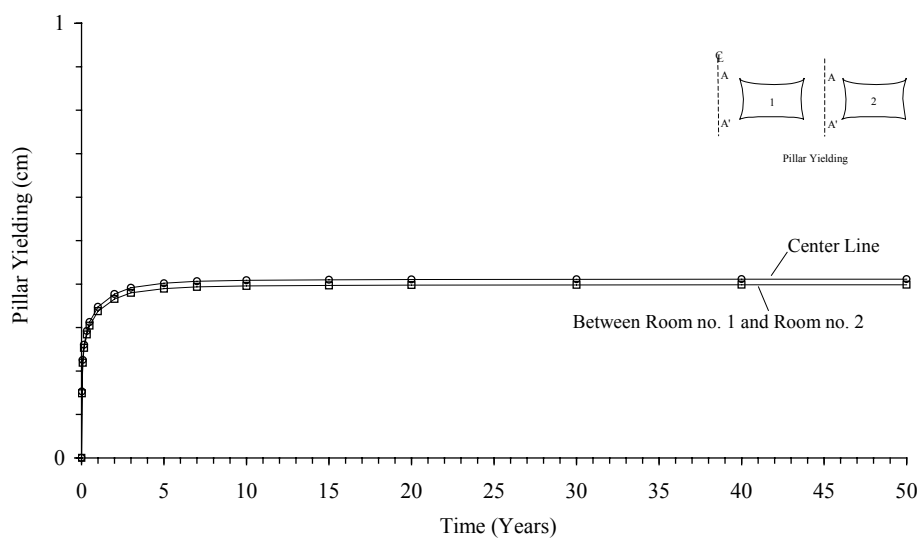


**Figure E.5** Predicted pillar yielding of the main entry for room 1 (inner) and room 2 (outer). The room is 5 m wide, 4.5 m high and 502 m deep, separated by 20 m wide pillar.

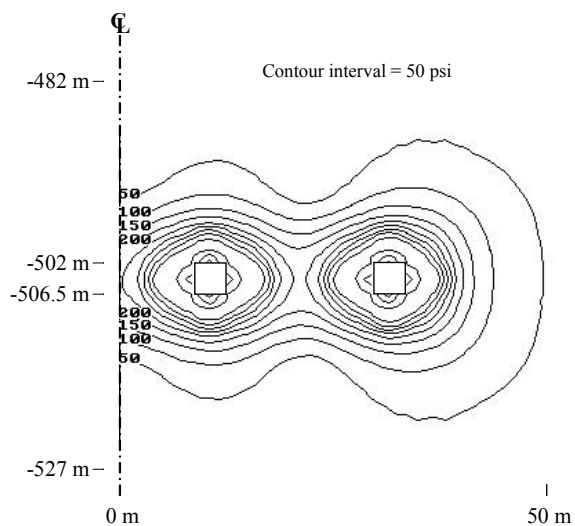


**Figure E.6** Contour of octahedral shear stress around main entries at 50 years (the maximum octahedral shear stress = 500 psi). The room is 5 m wide, 4.5 m high and 502 m deep, separated by 20 m wide pillar.



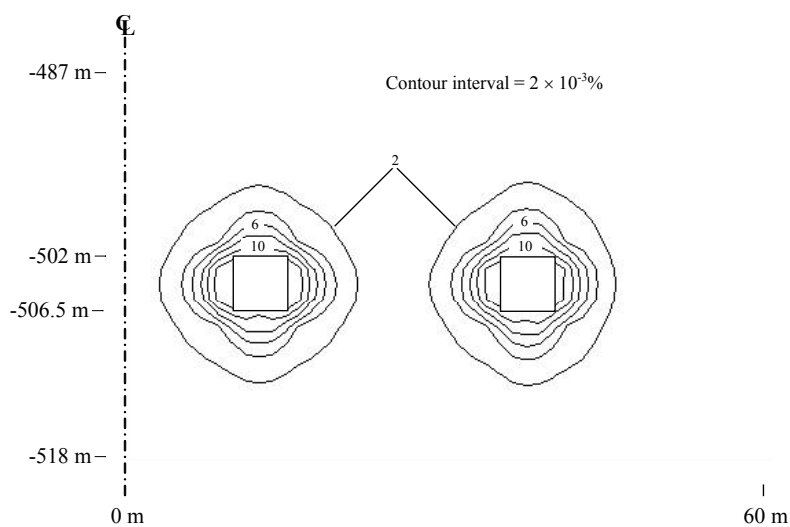


**Figure E.7** Contour of octahedral shear strain around main entries at 50 years (the maximum octahedral shear strain =  $14 \times 10^{-3}\%$ ). The room is 5 m wide, 4.5 m high and 502 m deep, separated by 20 m wide pillar.

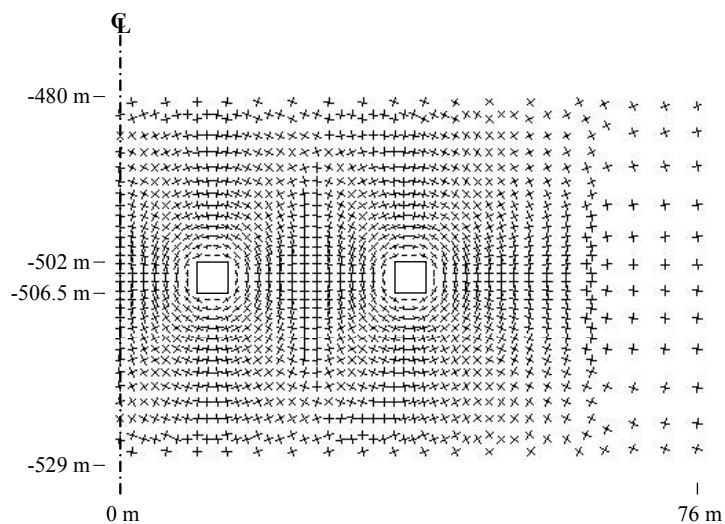


**Figure E.8** Principal stress vectors around main entries at 50 years (the maximum stress = 2,572 psi). Scale is 15,000 psi/inch. The room is 5 m wide, 4.5 m high and 502 m deep, separated by 20 m wide pillar.

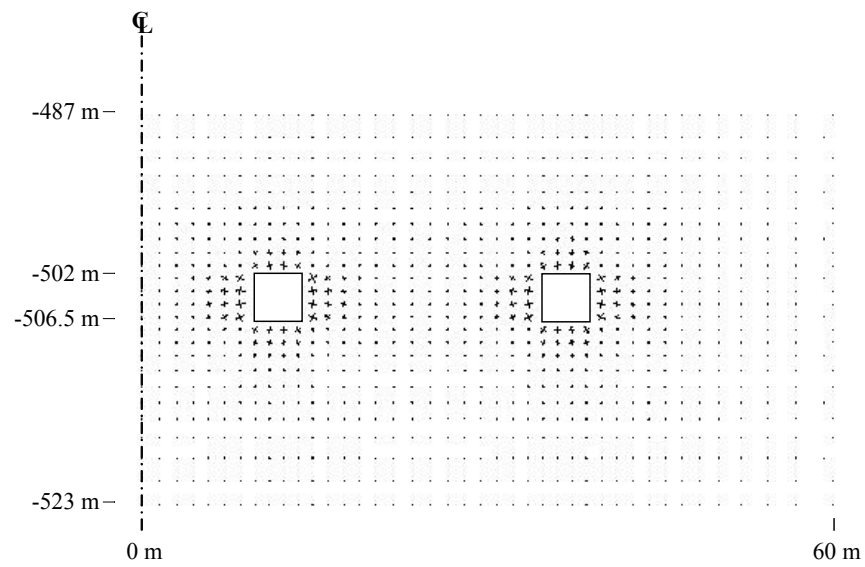


**Figure E.9** Principal strain vectors around main entries at 50 years (the maximum strain = 1.0 %). Scale is 10 % /inch. The room is 5 m wide, 4.5 m high and 502 m deep, separated by 20 m wide pillar.

## **BIOGRAPHY**

Mr. Kitcha Klayvimut was born in Nakhon Sawan province and graduated in geological engineering from Suranaree University of Technology (SUT) in 2001. For his post-graduate, he continued to study with a Master's Degree in Geological Engineering emphasis on rock mechanics at SUT. During graduation, 2001-2003, he was a part time worker in positions of teaching assistant at SUT and research assistant at the Department of Alternative Energy Development and Efficiency (DEDE), the Thailand Research Fund (TRF) and the Office of Atomic Energy for Peace (OAEP). Moreover, he also worked at the Asia Cement Public Company Limited, as a geologist assistant and for a mining engineering company as an assistant mining engineer. In 2004, he has published a technical paper related to rock salt mechanics at the 9<sup>th</sup> Australia New Zealand Conference on Geomechanics "*To the eNZ of the Earth*", Auckland, New Zealand. For his work, he is a good knowledge in geomechanics theory and practice.